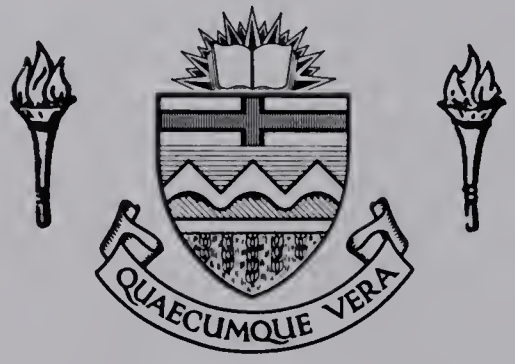

THE UNIVERSITY OF ALBERTA

NMR STUDY OF ELECTRON-NUCLEAR INTERACTIONS IN WHITE TIN USING THE TECHNIQUE OF MACROSCOPIC ROTATION

BY

© MICHAEL R. SMITH

A THESIS

SUBMITTED TO THE FACULTY OF GRADUATE STUDIES AND RESEARCH

IN PARTIAL FULFILMENT OF THE REQUIREMENTS FOR THE DEGREE

OF DOCTOR OF PHILOSOPHY

DEPARTMENT OF PHYSICS

EDMONTON, ALBERTA

SPRING, 1972

UNIVERSITY OF ALBERTA

FACULTY OF GRADUATE STUDIES

The undersigned certify that they have read, and recommend to the Faculty of Graduate Studies and Research for acceptance, a thesis entitled NMR STUDY OF ELECTRON-NUCLEAR INTERACTIONS IN WHITE TIN USING THE TECHNIQUE OF MACROSCOPIC ROTATION submitted by Michael R. Smith in partial fulfilment of the requirements for the degree of Doctor of Philosophy.

Abstract

This thesis describes an experimental study of the electron-coupled nuclear-nuclear interactions and the Knight Shift in white tin using macroscopic rotation techniques. A description is given of a high-speed gas turbine capable of operating to speeds in excess of 5 kHz at the 'magic' angle within a Varian crossed-coil probe.

Using this turbine the Sn^{117} and Sn^{119} resonances were observed in tin metal. The lineshape is governed by the spin-lattice relaxation time and the 'pseudo-exchange' coupling between nuclei. The theoretical lineshape has been synthesized assuming the Ruderman-Kittel model. By comparing the experimental and theoretical lineshapes it was found that the nearest-neighbour 'pseudo-exchange' coupling was 1.89 ± 0.09 kHz. This suggests that Alloul and Deltour have misinterpreted their data in obtaining a value of 4.1 kHz.

The room-temperature isotropic Knight Shifts of the Sn^{117} and Sn^{119} isotopes were determined to be 0.724 ± 0.003 and 0.726 ± 0.003 respectively. A redetermination of the ratio of the Sn^{119} and Sn^{117} magnetogyric ratios gave the value 1.046535 ± 0.000003.

Acknowledgements

I wish to express my sincere gratitude to Dr. D. G. Hughes, my research supervisor, for suggesting this project and for his continued interest, encouragement and help throughout my studies at the University of Alberta.

The cooperative attitude of members of the technical staff of the Department has been a definite asset. I wish in particular to thank Mr. M. Burke and Mr. W. Boyd, for their help on the instrumentation involved in the project, and Mr. D. Gerritsen and Mr. J. Cuthiell, for their patience and technical skill during the construction of the turbine assembly.

I wish to thank my wife, Pat, for her encouragement during the course of this research. Her help in drawing the figures for this thesis is greatly appreciated.

It is a pleasure to acknowledge the financial assistance that I received. I wish to thank the National Research Council for their support, and in particular for the award of a Graduate Scholarship. Also, I wish to thank the Killam Foundation for their continued support in the form of an Izaak Walton Killam Memorial Predoctoral Fellowship.

Finally, I would like to thank Mrs. Mary Yiu and Miss AnnaBelle Thibodeau for typing this thesis.

TABLE OF CONTENTS

CHAPTER 1. INTRODUCTION

When an ensemble of non-interacting spin $\frac{1}{2}$ nuclei is placed in a steady magnetic field H_o, the two magnetic energy levels of the system are separated by

$$\Delta E = \gamma_n \hbar H_o = h\nu$$

where γ_n is the magnetogyric ratio of the nuclei. The application of an rf magnetic field, of frequency ν, perpendicular to the main field, induces transitions between the levels. This would imply that the nmr spectrum of such a system consists of an infinitely sharp line at frequency ν. If the nuclei are interacting with each other, the nmr spectrum ceases to be a sharp line and becomes spread or broadened over a band of frequencies.

A common source of broadening in solids arises from the nuclear magnetic dipole-dipole interactions. A nuclear magnetic dipole produces, at a neighbouring lattice site, an effective additional magnetic field with an angular variation of $(3 \cos^2\theta - 1)$ where θ is the angle between the applied field and the internuclear vector. The presence of neighbouring nuclei can thus alter the resonance absorption lineshape. It was observed, however, that in many cases, the line would suddenly narrow when the sample was heated. This was taken as evidence of relative motion

between nuclei or groups of nuclei in the solid. A given neighbouring nucleus would then see only a time averaged field, and this, in general, is smaller than the static field. Gutowsky and Pake (1948) showed that when the frequency of motion became greater than the width of the absorption line (measured in frequency units), narrowing occurred.

Andrew, Bradbury and Eades (1958) and independently Lowe (1959) found that a similar narrowing was also obtained when the sample was macroscopically rotated. Further analysis (Andrew and Newing, 1958) showed that the maximum narrowing occurred when the axis of rotation was at the so-called 'magic' angle $\cos^{-1}(1/\sqrt{3})$ to the main magnetic field.

In metals there is an additional source of broadening above that of the dipolar. This arises from the interaction of the nuclei with the conduction electrons. This interaction is normally stronger than the dipolar interaction, so that the broadening arising from it dominates. There are three types of broadening; one more important at low temperatures, another at high temperatures and the third in large magnetic fields. The presence of the applied magnetic field polarises the conduction electrons in the metal. This polarization results in an additional magnetic field at the nuclear site, giving the nucleus a shift in resonant frequency relative to the same nucleus in a non-metallic salt. This shift is known as the Knight Shift (Knight, 1949). When the nucleus is in a non-cubic environment, this

shift depends upon the angle between the main field and the crystallographic axes of the metal. In a powder, therefore, a spread of resonant frequencies would result from the crystallites being randomly orientated. This broadening increases in proportion to the applied field. At high temperatures, the electron-nuclear interaction gives a finite lifetime to the nuclear states. This results in broadening due to the short spin-lattice relaxation time T_1. As the relaxation time is inversely proportional to temperature (Korringa, 1950) this source of broadening is relatively unimportant at low temperatures. The third effect is the electron-coupled nuclear-nuclear interaction, which at low temperatures and fields has a dominant effect on the metal spectrum (Bloembergen and Rowland, 1953; Rudermann and Kittel, 1954). This arises from an electron, scattered by its hyperfine interaction with one nucleus, interacting with a second nucleus, and effectively coupling the nuclei together. Whilst historically this effect was first seen in high resolution spectrometry in liquids (Hahn and Maxwell, 1952; Gutowsky, McCall and Slichter, 1953) it has since been noticed in many metals. In general this interaction has an anisotropic contribution.

In a similar fashion to the narrowing of lines broadened by dipole interactions, the macroscopic rotation of samples leads to the removal of other anisotropic interactions. This enables a study to be made of the scalar part (or pseudo-exchange) of the electron-coupled nuclear-

nuclear interaction without the necessity of considering a spectrum complicated by the presence of any anisotropic interaction.

In this thesis we describe an experiment conducted to measure the scalar 'pseudo-exchange' coupling in white (metallic) tin. Chapter 2 gives details of the theory and experimentation involved in the method of macroscopic rotation. Chapter 3 gives a brief account of the electron-coupled nuclear-nuclear interaction. Chapter 4 gives the analysis of the data obtained from tin. The results are discussed and a conclusion given in Chapter 5.

CHAPTER 2. MACROSCOPIC ROTATION

A) Theory

A number of studies have been undertaken to examine the electron-coupled interactions in tin (steady-state measurements: Karimov and Shchegolev, 1961; Sharma, Williams and Schone, 1969; pulse measurements: McLachlan, 1968; Alloul and Deltour, 1969). The measurements have involved both the anisotropic and scalar couplings. Whilst in principle it would be possible to remove the anisotropic interactions with a series of pulses (cf removal of dipolar line broadening: Mansfield and Ware, 1966; Ostroff and Waugh, 1966), in practice there are difficulties. If measurements were made using a single metal crystal there would be the difficulty of overcoming signal distortions due to the finite skin depth. On the other hand, if a powder was used, then the line shape would be complicated by the presence of the anisotropic Knight Shift. This is a macroscopic rather than a microscopic broadening of the line and therefore cannot be removed by a system of pulses (Andrew, 1970). Removing the anisotropic broadening by rotation therefore offers certain advantages.

It is interesting to note that historically the first measurements involving sample rotation were not made for the specific purpose of narrowing the line. Instead, Andrew, Bradbury and Eades (1958) used the

technique to confirm the theoretical predictions of Anderson (1954) and Pake (1956) that internal motion in a solid narrowed the dipolar-broadened spectrum in such a manner that its second moment remained constant, whilst its fourth moment increased. When Andrew et al. rotated a sample of NaCl, they found that the central part of the spectrum narrowed but satellite lines appeared. These were separated from the main line by multiples of the rotation frequency. This increase in intensity in the wings keeps the second moment invariant whilst increasing the fourth moment.

The effect of rotation is best seen by considering the simple case of an ensemble of pairs of nuclei with spin $\frac{1}{2}$ arranged in a static array with their internuclear vectors parallel to each other. The nmr spectrum of each pair of non-rotating nuclei consists of two lines of equal intensity at the angular frequencies

$$\omega_{\pm} = \gamma_a [H_o \pm \varepsilon \mu_b R^{-3} (3 \cos^2\theta - 1)], \qquad (1)$$

where γ_a is the magnetogyric ratio of the nuclei at resonance, $\underline{H}_o$ is the constant applied field, μ_b is the magnetic moment of the nuclear neighbour in each pair, $\underline{R}$ is the internuclear vector, θ is the angle between $\underline{H}_o$ and $\underline{R}$ and ε is 3/2 if the nuclei in the pair are identical and 1 if they are not (Pake, 1948). Thus the spectrum of this static array can be considered to arise from the

presence, at the site of the nuclei at resonance, of an effective local field whose component along H_o is given by

$$H_{loc} = \pm c(3 \cos^2\theta - 1) \tag{2}$$

where $$c = \varepsilon \mu_b R^{-3}. \tag{3}$$

Instead of considering a static array, let the nuclei be capable of being rotated about an axis making an angle α to $\underline{H}_o$, and, for simplicity, perpendicular to the inter-nuclear vector of the pair (see figure (2.1a)). Imagine that when there is no rotation, the nuclear pairs are distributed with random, but fixed, azimuth angle ϕ about the rotation axis. The spectrum for each pair, with a given ϕ, consists of two lines given by equation (1), in which we set

$$\cos\theta = \sin\alpha \cos\phi \ . \tag{4}$$

The spectrum for all pairs, taking all ϕ with equal probability, has a second moment

$$S_2 = \frac{1}{2\pi} \int_o^{2\pi} c^2 \gamma_a{}^2 (9 \sin^4\alpha\cos^4\phi - 6 \sin^2\alpha\cos^2\phi + 1) d\phi$$

$$= c^2 \gamma_a{}^2 (\frac{27}{8} \sin^4\alpha - 3\sin^2\alpha + 1). \tag{5}$$

If all the pairs are now allowed to rotate with the same uniform angular velocity ω_r, we then have

$$\phi = \phi_o + \omega_r t \ , \tag{6}$$

Figure (2.1)

(a) A system of two nuclei A and B capable of being rotated about an axis at an angle α to the main magnetic field $\underline{H}_o$.

(b) Nmr spectrum for the above pair of nuclei when they are rotating at a rate ω_r about an axis perpendicular to their internuclear vector. The frequencies ω_o and ω_1 are $\gamma_a H_o$ and $\frac{1}{2} c \gamma_a (3 \cos^2\alpha - 1)$ respectively.

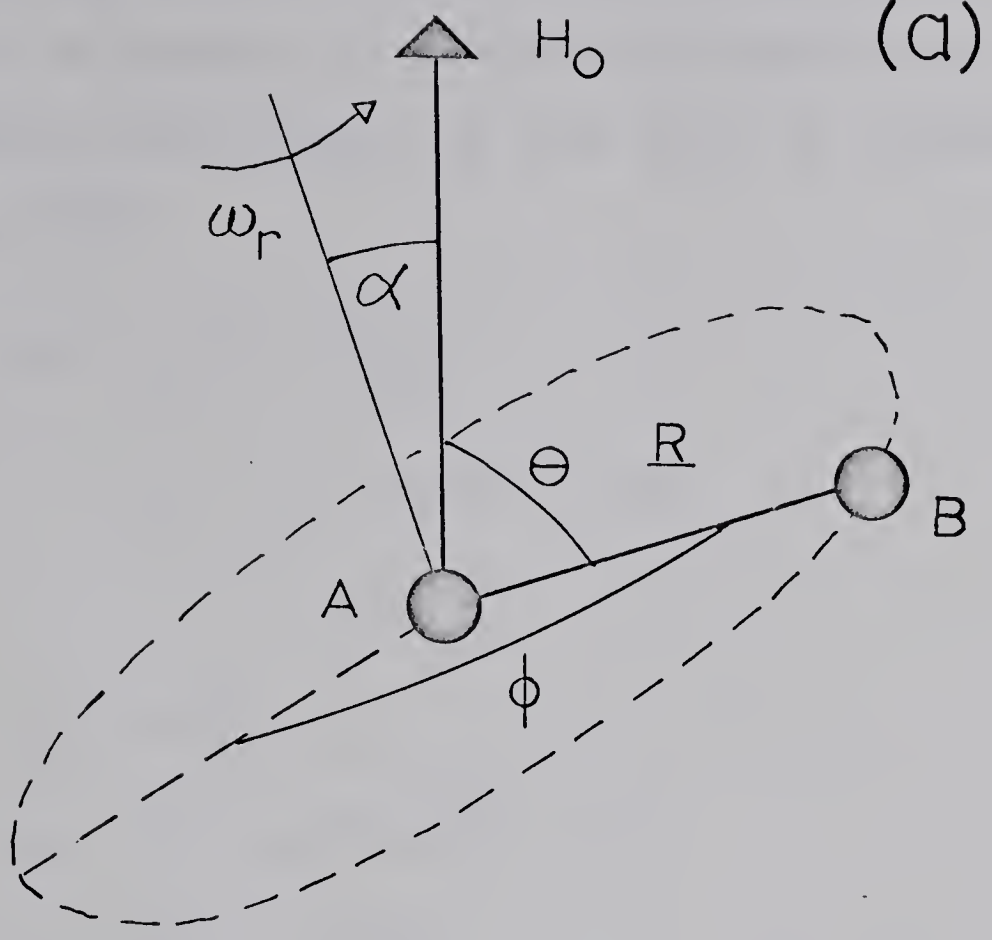
(a)
H_o
ω_r
α
θ
R
A
B
ϕ

(b)
$J_0^2(m)$
$J_2^2(m)$
$J_1^2(m)$
$J_1^2(m)$
$J_2^2(m)$
$\omega_o \pm \omega_1 - 4\omega_r$
$\omega_o \pm \omega_1 - 2\omega_r$
$\omega_o \pm \omega_1$
$\omega_o \pm \omega_1 + 2\omega_r$
$\omega_o \pm \omega_1 + 4\omega_r$
ANGULAR FREQUENCY

so that each nucleus experiences a local field which consists of static and fluctuating components. The Larmor frequency of the nuclei is then given by (Andrew and Newing, 1958)

$$\omega = \gamma_a(H_o + H_{loc})$$

$$= \omega_o \mp \omega_1 \pm \omega_2 \cos 2\omega_r t \qquad (7)$$

where

$$\omega_o = \gamma_a H_o$$

$$\omega_1 = \frac{1}{2} c \gamma_a(3 \cos^2\alpha - 1) \qquad (8)$$

$$\omega_2 = \frac{3}{2} c \gamma_a \sin^2\alpha \quad .$$

We note that the Larmor frequency is frequency-modulated at $2\omega_r$. Thus the spectrum consists of two carrier components at frequencies $\omega_o \pm \omega_1$, each of which has an infinite set of sidebands situated at multiples of $2\omega_r$ (see figure (2.1b)). The intensity of the nth sideband relative to that of the central component is $J_n^2(m)/J_o^2(m)$ where $J_n(m)$ is the Bessel function of order n, and m is given by

$$m = \omega_2/2\omega_r. \qquad (9)$$

The second moment of this spectrum is

$$S_2 = \frac{1}{2} \sum_{n=-\infty}^{+\infty} \{(\omega_1 + 2n\omega_r)^2 J_n^2(m)$$

$$+ (-\omega_1 + 2n\omega_r^2)^2 J_n^2(m)\} \qquad (10)$$

which, by making use of the theorems of Watson (1922), becomes

$$S_2 = \omega_1^2 + \frac{1}{2}\omega_2^2 \quad . \tag{11}$$

Making use of equations (8) and (11) one finds that the second moment is identical to that of the static array. As ω_r increases, the sidebands move out and become less intense. If we ignore their contributions, the spectrum then consists of two carrier frequencies. The second moment of these is ω_1^2, which is smaller than the static second moment. We can generalize this analysis to a more random array of nuclei, whose spectrum is broad rather than consisting of delta functions, and see that rotation would lead to a narrower line. We note from equation (8) that if

$$\alpha = \cos^{-1}(1/\sqrt{3}) = 54°44' \tag{12}$$

the centre lines collapse into a single line at ω_o, and the dipolar second moment (excluding the contribution of the sidebands) reduces to zero.

We shall now proceed to consider macroscopic rotation in a more general fashion. Theoretical considerations have been made on the narrowing of dipolar-broadened lines (Andrew and Newing, 1958; Andrew and Jenks, 1962) and on the removal of the anisotropic Knight Shift (Schwind, 1967), but the most general comprehensive study has been undertaken

by Andrew and Farnell (1968) who were able to point out a limitation to the rotation technique in removing anisotropic effects.

The truncated Hamiltonian which determines the nmr spectrum is, excluding quadrupole interactions,

$$H = H_z + [H_D]_{trunc.} + H_J \quad . \tag{13}$$

H_z is the Zeeman interaction between the nuclei and the applied field:

$$H_z = - \sum_i \gamma_i \hbar \underline{I}_i \cdot (\underline{\underline{1}} - \underline{\underline{K}}_i) \cdot \underline{H}_o \tag{14}$$

where $\underline{I}_i$ is the spin operator of the nucleus i, γ_i is the magnetogyric ratio, and $\underline{\underline{K}}_i$ is the Knight Shift tensor. H_D is the truncated dipolar interaction (Van Vleck, 1948; Slichter, 1963):

$$[H_D]_{trunc.} = \sum_{i<j} h \underline{I}_i \cdot \underline{\underline{D}}_t \cdot \underline{I}_d \tag{15}$$

where $\underline{\underline{D}}_t$ is the truncated dipolar interaction tensor, all terms of which contain the factor $(3 \cos^2\theta_{ij} - 1)$, with θ_{ij} being the angle between $\underline{H}_o$ and the internuclear vector $\underline{R}_{ij}$. H_J is the indirect electron-coupled nuclear-nuclear spin interaction:

$$H_J = \sum_{i<j} h \underline{I}_i \cdot \underline{\underline{J}}_{ij} \cdot \underline{I}_j \tag{16}$$

where $\underline{\underline{J}}_{ij}$ is the indirect interaction tensor.

When the sample is rotated, the Hamiltonian becomes

time-dependent. It can then be expressed as

$$H = \bar{H} + H(t) \tag{17}$$

where $\bar{H}$ is the time-averaged Hamiltonian, and H(t) is the time-dependent interaction whose average value is zero. H(t), which is small compared to $\bar{H}$ when the main field is strong, is responsible for the generation of the satellite lines discussed above. $\bar{H}$, which determines the central part of the spectrum, is given by the sum of $\bar{H}_J$, $\bar{H}_z$ and $\bar{H}_D$. We shall consider the case where the satellites are sufficiently far removed from the centre of the spectrum, so that they are not observed; i.e. only the time-averaged Hamiltonian will be examined. Since the Knight Shift components are so small, only the components along H_o need to be considered (Abragam, 1961) and $\bar{H}$ may be written as

$$\bar{H} = -\hbar \sum_i \gamma_i (1 - \bar{K}_{izz}) I_{iz} H_o + \sum_{\alpha\beta} \sum_{i<j} (h \bar{J}_{ij\alpha\beta} + \bar{D}_{ij\alpha\beta}) I_{i\alpha} I_{j\beta} \tag{18}$$

where α and β are suffixes for cartesian axes in the lab frame and

$$\bar{K}_{zz} = \overline{K + K_z' \lambda_3^2 + K_x' \lambda_1^2 + K_y' \lambda_2^2} \tag{19}$$

with λ_p being the direction cosines of the principal axes of the anisotropic Knight Shift relative to $\underline{H}_o$, K_p' is the pth component of the anisotropic Knight Shift tensor K'

and K is the isotropic Knight Shift.

Now, when the sample is rotated with an angular velocity ω_r about an axis inclined at an angle α_3 to $\underline{H}_o$, and at an angle μ_1, μ_2 and μ_3 to the principal axes of K', we have that

$$\lambda_{i'} = \cos\alpha_3\cos\mu_{i'} + \sin\alpha_3\sin\mu_{i'}\cos(\omega_r t + \psi_{i'}) \qquad (20)$$

where $\psi_{i'}$ is the azimuth angle of the ith principal axis at t = 0. Using eqn. (20) in equation (19) we find

$$\bar{K}_{zz} = K + \frac{1}{2}\sin^2\alpha_3(K'_x + K'_y + K'_z)$$

$$+ \frac{1}{2}(3\cos^2\alpha_3 - 1)\sum_{i'} K'_{i'}\cos^2\psi_{i'}. \qquad (21)$$

When α_3 has the special value, $\cos^{-1}(1/\sqrt{3})$, the so-called magic angle, this mean value reduces to

$$\overline{K_{zz}} = K \qquad (22)$$

as $K'_x + K'_y + K'_z = 0$.

The dipolar interaction is treated in a similar fashion;

$$\sum_{i>j}\sum_{\alpha\beta}\overline{D_{ij\alpha\beta}\, I_{i\alpha} I_{j\beta}}$$

$$= \sum_{i>j}\gamma_i\gamma_j(8\pi^2 r_{ij}^3)^{-1}\overline{(3\cos^2\theta_{ij}-1)}\,(\underline{I}_i\cdot\underline{I}_j - 3I_{iz}I_{jz}). \qquad (23)$$

Since

$$\cos\theta_{ij} = \cos\alpha_3\cos\Omega_{ij} + \sin\alpha_3\sin\Omega_{ij}\cos(\omega_r t + \phi_{ij}) \qquad (24)$$

Figure (2.2)

A diagram of a general system of rotating axes to illustrate the nomenclature used in Chapter 2.

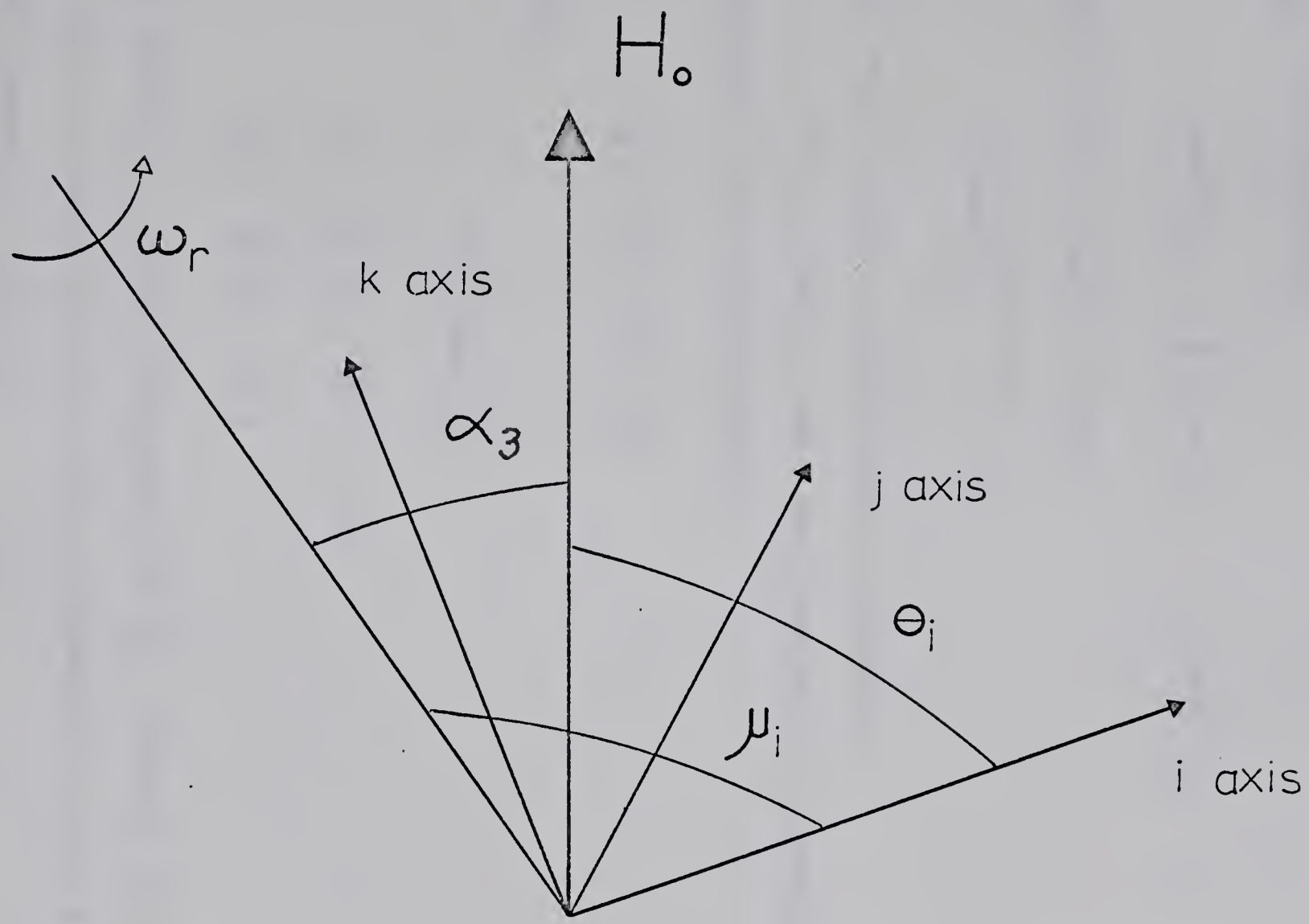
H_o
ω_r
k axis
α_3
j axis
θ_i
μ_i
i axis

where Ω_{ij} is the angle between the axes of rotation and $\underline{R}_{ij}$, with ϕ_{ij} being the azimuth angle, at zero time, of $\underline{R}_{ij}$, we find that

$$\cos^2\theta_{ij} = \frac{1}{6}(3\cos^2\alpha_3 - 1)(3\cos^2\Omega_{ij} - 1) + \frac{1}{3}. \qquad (25)$$

Thus, at the 'magic angle',

$$\overline{(3\cos^2\theta_{ij} - 1)} = 0 \qquad (26)$$

and the dipolar contribution vanishes.

The $\underline{\underline{J}}$ tensor must be treated differently. It may be split into three parts;

$$\underline{\underline{J}} = J\underline{\underline{1}} + \underline{\underline{J}}^* + \underline{\underline{J}}^\dagger \qquad (27)$$

where

$$J = 1/3 \text{ trace } \underline{\underline{J}}$$

$$\underline{\underline{J}}^* = \frac{1}{2}(\underline{\underline{J}} + \underline{\underline{J}}') - J\underline{\underline{1}}$$

$$\underline{\underline{J}}^\dagger = \frac{1}{2}(\underline{\underline{J}} - \underline{\underline{J}}')$$

in which $\underline{\underline{J}}'$ is the transpose of $\underline{\underline{J}}$. Clearly this divides $\underline{\underline{J}}$ into an isotropic part $J\underline{\underline{1}}$, a symmetric part $\underline{\underline{J}}^*$ and an antisymmetric part $\underline{\underline{J}}^\dagger$.

In tin, symmetry considerations show that $\underline{\underline{J}}^\dagger$ should be zero (see Appendix II). (In fact, no case has yet been observed in solids where this is not the case (Andrew, 1970).) We shall therefore take $\underline{\underline{J}}^\dagger$ as zero.

The component $J\underline{\underline{1}}$ is unaffected by the rotation. The term $\underline{I}_i \cdot \underline{\underline{J}}_{ij} \cdot \underline{I}_j$ can be written as

$$\sum_{i>j} \underline{I}_i \cdot \underline{\underline{J}}^*_{ij} \cdot \underline{I}_j = \sum_{i<j} \sum_{\alpha\beta} J^*_{ij\alpha\beta} I_{i\alpha} I_{j\beta}$$

$$= \sum_{i<j} \sum_{n} \sum_{\alpha\beta} C_{ij\alpha n} C_{ij\beta n} I_{i\alpha} I_{j\beta} J_{ijn} \qquad (28)$$

where $C_{\alpha n}$ are the direction cosines of the nth principal axis of the tensor J^*_{ij} relative to the laboratory axes. For each set (i, j) there are 27 terms, not all of which correspond to transitions near the main resonance line. Truncating as for the dipolar term we obtain

$$\left[\sum_{i<j} \sum_{\alpha\beta} J^*_{ij\alpha\beta} I_{i\alpha} I_{j\beta}\right]_{trun.} = \sum_{i<j} -\frac{1}{4}\Big[J_{ij3}(3C^2_{ij33} - 1) \qquad (29)$$

$$+ (J_{ij2} - J_{ij1})(C^2_{ij32} - C^2_{ij31})\Big] \quad (\underline{I}_i \cdot \underline{I}_j - 3I_{iz} I_{jz}) \ .$$

When the crystal is rotated, the direction cosines become time-dependent and the average value of their squares is

$$\overline{C^2_{ij3n}} = \frac{1}{6}(3\cos^2\alpha_3 - 1)(3\cos^2\mu_{ijn} - 1) + \frac{1}{3} \qquad (30)$$

where μ_{ijn} are the angles between the axis of rotation and the principal axes of the tensor J^*_{ij}. Thus, at the magic

angle,

$$\left[\sum_{i<j} \sum_{\alpha\beta} \overline{J^{*}_{ij\alpha\beta} I_{i\alpha} I_{j\beta}} \right]_{trun} = 0. \qquad (31)$$

Collecting terms, we see that on macroscopic rotation at the magic angle the resonance line is determined by the time-averaged Hamiltonian

$$\bar{H} = - \sum_{i} \gamma_i \hbar I_{z_i} (1 - K_i) H_o + \sum_{i<j} J_{ij} h \underline{I}_i \cdot \underline{I}_j . \qquad (32)$$

We find that the nmr spectrum is determined by the Knight Shift K and the coupling constant J as in the case of an isotropic liquid. (In a liquid the Knight Shift is replaced by the scalar chemical shift.) We shall attempt to analyse the data using a Hamiltonian of this form in chapter 4.

Andrew, Carolan and Randall (1971a, 1971b) have undertaken the only other study of this kind. Their measurements were made on Cu^{63} and Cu^{65} in metallic copper and the value of the J coupling was obtained by measuring the second moment of the resonance absorption. However, as will be seen in Chapter 4, we have used an entirely different approach in obtaining the value of the J coupling.

B) Experimentation

To obtain a spectrum determined by the 'liquid-like' Hamiltonian, it is necessary to rotate the sample relative to the external field. This may be achieved by rotating either the sample or the field. The field may be rotated electrically much faster than the sample can be mechanically spun. Bradbury, Eades and McCarten (1968) report generating a 270 gauss field rotating at 27kHz. However, the problem here is to create a field that is large enough to be useful. Overcoming this problem, by spinning the sample, limits the speeds to about 10kHz. The sample is normally held in some type of container which is suspended upon a set of air bearings. This means that if the sample is slightly unbalanced, it can choose its own axis of rotation and spin freely.

If the sample was mounted on a rigid shaft as is shown in figure (2.3a) then a slight imbalance would, at high speeds, create such large forces that the mechanical bearings supporting the shaft would quickly fail. Instead of making use of air bearings, it is possible to rotate a sample that is suspended on magnetic bearings (Beams, 1964). However, this type of suspension is not suitable because, even if the sample was sufficiently magnetic to be supported, the need to use a magnetic field gradient is in conflict with the homogeneous field required in nmr; the axis of rotation is normally in such a direction that

Figure (2.3)

(a) Schematic of stiff-shaft turbine.

(b) Simplified version of air turbine.

The thrust gases are issuing at a velocity v.

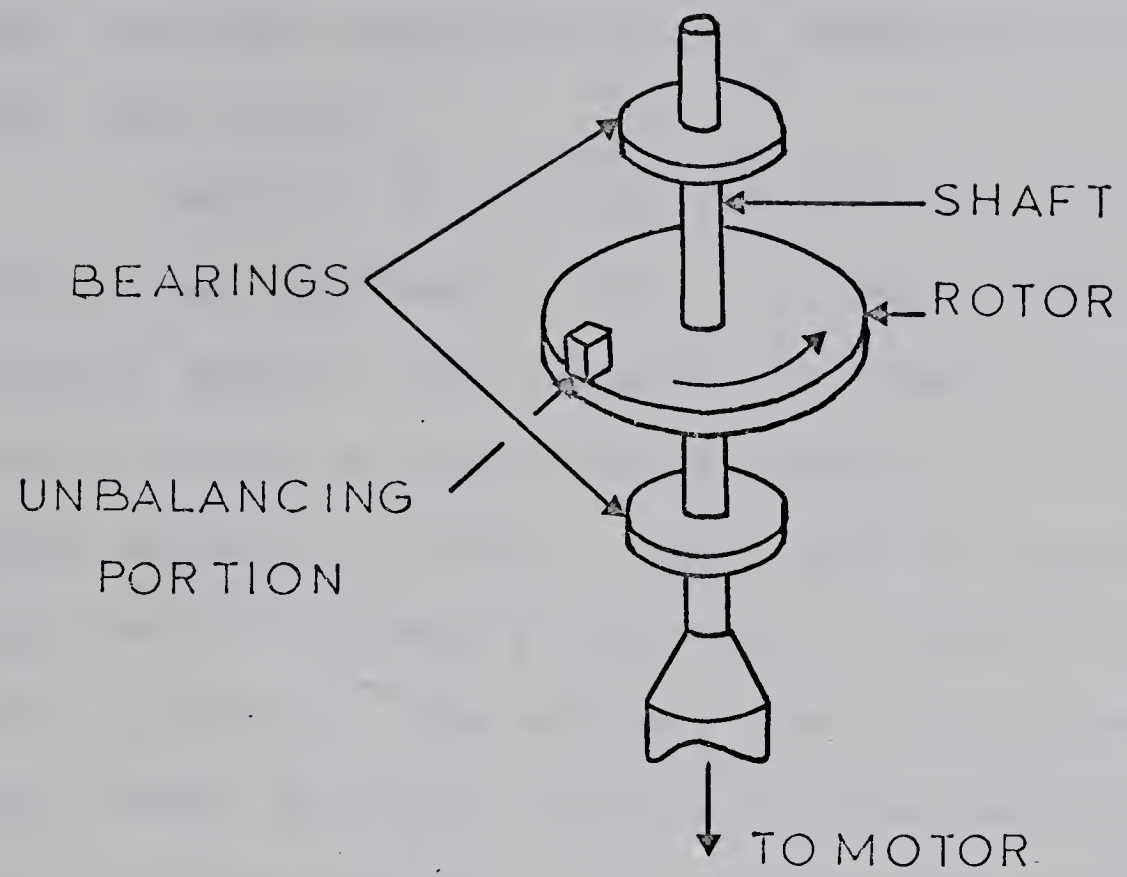
SHAFT
BEARINGS
ROTOR
UNBALANCING
PORTION
TO MOTOR

(a)

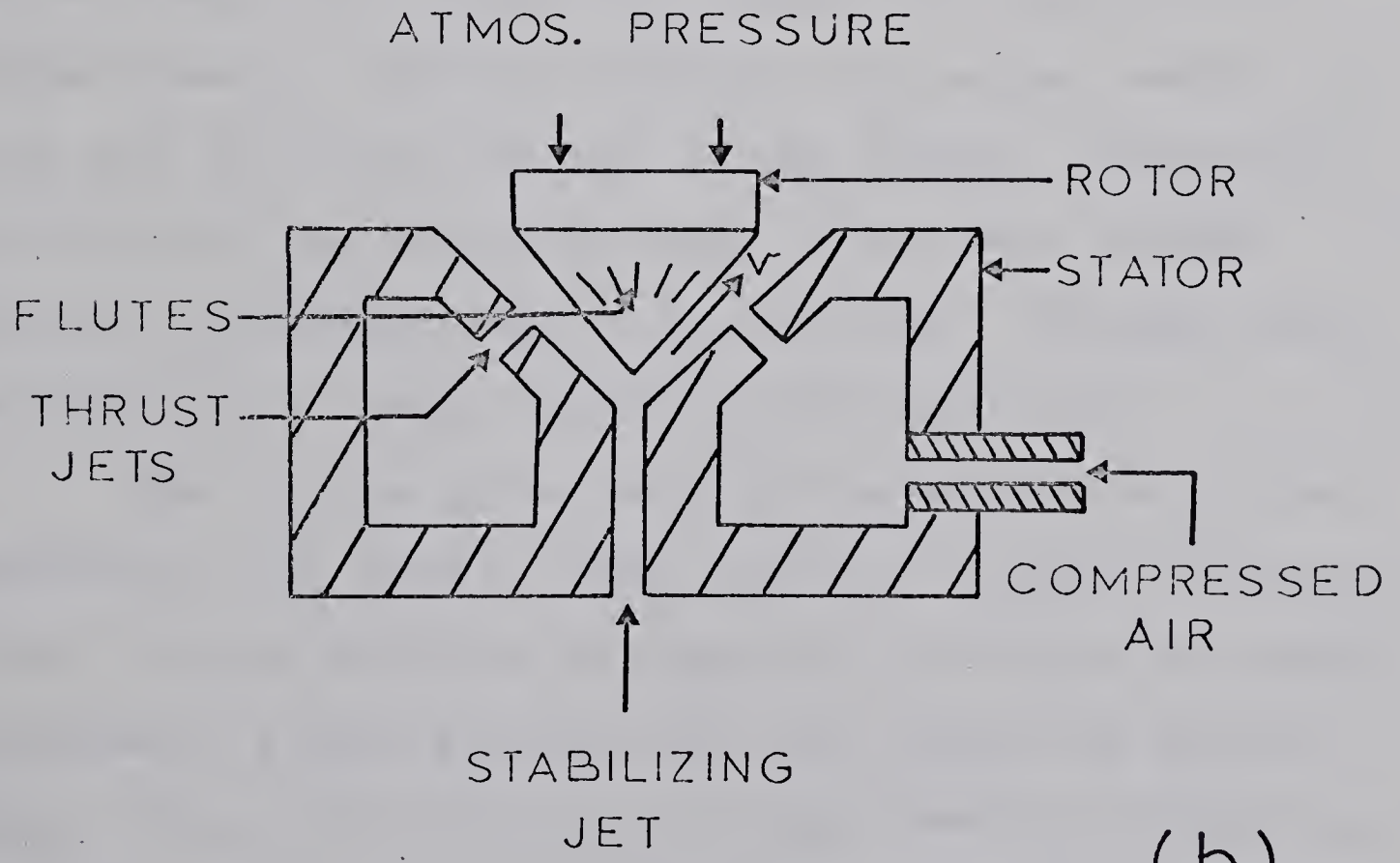
ATMOS. PRESSURE
ROTOR
STATOR
FLUTES
THRUST
JETS
COMPRESSED
AIR
STABILIZING
JET

(b)

the field gradients would not be averaged out. Furthermore, this fact also implies that the rotation would not be at the 'magic angle'.

Details of an early air turbine were given by Henriot and Huguenard (1925). A simple adaptation of their turbine (Beams, 1937) is shown in figure (2.3b). The turbine or rotor is supported by a series of air jets in the lower support or stator. These jets are angled away from the vertical in such a manner as to provide both support and propulsion. The turbine, when spinning steadily, is very stable and will actually operate upside-down. However, when it starts it does not normally spin centrally on the stator but instead tends to bounce around. This motion must be damped out before the turbine will achieve its highest speeds. The most efficient and easiest method of doing this is to use the tips of the fingers. Mechanical self-starting was tried, but when it was used needed constant readjustment due to turbine wear. (Fingers have the advantage of being naturally self-repairing.)

The turbine system used in the measurements is an adaptation of that used by Beams (1937) to support a rotating mirror. It was modified to allow its use inside the Varian crossed-coil probes provided with the Varian nmr spectrometer. It was felt that as the sample need not rotate in the vertical position, it would be preferable to orient it at 54°44' to a horizontal magnetic field rather than risk

straining the magnet yoke in orientating the field at the magic angle to a vertically spinning sample (contrast Andrew, 1970). The fact that the sample spins stably can be explained in terms of Bernoulli's principle. Referring to the simplified version of the air turbine and bearing shown in figure (2.3b) we see that

$$P_{\text{lower surface}} + \rho v^2/2 = P_{\text{atmos}} \qquad (20)$$

and therefore the atmospheric pressure prevents the turbine from being ejected from the stator by the propelling gas. If we now suppose that the turbine shifts away from the centre of the stator, then there is a decrease in the velocity of air flowing through the gap between the turbine and stator. The resulting pressure increase recentralizes the rotor.

Details of the construction of the rotor are shown in figure (2.4). The turbine (figure (2.4a)) is constructed from nylon. Great care and precision is needed to insure that the flutes are all milled equally deep, uniformly wide and correctly placed on the surface of the rotor relative to the air holes in the stator. (Despite this careful construction, there was often a failure rate of one in two.) The hollow in the centre of the turbine is used to contain the sample. It is necessary to construct the stator in two parts. The upper piece (figure (2.4c)) contains the jets to spin the turbine.

Figure (2.4)

Construction of the turbine used in the macroscopic rotation of the nmr sample.

(a) Diagram of the turbine.

(b) Diagram of the lower part of the stator.

(c) Diagram of the upper part of the stator showing position of air jets.

(d) Diagram showing the total turbine assembly as used experimentally.

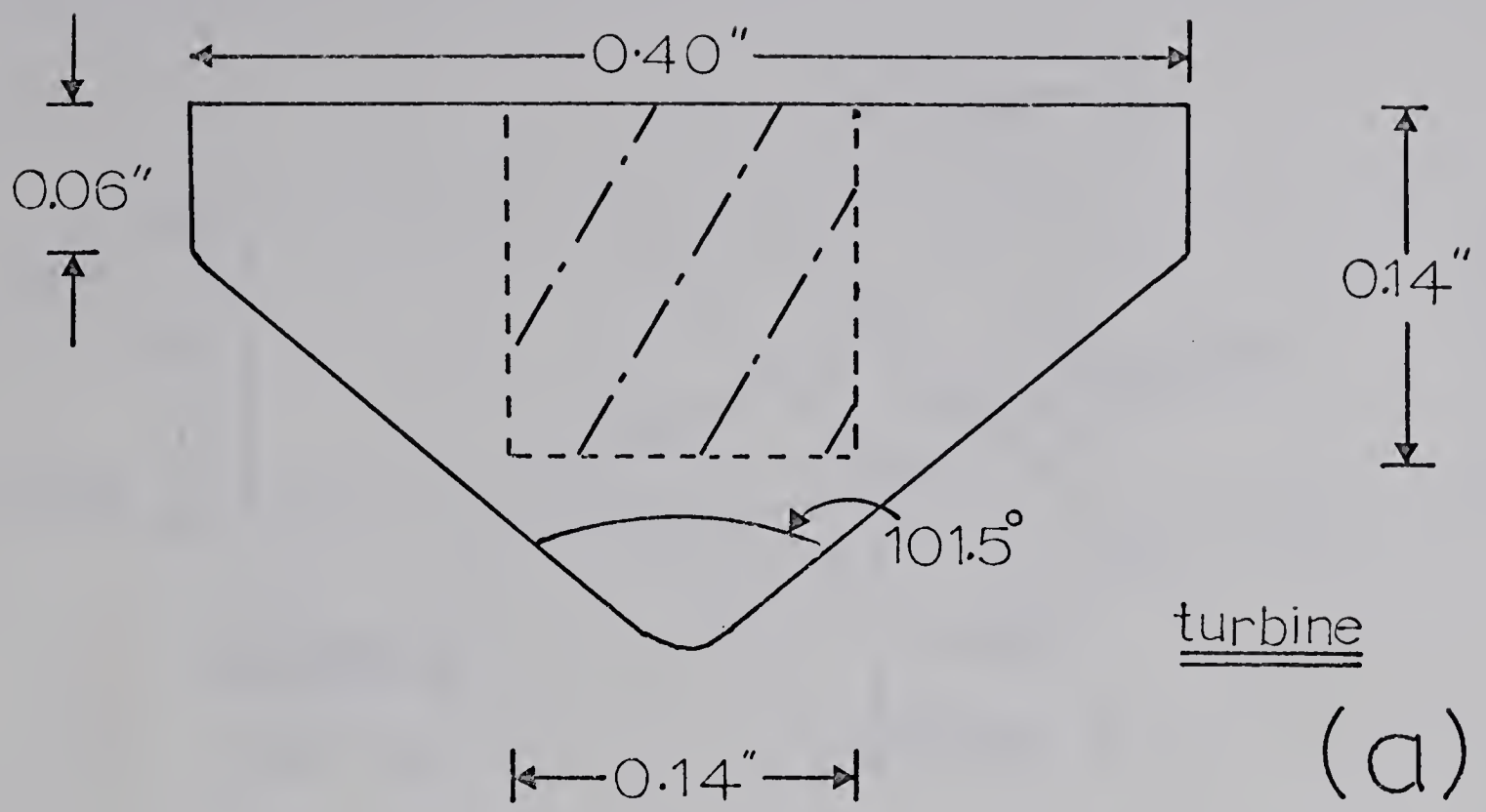

turbine

(a)

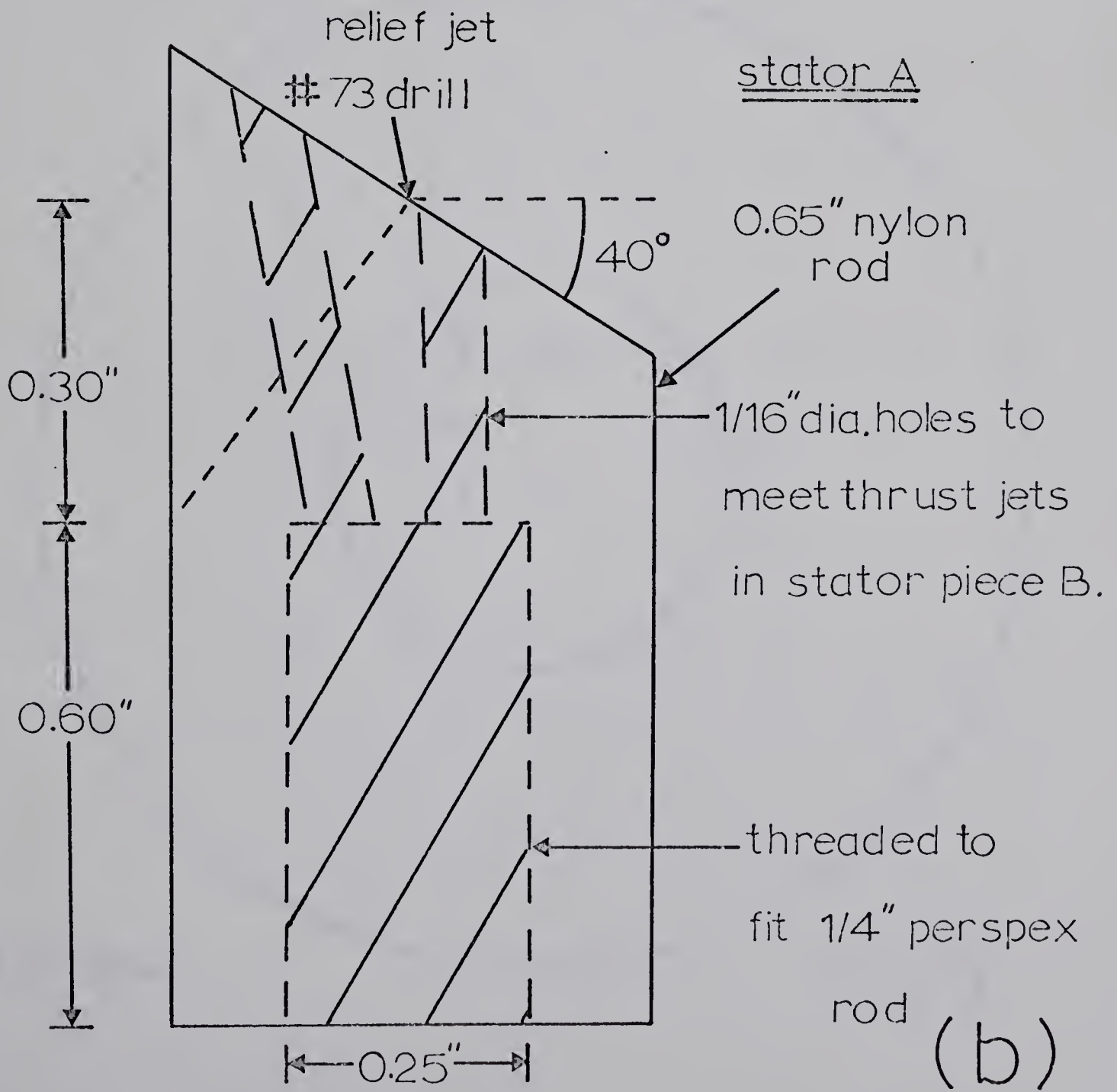

stator A

0.65" nylon rod

1/16" dia. holes to meet thrust jets in stator piece B.

threaded to fit 1/4" perspex rod

(b)

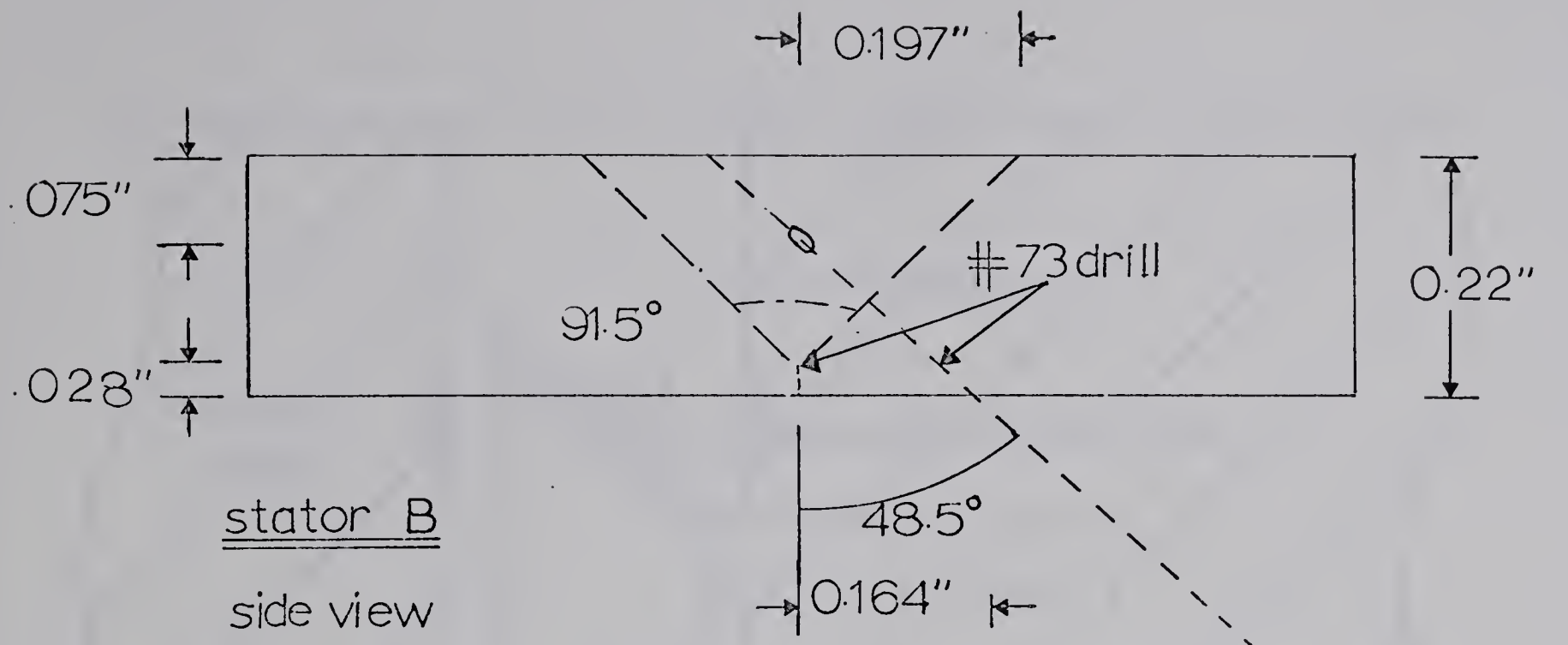

stator B

side view

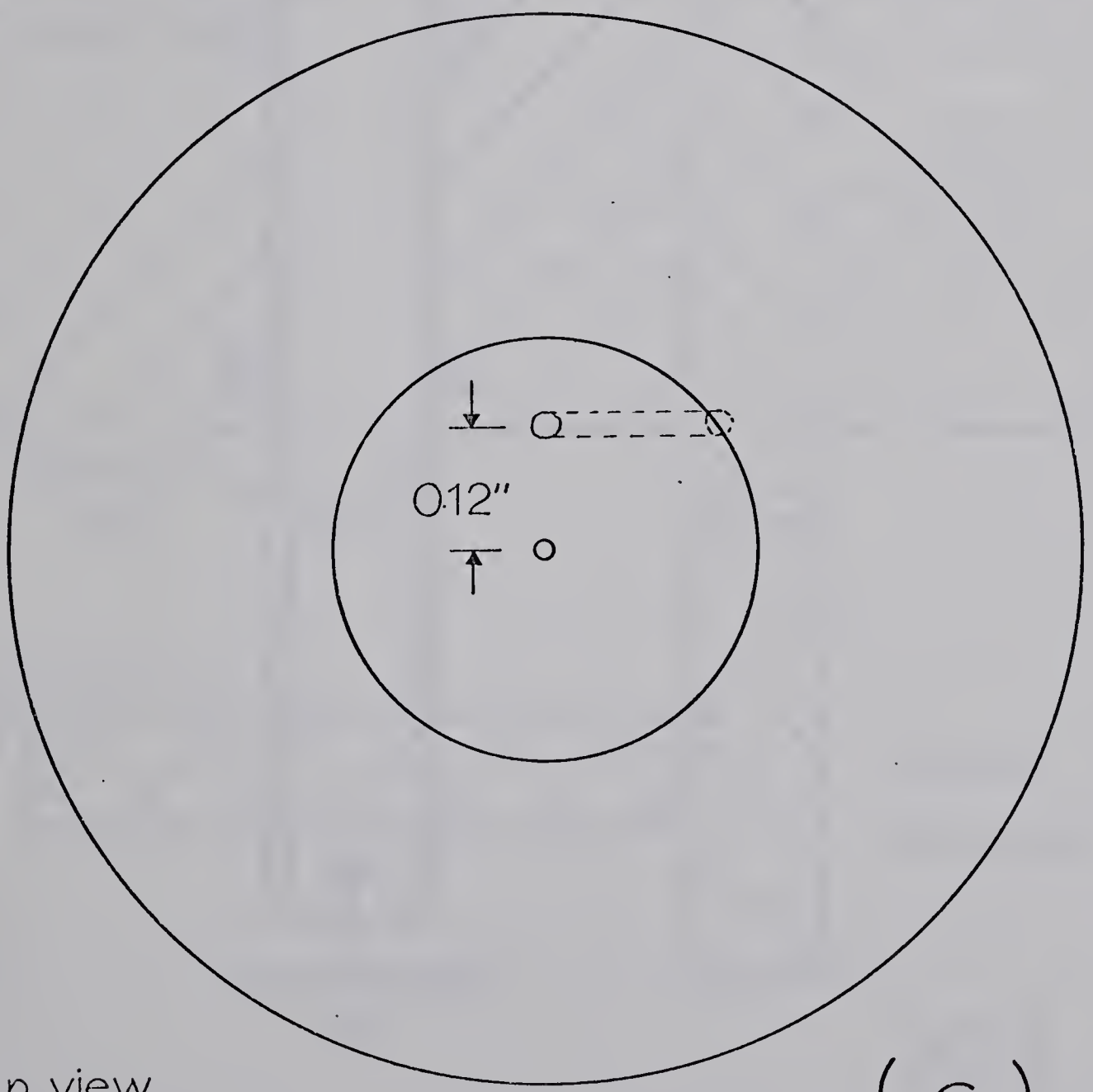

top view

(C)

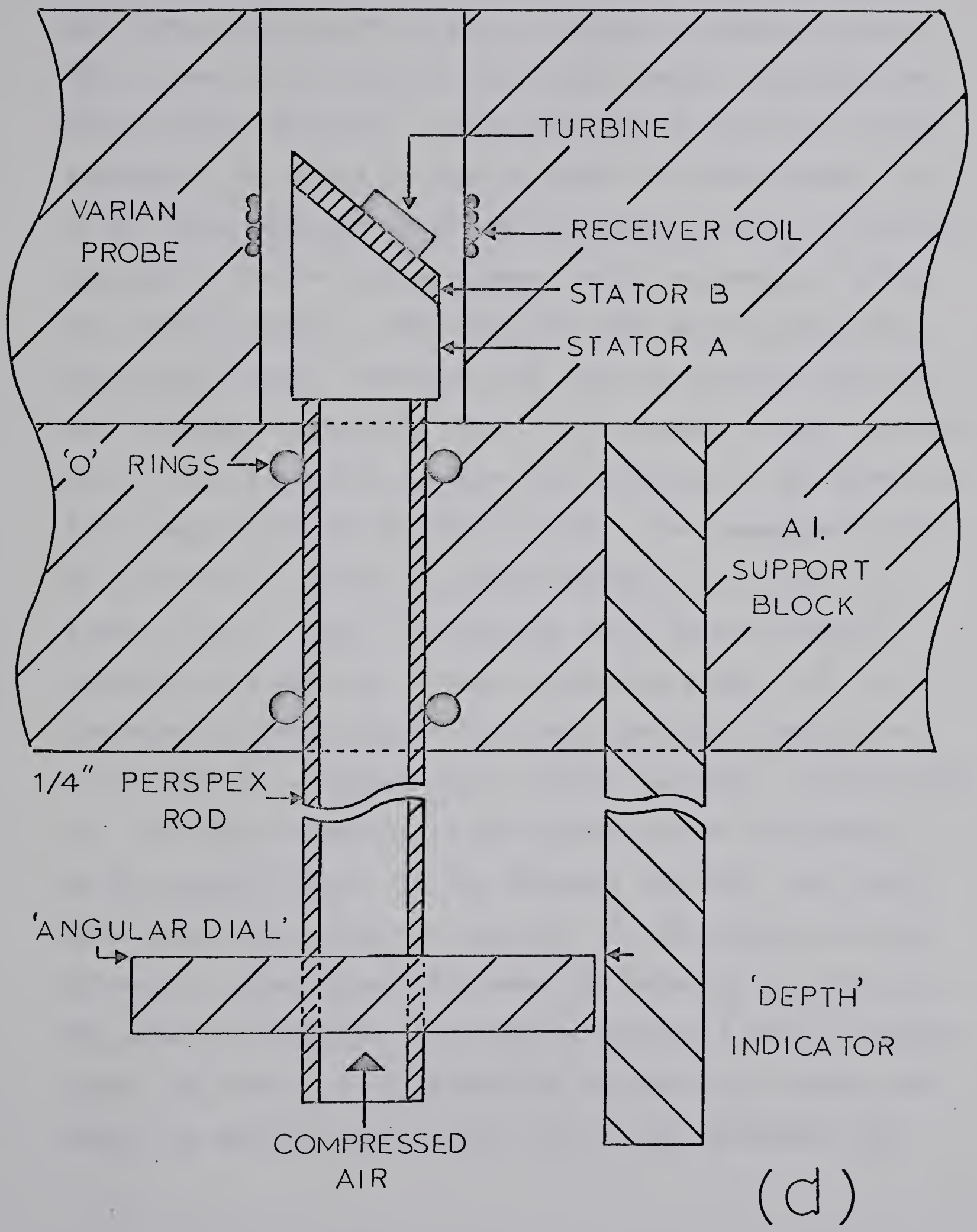
TURBINE
VARIAN PROBE
RECEIVER COIL
STATOR B
STATOR A
'O' RINGS
A.I. SUPPORT BLOCK
1/4" PERSPEX ROD
'ANGULAR DIAL'
'DEPTH' INDICATOR
COMPRESSED AIR

(d)

The piece shown in figure (2.4c) is set on top of the lower stator part (figure 2.4b)) at an angle of about 50° to the central axis of the lower piece. Rotating the whole stator, therefore, allows the axis of rotation of the turbine to be turned so that it makes an angle between 50° to 90° to a magnetic field applied perpendicular to the stator axis. The two stator pieces, which are made of nylon, are fused together, after cleaning with trichloroethylene, with formic acid. Provided that the two surfaces have not been machined 'optically flat', this creates a very effective seal. After fusing, the pieces are machined to fit down the 3/4" sample-hole of the Varian probe. The assembled stator is mounted on a piece of perspex tubing as is shown in figure (2.4d). This is necessary as it is not normally possible to start the turbine inside the probe. It is therefore started outside the probe and then brought down level with the receiver coils inside the probe. Unfortunately, this type of motion is one against which the turbine is the least stable. If the movement is jerky, the rotor will touch the stator and fly out. As the turbine circumference is often travelling near the velocity of sound in the propelling medium, the turbine travels a great distance along the floor. It is therefore advisable to enclose the magnet to prevent loss of the rotor. The enclosure can

also provide increased thermal stability for the magnet. Of the turbines that spin, only 50% will do so inside the probe. This is apparently due to the unbalancing effect of the air stream from the stator being reflected back onto the turbine from the probe walls.

The maximum theoretical rotation rate for the turbine occurs when its circumference is travelling at the velocity of sound in the propelling medium. Normally this maximum is not reached as a number of speed-limiting factors are present. Imbalance will cause the rotor to spin unstably or 'jump'. Frictional forces acting on the sides of the rotor will counterbalance the thrust provided by the jets. The stator support may vibrate causing the turbine and stator to touch. In addition, when the propulsion pressure is high, it is likely that there will be a certain amount of turbulence in the pipes supplying air to the turbine, which is capable of upsetting the turbine. It should therefore be expected that Helium gas would generate higher speeds than Nitrogen or Air. This was found to be the case experimentally. Figure (2.5) shows the variation of rotation speeds measured as a function of thrusting pressure for both Helium and Nitrogen. Hydrogen is even more effective but because of the danger involved, it is not normally used. (Sparks may be generated when the stator and turbine touch.)

The actual rotation rates are easy to measure.

Figure (2.5)

Variation of rotational rate as a function of thrust when Helium and Nitrogen are used as propelling gases.

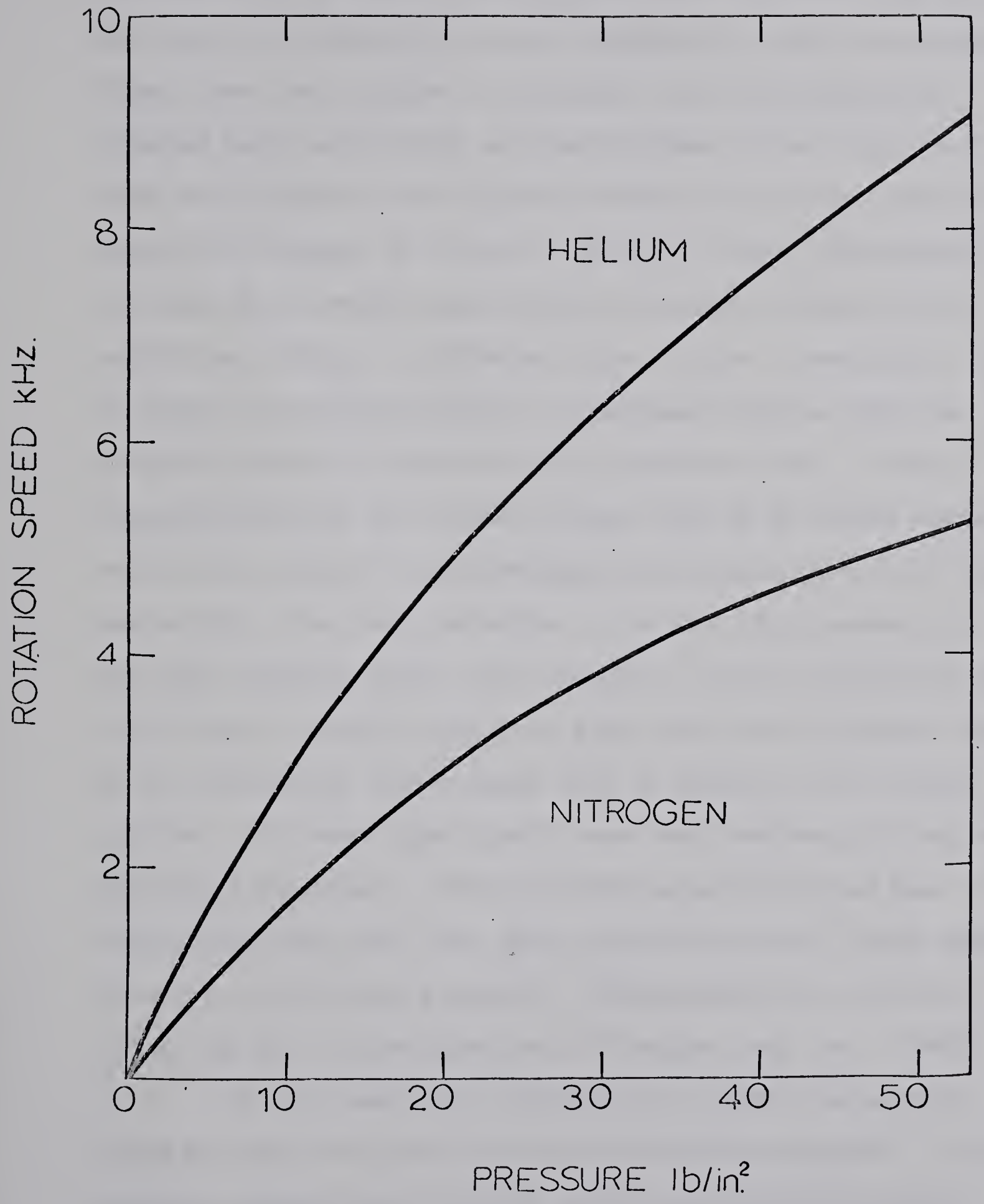
ROTATION SPEED kHz.
10
8
6
4
2
0
10
20
30
40
50
HELIUM
NITROGEN
PRESSURE lb/in.²

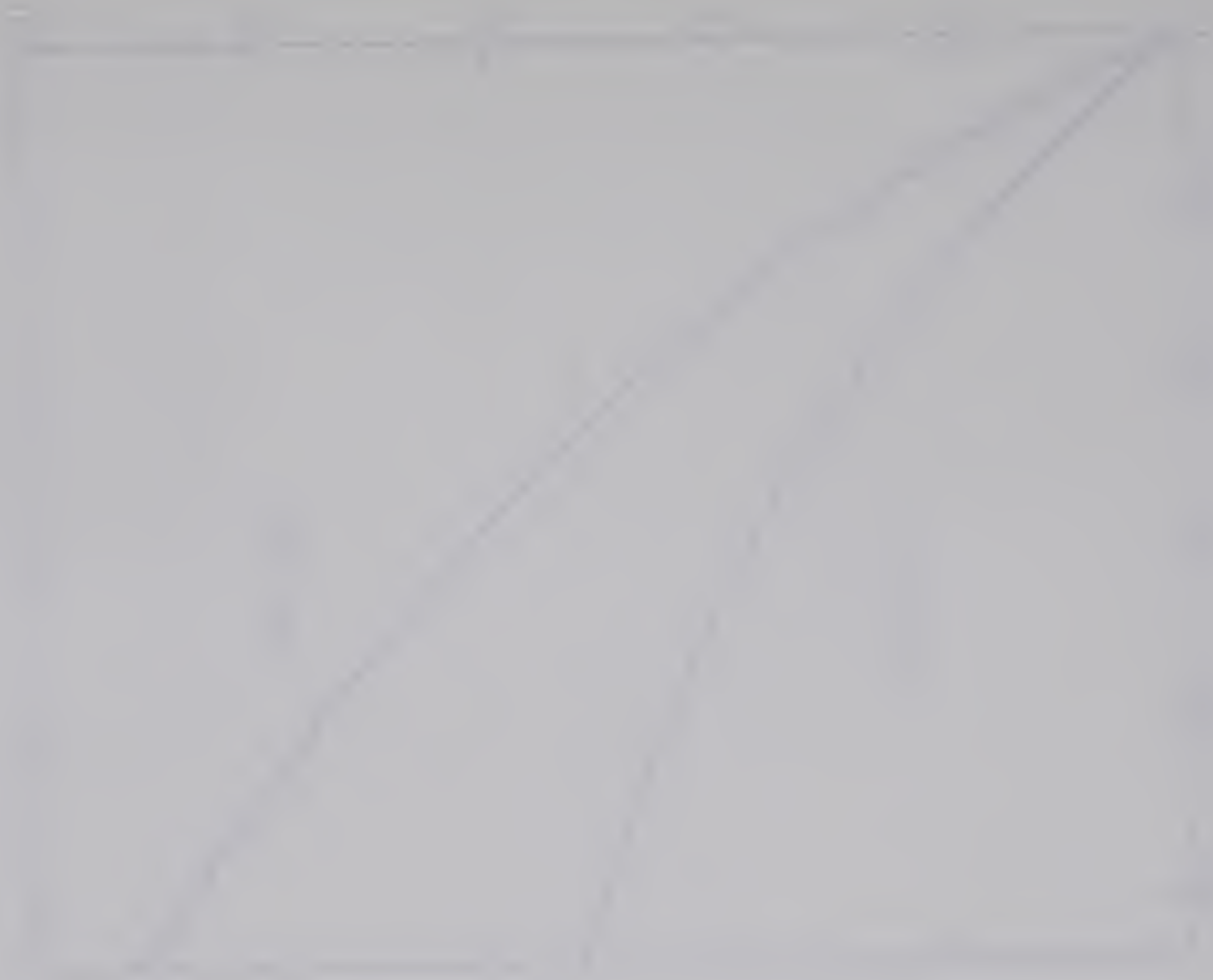

At low speeds, it is possible to use a stroboscope to 'stop' the motion. At speeds much greater than 100,000 rpm it is not easy to determine at what harmonic of the stroboscope flash rate the turbine is turning. If the turbine is painted half matt-black and half silver, then light reflected from the turbine onto a photo-transistor creates sufficient signal to trigger a counter. However, when the turbine is sitting at an angle deep inside the probe, there is insufficient light reflected back to the transistor. On hearing the turbine rotate, it becomes obvious what is another method of measuring the rotation rate. Small imperfections on the rotor surface set up an audio signal with tones equal to the fundamental rotation rate and its harmonics. (We have detected up to the 12th harmonic.) At high rotation rates the harmonics are not perceived and it is then a simple manner to beat the signal against that of an oscillator which feeds both a counter and a loudspeaker. At very high speeds even the fundamental may be difficult to detect. The greatest speed obtained was 12kHz (720,000 rpm), but this was with a solid rotor rather than one containing a sample. That particular turbine 'blew' up at a later time when 'turning over' at 7.2kHz.

If the sample is nonmetallic, it may be packed tightly into the centre of the turbine and capped. At low speeds, plastic wood is very useful but at high speeds the edges of the turbine begin to creep, allowing the cap

to shift. This either unbalances the turbine and/or scatters the sample. A better method is to mix the sample with an epoxy which is then allowed to set in the turbine. A good room-temperature-setting epoxy is STYCAST 2850FT manufactured by Emerson and Cuming, Inc., Canton, Mass., U.S.A. When used in conjunction with catalyst 24, it is very liquid with a pot life of about 45 mins. The fact that the epoxy flows freely means that a large amount of sample may be mixed in before the epoxy is too stiff to pour. To prevent the formation of air bubbles, which would unbalance the turbine, it is placed, after filling, in a bell jar, which is then evacuated. This improves the number of turbines that rotate after filling to 50% from the 10% that would spin before the evacuation technique was used. This number could be even further increased if less sample was mixed in with the epoxy. The decrease in sample volume is, however, undesirable, as it decreases the filling factor and hence the signal-to-noise ratio. If an enriched sample was to be mixed in with the epoxy, it would be advisable to leave the epoxy very liquid to avoid wasting the sample. Using epoxy rather than plastic wood offers a large number of advantages. The epoxy has very good mechanical strength. Even if the turbine breaks up, the epoxy will hold together, preventing the sample from contaminating the probe. When a metal powder sample is used, the high resistance of the epoxy efficiently isolates the

particles from each other, alleviating any problem of skin depth. The epoxy is distributed evenly throughout the turbine rather than sitting on top as a cap would. This, together with the fact that the epoxy binds onto the edges of the nylon preventing them from spreading, leads to a greater mechanical stability at high speeds.

The problem of a poor filling-factor, when using a sample-epoxy mix, could be avoided if it were possible to machine the whole turbine from the mix. This was tried, but it was found that the epoxy, especially when metal particles were added, was so abrasive that it was impossible to machine the turbines to any accuracy. To overcome the signal-to-noise problem, it was necessary to employ signal averaging.

The actual experimental set-up is shown as a block diagram in figure (2.6). The turbine is driven with air supplied by a compressor with an operating output pressure fluctuating between 90 and 110 lbs/sq in. By the use of a series of regulators and storage tanks, the air flow to the turbine could be regulated. Over a day the rotation rate was stable to around 1 part in 10^4. To gain the stability needed for long-term signal-averaging, the frequency of the Varian spectrometer, operating at 6MHz, is phase-locked to a 1MHz frequency standard and is stable to 1 part in 10^7. The magnet field is controlled by the Varian Mark II Fieldial via a Hall probe sensing element. We have attached a blackened disk with small silver markings

Figure (2.6)

Block diagram of experimental arrangement used when nmr samples are being macroscopically rotated.

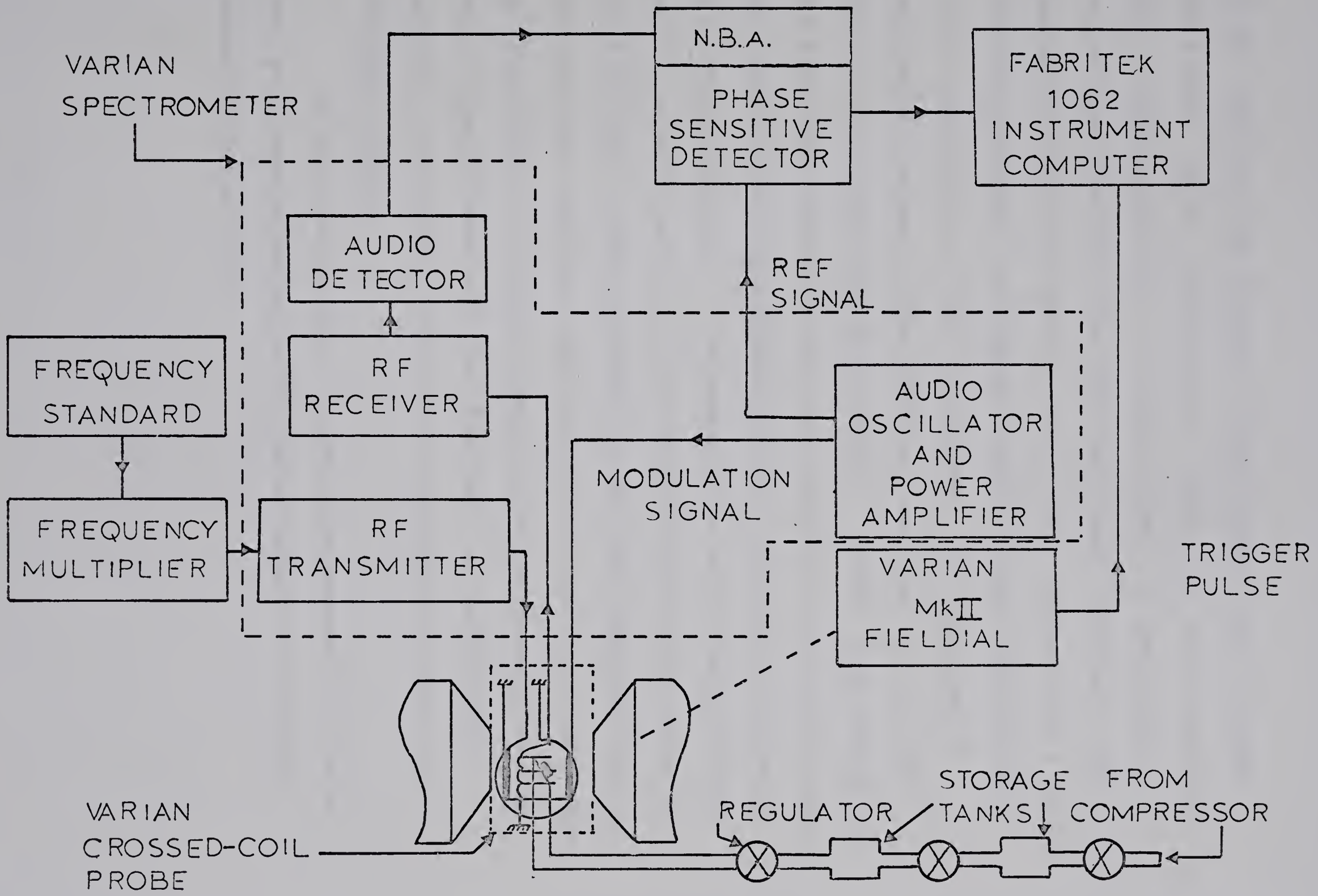
VARIAN
SPECTROMETER
N.B.A.
PHASE
SENSITIVE
DETECTOR
FABRITEK
1062
INSTRUMENT
COMPUTER
AUDIO
DETECTOR
REF
SIGNAL
FREQUENCY
STANDARD
RF
RECEIVER
AUDIO
OSCILLATOR
AND
POWER
AMPLIFIER
MODULATION
SIGNAL
FREQUENCY
MULTIPLIER
RF
TRANSMITTER
VARIAN
MkII
FIELDIAL
TRIGGER
PULSE
STORAGE
TANKS
FROM
COMPRESSOR
REGULATOR
VARIAN
CROSSED-COIL
PROBE

to the shaft of the Fieldial potentiometer used to sweep the field. By the reflection of light from these markings onto a phototransistor, a trigger signal is generated for controlling the Fabri-Tek 1062 instrument computer. The generated signal was squared up to give a pulse with a good rise-time so that the computer would trigger consistently at the same point in the field sweep. The microswitch provided by Varian in the Fieldial was found to be insufficiently accurate for this purpose. Pulses from points on the disk other than the starting position could be fed into the computer and superimposed on the resonances to provide calibration markings. The sweep rates of the magnet field were altered to match up with the available sweep times on the Fabri-Tek. This provides for the most efficient use of the computer; its 'dead time' relative to the field sweep time is less than 6%. The nmr signal is audio-detected in the Varian spectrometer and then fed into a narrow-band amplifier and lockin detector of the type described by Schuster (1951).

In the case of tin, it was often necessary to make 2048 runs over a period of 48 hrs to achieve an adequate signal-to-noise ratio.

CHAPTER 3. THEORY OF THE ELECTRON-COUPLED NUCLEAR-NUCLEAR INTERACTION

In a study made on thallium oxide, Bloembergen and Rowland (1953) found that the linewidth of one of the thallium isotopes was much greater than that of the other. The extra width of Tl^{203} compared to Tl^{205} was surprising as their magnetic moments only differ by 1%, so that it could be expected that both isotopes would interact with their surroundings to the same extent. The only manner in which the isotopes differ greatly is in their natural abundances. The Tl^{203} is 30% abundant compared to 70% for the Tl^{205}, so that a Tl^{203} nucleus will on average have a larger number of unlike neighbours compared to a Tl^{205} nucleus. The experimental data may be explained if there is an exchange interaction. Exchange interactions between unlike nuclei broaden the resonance line whilst those between like neighbours narrow it (Van Vleck, 1948). Hahn and Maxwell (1952) and independently Gutowsky, McCall and Slichter (1953) have shown that there exists a coupling between the magnetic moments of two nuclei in a molecule, via their hyperfine interaction with the surrounding electrons. Ruderman and Kittel (1954) showed that a similar coupling could arise in a metal with the nuclear spins interacting with the conduction electrons. The existence of such a coupling can best be explained in terms of a

simple model.

We take as a model a metallic crystal in which only two of the nuclei are magnetic. The electron wave function in the periodic lattice will be scattered by the interaction with each magnetic nucleus. The effect of the magnetic moment of a nucleus at any lattice site is to make that site favourable for an electron of parallel magnetic moment but unfavourable for an electron with anti-parallel moment. In order to take advantage of the magnetic interaction, an electron of parallel spin will distort its wave function so that the wave function is slightly larger in the vicinity of the nucleus. The distortion is brought about by mixing in other states of the same spin orientation. The wavefunctions of the additional Bloch states are added in phase with the unperturbed function at the nucleus in order to interfere constructively at that point, but because of the spread in wavelengths, they quickly get out of step as one moves away from the nucleus. As a result of the difference between the unperturbed and perturbed functions, the original uniform distribution of spin density is changed to have a damped oscillatory behaviour. The total electron wavefunction seen by one magnetic nucleus will therefore depend upon the spin orientation of the other, thus establishing an indirect spin-dependent coupling between the nuclei.

The strength of the coupling in the general case may be calculated from the total electron-nuclear Hamiltonian.

This interaction between the nuclei and the electrons ℓ is written as

$$H_{en} = \sum_i c_i \underline{I}_i \cdot \sum_\ell \underline{S}_\ell \, \delta(\underline{r}_\ell - \underline{R}_i) + \sum_i D_i \underline{I}_i \cdot \sum_\ell \underline{\underline{A}}_{\ell i} \cdot \underline{S}_\ell \,, \tag{1}$$

where

$$c_i = 8\pi\gamma_e\gamma_i \hbar^2/3, \tag{2}$$

$$D_i = \gamma_e\gamma_i \hbar^2 \,, \tag{3}$$

and

$$\underline{\underline{A}}_{\ell i} = \sum_\ell \frac{1}{|\underline{r}_\ell - \underline{R}_i|^3} - \frac{(\underline{r}_\ell - \underline{R}_i)(\underline{r}_\ell - \underline{R}_i)}{|\underline{r}_\ell - \underline{R}_i|^5} \,. \tag{4}$$

The first term in equation (1) is the 'contact' interaction between the electrons and nuclei, whilst the second term gives the dipolar interaction. Equation (1) may be rewritten in the form

$$H_{en} = \sum_i \underline{I}_i \cdot \underline{G}_i = \sum_i H_i \tag{5}$$

where $\underline{G}_i$ does not involve the nuclear spin coordinates. The interaction energy associated with H_{en} is given, to second order, by

$$\Delta E = \langle 0|H_{en}|0\rangle + \sum_n{}' \, |\langle n|H_{en}|0\rangle|^2 (E_n - E_o)^{-1} \,. \tag{6}$$

The terms in ΔE such as $\langle 0 | H_i | 0 \rangle$ and $|\langle n|H_i|0\rangle|^2 (E_n - E_o)^{-1}$ are just those that would

arise if each nucleus was isolated from the other nuclei. This energy is associated with parts of the electron-nucleus interaction which give rise to the Knight Shift and the relaxation processes in metals. The cross terms, i.e. those involving two nuclei e.g. $\langle 0|H_i|n\rangle \langle n|H_j|0\rangle (E_n-E_o)^{-1}$, represent the interaction energy associated with the electron-coupled nuclear-nuclear interaction. These may be expressed as

$$\Delta E_{0\alpha} = \sum_{i>j} \sum_{n\alpha'} \frac{(0\alpha|H_i|n\alpha')(n\alpha'|H_j|0\alpha)}{E_0+E_\alpha-E_n-E_{\alpha'}} + \text{c.c.}, \qquad (7)$$

where $|n\alpha')$ is a product of a many-electron state $|n)$ with energy E_n and the many-nucleus state $|\alpha')$ with energy $E_{\alpha'}$, $|0\alpha)$ being the ground state. Substituting equation (5) into equation (7) we obtain

$$\Delta E_{0\alpha} = \sum_{i>j} \sum_{n} \sum_{\beta\beta'} (0|G_{i\beta}|n)(n|G_{i\beta'}|0)(E_o-E_n)^{-1}$$

$$\times (\alpha|I_{i\beta}I_{j\beta'}|\alpha) + \text{c.c.} \qquad (8)$$

where the nuclear energies have been ignored in comparison with the electron energies. This energy $\Delta E_{0\alpha}$ is just that which would be expected from a first-order perturbation contribution of an extra term in the nuclear Hamiltonian H_{eff} given by

$$H_{eff} = \sum_{i>j} \sum_{\beta\beta'} I_{i\beta} I_{j\beta'} \sum_{n} \frac{(0|G_{i\beta}|n)(n|G_{j\beta'}|0)}{E_o - E_n} + c.c.$$

$$= \sum_{i>j} \underline{I}_i \cdot \underline{\underline{J}}_{ij} \cdot \underline{I}_j \qquad (a)$$

where $\underline{\underline{J}}_{ij}$ is the spin coupling tensor between the i and j nuclei. Taking the electron wave functions to be products of Bloch functions, it is possible to calculate the $\underline{\underline{J}}_{ij}$ (Abragam, 1961; Slichter, 1963).

The most important term arises from the cross terms involving the contact interaction between the nuclei and the electrons. This is given by

$$H_{contact\text{-}contact} = \sum_{i>j} c_i c_j \sum_{n} \underline{I}_i \cdot (0|\sum_{\ell} \underline{S}_\ell \, \delta(\underline{r}_\ell - \underline{R}_i)|n)$$

$$\times (n|\sum_{\ell} \underline{S}_\ell \delta(\underline{r}_\ell - \underline{R}_j)|0) \cdot \underline{I}_j (E_o - E_n)^{-1} + c.c.$$

$$= \sum_{i>j} \underline{I}_i \cdot \underline{I}_j . J_{ij} \, h \qquad (10)$$

where

$$(c_i c_j)^{-1} J_{ij} h = \sum_{\underline{k}\underline{k}'} |U_{\underline{k}'}(0)|^2 |U_{\underline{k}}(0)|^2 \cos\{(\underline{k}-\underline{k}') . (\underline{R}_j - \underline{R}_i)\}$$

$$\times f(\underline{k})(1 - f(\underline{k}'))(E_{\underline{k}} - E_{\underline{k}'})^{-1} . \qquad (11)$$

$U_{\underline{k}}(0)$ is the value of the spatial part of the electron wave function at the nucleus and $f(\underline{k})$ is the Fermi probability function. It can be seen from the form of $H_{contact\text{-}contact}$ that it has the appearance of an exchange interaction.

Hence its name of 'pseudo-exchange' coupling.

It is not possible to evaluate the summation without either some further approximations or some explicit information on the $\underline{k}$ dependence of the wave functions and energy. We assume that the energy surfaces are spherical and there is an effective mass $m^*(k)$. As the greatest contribution to J_{ij} comes when $k \simeq k' \simeq k_f$, $|U_{\underline{k}}(0)|^2$ and $|U_{\underline{k}'}(0)|^2$ may be replaced by a value appropriate to $\underline{k}$ and $\underline{k}'$ near the Fermi surface and the sums may then be evaluated (Slichter, 1963). This leads to a value of the scalar coupling constant J_{ij} given by

$$h J_{ij} = - \frac{32}{9\pi} \gamma_e^2 \gamma_i \gamma_j \hbar^2 m^* |U_{k_f}(0)|^4 k_f^4 F(2k_f|\underline{R}_{ij}|) \qquad (12)$$

where

$$F(x) = \frac{\sin x - x \cos x}{x^4} \quad . \qquad (13)$$

This is the Ruderman-Kittel approximation (Ruderman and Kittel, 1954). The oscillatory part $F(x)$ is plotted in figure (3.1). The dependence on $|U_{k_f}(0)|^4$ shows that the coupling will be greatest for a nucleus with a large Z.

The second term from H_{eff} arises from the cross-terms between the contact and dipolar interactions. This is given by

$$H_{\text{contact-dipolar}} = \sum_{i>j} (B_{ij} + B_{ji}) + \text{cc}$$

Figure (3.1)

The spatial dependence of the Ruderman-Kittel 'pseudo-exchange' interaction F(x). The figure also shows the distances of the neighbouring nuclei in white tin. $(x_o)_{Sn}$ indicates the value of x taken for the start of the continuum, as discussed in chapter 4.

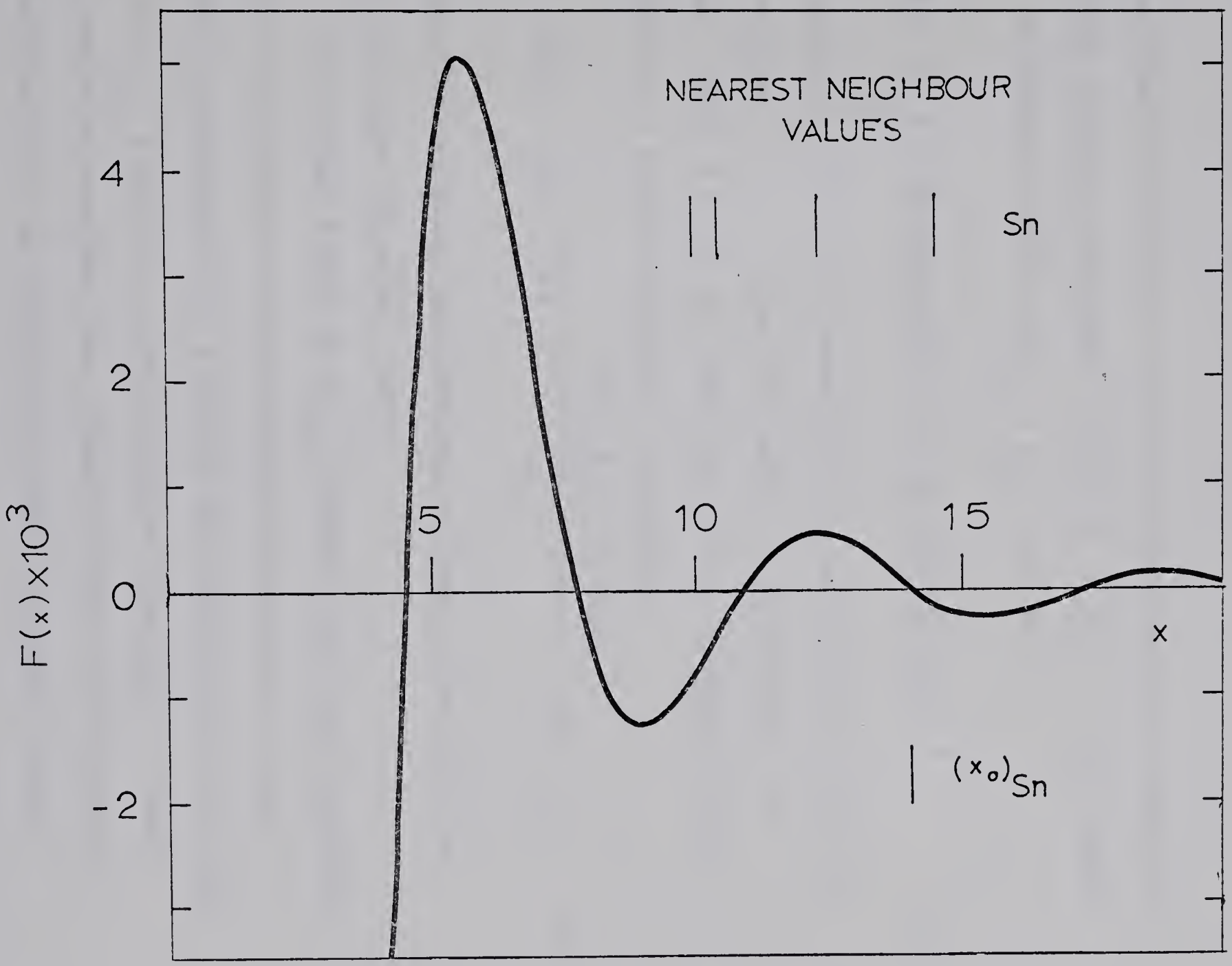
NEAREST NEIGHBOUR
VALUES
Sn
4
2
0
-2
5
10
15
x
$F(x) \times 10^3$
$(x_o)_{Sn}$

where

$$B_{ij} = c_i D_j \sum_n \sum_\ell (0|\delta(\underline{r}_\ell - \underline{R}_i)(\underline{S}_\ell \cdot \underline{I}_i)|n)$$

$$\times (n|\underline{S}_\ell \cdot \underline{\underline{A}}_{\ell j} \cdot \underline{I}_j|0)(E_n - E_o)^{-1} \qquad (14)$$

Summing over the electron spins as previously, we obtain a traceless coupling (Abragam, 1961) $\underline{I}_i \cdot \underline{\underline{J}}''_{ij} \cdot \underline{I}_j$ where $\underline{\underline{J}}''_{ij}$ is proportional to $\underline{\underline{P}}_{ij} + \underline{\underline{P}}_{ji}$ + cc with

$$\underline{\underline{P}}_{ij} = \sum_{\underline{k}\underline{k}'} (\underline{k}|\delta(\underline{r}_{\underline{k}} - \underline{R}_i)|\underline{k}')(\underline{k}'|\underline{\underline{A}}_{kj}|\underline{k})(E_{\underline{k}} - E_{\underline{k}'})^{-1} . \qquad (15)$$

This coupling will be removed by the macroscopic rotation (see chapter 2). In special cases, (Bloembergen and Rowland, 1955) it may be shown that this coupling takes the form of a pseudo-dipolar interaction

$$\underline{I}_i \cdot \underline{\underline{J}}''_{ij} \cdot \underline{I}'_j = D'_{ij} \left\{ \frac{3(\underline{I}_i \cdot \underline{R}_{ij})(\underline{I}_j \cdot \underline{R}_{ij})}{R_{ij}^2} - \underline{I}_i \cdot \underline{I}_j \right\} \qquad (16)$$

but there is no group theoretical argument that this is always the case (Abragam, 1961).

The final terms in $\Delta E_{0\alpha}$ involve the cross-products between the electron-nuclear dipole interaction terms. This may be expressed as a sum of two tensors, one with the form of $J'_{ij}\ \underline{\underline{1}}$ and the other with the form $\underline{\underline{J}}''_{ij}$. These terms are much smaller than those already considered and may be thought of as correction terms (Abragam, 1961).

CHAPTER 4. TIN

A) Theoretical analysis

Van Vleck (1948) showed that spin-spin coupling between nuclei, corresponding to a Hamiltonian of the form

$$H_{ss} = J\, h\, \underline{I_1} \cdot \underline{I_2} \quad ,$$

has two effects on the resonance line-shape. If the coupling is between unlike nuclei, the second moment is increased, implying that the line is broadened. When the nuclei are alike, however, the coupling produces an increase in the fourth moment but leaves the second moment unchanged. This means the line narrows but there is an intensity shift towards the wings. A number of studies have been made on tin spectra using the 'method of moments' (Karimov and Schegolev, 1961; McLachlan, 1968; Schone, 1969; Sharma et al., 1969; Alloul and Deltour, 1969). This approach is difficult. The experimental line shape is somewhat Lorentzian, implying that there is considerable intensity in the wings which makes accurate determination of moments difficult (Sharma et al., 1969). In addition, interpretation of the results is complicated by the necessity of unravelling the effects of the spin-spin scalar coupling from those of the spin-spin 'pseudo-dipolar' coupling.

A second approach which has been used to determine the scalar coupling is to apply the Anderson-Weiss theory

(Anderson and Weiss, 1953). This, being useful when the line is very exchange-narrowed, is only applicable to resonances from isotopically enriched tin. The experimental line width $\delta\omega$ is given in this theory by

$$\delta\omega = \pi\langle\Delta\omega^2\rangle/\sqrt{3}\ J \qquad (1)$$

where $\langle\Delta\omega^2\rangle$ is the theoretical second moment in the absence of exchange narrowing and J is an average value of the scalar coupling constants over the nearest neighbours (McLachlan, 1968; Sharma et al., 1969).

In this thesis an entirely different approach is used. An attempt is made to build up the tin spectrum from first principles. This is possible in natural tin because of the low isotopic abundance of the magnetically active nuclei (Sn^{117}, 7.67%; Sn^{119}, 8.68%) and the fact that the macroscopic rotation has given the Hamiltonian the same form as for a liquid. This allows the possibility of applying high resolution nmr spectroscopy techniques in a situation where they would not normally prove useful. The low isotopic abundance permits the splitting of the sample into groups of interacting nuclei; each group being effectively isolated from the next. The distances from a nucleus to its four shells of nearest neighbours are 3.016 Å, 3.175 Å, 3.760Å and 4.140Å (see figure (4.1)). From an examination of the form of the Ruderman-Kittel interaction (figure (3.1)) we see that after the third

Figure (4.1)

Diagram of the tin crystal structure. The numbers 1, 2 3 and 4 indicate the nearest neighbour relationships.

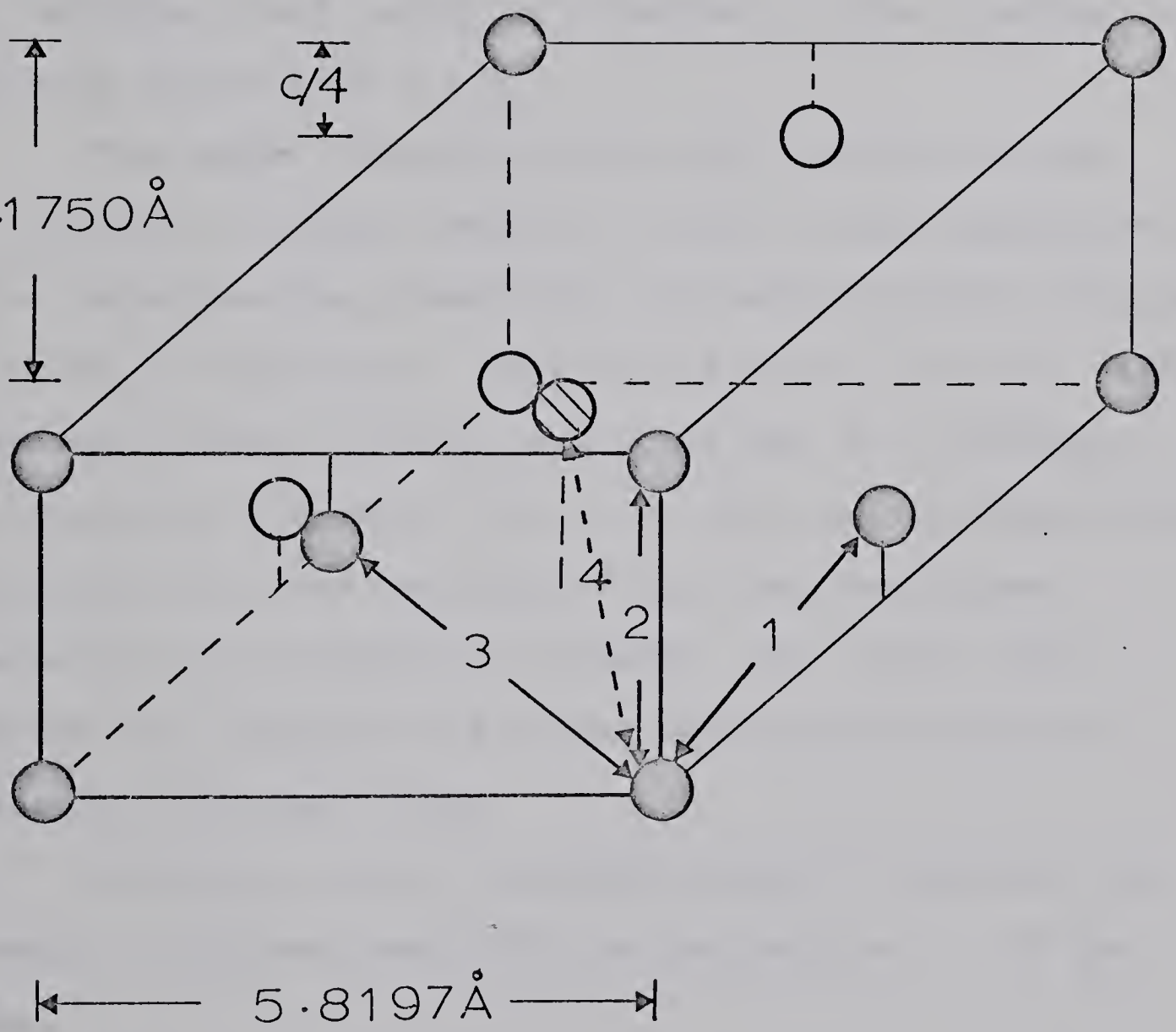
c/4
3.1750Å
4
2
3
1
5.8197Å

nearest neighbour, the spin-spin coupling is small. We therefore consider in some detail the effects on a central nucleus of its neighbours in the first three shells and treat the other nuclei as part of a continuum. The analysis is facilitated by the fact that Sn^{117} and Sn^{119} both have spin $\frac{1}{2}$. However, provided the macroscopic rotation has removed any effect of quadrupolar coupling, the technique could easily be extended to cover spectra involving nuclei with $I > \frac{1}{2}$.

The nuclei interacting with the central nucleus are situated in shells having 4, 2 and 4 sites respectively. We can determine the probability of finding certain groupings of nuclei in the sample. These are given in table I. With techniques similar to High Resolution nmr it is possible to calculate the spectra that arise from these configurations. In metallic tin, the presence of the electron-nuclear interaction very effectively relaxes the nuclei; this broadens the resonance and leaves little possibility of resolving individual lines.

Taking one of the isolated groups we construct an ensemble of systems each with the Hamiltonian H of the group,

$$H = E_o + E_1 + G(t) + H_{rf}(t) \qquad (2)$$

The time independent term E_o is the Hamiltonian of the isolated nuclei. It has eigen-functions ψ'_α,, ψ'_β,, etc.

Table I

Probability of finding certain configurations of tin nuclei in a sample of natural tin.

Nucleus At Centre Of The 10 Sites	117	119
Surrounding 10 Sites Contain	Probability	
0 Unlike Nuclei	0.4033	0.4502
1 Unlike Nucleus ★	0.1740	0.1540
2 Unlike Nuclei ★★	0.0813	0.0635
1 Unlike Nucleus 1 Like ★★★	0.1440	0.1440
Total	0.8026	0.8117
Not Accounted For	0.1974	0.1883

Key Overleaf

PROBABILITIES ARE DIVIDED AMONGST THE VARIOUS SHELLS AS FOLLOWS:

Sn^{119} VALUES IN BRACKETS	★	★★	★★★
IN 1st. SHELL	0.0696 (0.0616)	0.01084(0.00847)	0.0192
IN 2nd. SHELL	0.0348 (0.0308)	0.00181(0.00141)	0.0032
IN 3rd. SHELL	0.0696 (0.0616)	0.01084(0.00847)	0.0192
1 IN 1st. AND 1 IN 2nd.		0.01446(0.01129)	
1 IN 1st. AND 1 IN 3rd.		0.02892(0.02258)	
1 IN 2nd. AND 1 IN 3rd.		0.01446 (0.01129)	
LIKE IN 1st. UNLIKE IN 2nd.			0.0128
UNLIKE IN 1st. LIKE IN 2nd.			0.0128
LIKE IN 1st. UNLIKE IN 3rd.			0.0256
UNLIKE IN 1st LIKE IN 3rd			0.0256
LIKE IN 2nd. UNLIKE IN 3rd.			0.0128
UNLIKE IN 2nd. LIKE IN 3rd.			0.0128

★★★ Sn^{119} identical to Sn^{117}

with eigenvalues α', β', etc. The time-independent term E_1 is produced by the electron-nuclear interactions and is responsible for the Knight Shift and the electron-induced spin-spin coupling. By use of perturbation theory it is possible to determine the eigen-functions ψ_α, ψ_β, etc. of the Hamiltonian $E_o + E_1$. The Hermitian perturbation $G(t)$ is random in time. It takes into account the effect on the nuclei of the random magnetic fields produced by the electrons. $G(t)$ is therefore responsible for the electron part of the nuclear relaxation. The externally applied rf field Hamiltonian is denoted by $H_{rf}(t)$. In general the wave functions of the ensemble can be written

$$\underline{\psi} = \sum_\alpha C_\alpha \psi_\alpha . \tag{3}$$

We define the density matrix in the Schrodinger representation by

$$\rho_{\alpha\alpha'} = \langle C_\alpha^* \, C_{\alpha'} \rangle \tag{4}$$

where $\langle\rangle$ indicates an ensemble average. The density matrix elements satisfy the following differential equation

$$\hbar \frac{d\rho_{\alpha\alpha'}}{dt} = i(E_{\alpha'} - E_\alpha)\rho_{\alpha\alpha'}$$

$$+ i \sum_{\alpha''} \left[\rho_{\alpha\alpha''}(\alpha''|H_{rf}(t)|\alpha') - (\alpha|H_{rf}(t)|\alpha'')\rho_{\alpha''\alpha'}\right]$$

$$+ \sum_{\beta\beta'} \hbar R_{\alpha\alpha'\beta\beta'} \left[\rho_{\beta\beta'} - \rho_{\beta\beta'}(T)\right] \tag{5}$$

where $\rho_{\beta\beta'}(T)$ is the thermal equilibrium value of $\rho_{\beta\beta'}$ (Redfield, 1957). The R's are defined by

$$2\hbar^2 R_{\alpha\alpha'\beta\beta'} = J_{\alpha\beta\alpha'\beta'}(\alpha'-\beta') + J_{\alpha\beta\alpha'\beta'}(\alpha-\beta)$$

$$- \sum_{\gamma}(\delta_{\alpha'\beta} J_{\gamma\beta\gamma\alpha}(\gamma-\beta) + \delta_{\alpha\beta} J_{\gamma\alpha'\gamma\beta'}(\gamma-\beta')). \qquad (6)$$

The J's are the random-field spectral densities and are defined by

$$J_{\alpha\beta\alpha'\beta'}(\omega) = \int_{-\infty}^{+\infty} \langle(\alpha|G(t)|\beta)(\beta'|G(t+\tau)|\alpha')\rangle \exp(-i\omega\tau)\, d\tau. \qquad (7)$$

It may be shown (Redfield, 1957) that $R_{\alpha\alpha'\beta\beta'} = 0$ unless

$$(E_\alpha - E_{\alpha'} - E_\beta + E_{\beta'})\tau_c << h, \qquad (8)$$

where τ_c is the correlation time of the random fields. We may use the density matrix in determining the expectation value of an operator M. It is given by

$$\langle M\rangle = \sum_{\alpha,\alpha',\alpha''} \rho_{\alpha\alpha'} M_{\alpha'\alpha''}. \qquad (9)$$

Having introduced the density matrix we make use of it in determing the tin spectrum.

Case 1: No active nuclei in next three shells.

In this instance there is no spin-spin coupling present and the spectrum is a single line whose width is determined by relaxation broadening. We shall however

treat this simple case in some detail to show the approach to be used in the more complicated systems.

The Hamiltonian of the single nucleus is

$$H = -\gamma \hbar I_z(1-K) H_o + G(t) + H_{rf}(t) \qquad (10)$$

where K is the isotropic Knight Shift constant. The isolated nucleus has two energy states, with its spin either parallel to the magnetic field (state $|1)$) or antiparallel (state $|2)$). The density matrix therefore has four elements ρ_{11}, ρ_{22}, ρ_{12}, ρ_{21}. The rf field produces transitions between states $|1)$ and $|2)$. Writing

$$(1| H_{rf}(t) |2) = H_{12} , \qquad (11)$$

we have from equation (5)

$$\hbar \frac{d\rho_{11}}{dt} = -\hbar \frac{d\rho_{22}}{dt}$$

$$= \hbar R_{1111}(\rho_{11}-\rho_{11}(T)) + \hbar R_{1122}(\rho_{22}-\rho_{22}(T))$$

$$+ i(\rho_{12}H_{21} - \rho_{21} H_{12}), \qquad (12)$$

$$\hbar \frac{d\rho_{12}}{dt} = \hbar R_{1212} \rho_{12} + i(E_2 - E_1) \rho_{12} + i(\rho_{11} - \rho_{22})H_{12} \qquad (13)$$

and

$$\rho_{12} = \rho_{21}^* . \qquad (14)$$

In the limit of small rf fields, i.e. ignoring terms of the order H_{12}^2, we have from equation (12),

$$\rho_{11} = \rho_{11}^{(T)} \tag{15a}$$

$$\rho_{22} = \rho_{22}^{(T)} . \tag{15b}$$

Taking $E_2 > E_1$ and assuming that $H_{rf}(t)$ is sinusoidal at a frequency ω, we try a solution of the form

$$\rho_{12} = r_{12} e^{i\omega t} \tag{16a}$$

$$\rho_{21} = r_{21} e^{-i\omega t} . \tag{16b}$$

Taking $H_{rf}(t) = V \cos \omega t = V(\exp(i\omega t) + \exp(-i\omega t))/2$ (17)

we have

$$r_{12} i\omega = (R_{1212} + i\omega_o) r_{12} + V_{12}(\rho_{11} - \rho_{22})/2 \tag{18}$$

where $E_2 - E_1 = \hbar \omega_o$. To evaluate the R's it is necessary to make a number of approximations. First is that the random fields produced at the nuclear sites by the electrons do not have any preferred direction. (This assumption will be discussed in detail later.) We also assume that the frequency spectrum of the random fields is white to frequencies much greater than the Larmor frequencies of the nucleus. This implies that inequality (8) is satisfied. As

$$(E_\alpha - E_\beta)/\hbar \simeq 10^8 \text{ sec}^{-1} \text{ and } \tau_c \simeq 10^{-11} \text{ sec}$$

(τ_c being the electron spin-lattice relaxation time), this is not unreasonable. We can now evaluate the R's. From equation (6)

$$2\hbar^2 R_{1212} = 2(J_{1122}(0) - J_{1111}(0)) - J_{2121}(\omega) - J_{1212}(\omega) - J_{2222}(0). \quad (19)$$

$$\text{Now } G(t) = -\gamma_n \hbar \underline{H_r}(t) \cdot \underline{I} \quad , \quad (20)$$

where $\underline{H_r}$ is the random magnetic field produced by the electrons at the nuclear site, so that

$$J_{\alpha\beta\alpha'\beta'}(\omega) = \int_{-\infty}^{+\infty} <(\alpha|\underline{H_r}(t).\underline{I}|\beta)(\beta'|\underline{H_r}(t+\tau).\underline{I}|\alpha')> \times \gamma_n^2\hbar^2 \exp(-i\omega\tau)d\tau$$

$$= \sum_{qq'} 2\hbar^2\gamma_n^2(\alpha|I_q|\beta)(\beta'|I_{q'}|\alpha')k_{qq'}(\omega) \quad (21)$$

where

$$2k_{qq'}(\omega) = \int_{-\infty}^{+\infty} <H_{r_q}(t)H_{r_{q'}}(t+\tau)> \exp(-i\omega\tau)d\tau \quad (22)$$

and $H_{r_q}(t)$ is the qth component of $\underline{H_r}(t)$. If the random field in perpendicular directions are assumed to be uncorrelated then

$$<H_{r_q}(t)H_{r_{q'}}(t+\tau)> = 0 \quad (23)$$

unless q' = q. We have that

$$J_{1111}(\omega) = -J_{1122}(\omega) = \gamma_n^2 \hbar^2 k_{zz}(\omega)/2 \tag{24}$$

and $$J_{2121}(\omega) = \gamma_n^2 \hbar^2 (k_{xx}(\omega) + k_{yy}(\omega))/2 \,. \tag{25}$$

The assumption of a white frequency spectrum for the random fields leads to

$$k_{qq}(\omega) = k_{qq}(0). \tag{26}$$

If the random fields have values independent of direction then

$$k_{xx} = k_{yy} = k_{zz} \tag{27}$$

and
$$R_{1212} = -\gamma_n^2 (k_{zz} + k_{yy})$$
$$= -2W \tag{28}$$

where $W = \gamma_n^2 k_{zz}$. Substituting equation (28) back into equation (18) we obtain

$$r_{12} = -iV_{12}(\rho_{11}-\rho_{12})[\{i(\omega_o-\omega) - 2W\}2\hbar]^{-1}. \tag{29}$$

Now

$$\rho_{11} = \exp(-E_1/kT)\{\exp(-E_1/kT) + \exp(-E_2/kT)\}^{-1}$$

$$\simeq \{\exp(-E_1/kT)\}/2 \tag{30}$$

so that $$\rho_{11}-\rho_{22} = \hbar\omega_o/2kT. \tag{31}$$

Using the density matrix we find that the magnetization in

the x direction is

$$\langle M_x(t)\rangle = \rho_{12}(2|M_x|1) + \rho_{21}(1|M_x|2)$$

$$= r_{12}(2|M_x|1)\exp(i\omega t) + r_{21}(1|M_x|2)\exp(-i\omega t)$$

$$= 2 \text{ Real } [r_{12}\exp(i\omega t)(2|M_x|1)], \tag{32a}$$

which by definition equals the real part of

$$\chi(\omega)\, H_{xo}\exp(i\omega t). \tag{32b}$$

Therefore, we have

$$\chi(\omega) = 2r_{12}(2|M_x|1)/H_{xo}. \tag{33}$$

Using the fact that

$$V_{12} = -(1|M_x H_{xo}|2) \tag{34}$$

leads to a value of the nuclear susceptibility

$$\chi(\omega) = i|(1|M_x|2)|^2\omega_o\{2kT(i(\omega_o-\omega)-2W)\}^{-1}$$

$$= 4i\, Z_o\, \{i(\omega_o-\omega) - 2W\}^{-1} \tag{35}$$

where Z_o is defined as $\gamma_n^2\hbar^2\omega_o(32kT)^{-1}$. We see that the line is, as expected, a Lorentzian with a width proportional to W.

Case 2: One active nucleus in next three shells.

We now suppose that there is an other magnetically-active nucleus within the first three shells. In this case we would expect two types of spectra; one when the two nuclei are alike, the other when they are not. In the first instance, the presence of the spin-spin coupling does not change the spectrum from that of an isolated nucleus, but in the other case, the system produces what a chemist would call an AX spectrum. As the nuclei are unlike, their resonance lines do not overlap and can be treated separately. The effect of the J coupling of the A nucleus on the X spectrum is to split it into two lines. It is as though the X nucleus would be found in two magnetic environments; one when the A nucleus has spin parallel to the main field, and the other when antiparallel. The J coupling from A acts as an 'extra' magnetic field at the X site. The random fields at the A nuclear site can be thought of as flipping it from spin up to spin down and vice-versa. This change effectively switches the magnetic environment of nucleus X. If the flip rate is high enough, the effect is to decouple the X nucleus from the A so that the X doublet collapses into a line centered at the natural frequency of X. The coalescing of the lines is a common enough effect in high resolution nmr (Arnold, 1956). There, it is often produced by the jumping of nucleus X from a molecule where the A spin is up to another where it is down. This also has the effect of changing the X magnetic environment. In liquids the

collapse of the lines is very apparent, but in a metal the effect of the relaxation broadening (determined by W) is so great that the multiplets will not be resolved and their collapse will be manifested only by a slight narrowing of the line.

It should be realized that there is a difference between the disappearance of the satellites under this flipping process and the disappearance of the dipolar broadening when the sample is spun. Rotation keeps the relative spin positions unchanged and produces a spatial average leaving the multiplet structure. The flipping however changes the spin positions and thus collapses the multiplet.

We shall now proceed to show that when the two nuclei are identical there is only one line. The Hamiltonian has the form

$$H = -\gamma_A \hbar I_{z_A} (1-K_A) H_o - \gamma_{A'} \hbar I_{z_{A'}} (1-K_{A'}) H_o$$

$$+ J_{AA'} h \underline{I_A} \cdot \underline{I_{A'}} + G(t) + H_{rf}(t). \qquad (36)$$

The time-independent part of the Hamiltonian has four eigenfunctions. Three of these are associated with a total spin of 1, and the other is of spin 0. It is not possible for the applied rf field to induce transitions between states of different total spin. The nmr lines will therefore only be produced by transitions between the states

of total spin 1 corresponding to $m_z = -1$, 0 and +1 where m_z is the z component of the total spin. It can be shown that these states have energies $\gamma_A H_o \hbar + J_{AA}, h/4$, $J_{AA}, h/4$, and $-\gamma_A H_o \hbar + J_{AA}, h/4$ respectively. It follows that the energy required to induce transitions is independent of J_{AA}, and the spectrum is the same as for the isolated nucleus.

For non-identical nuclei the Hamiltonian becomes

$$H = -\gamma_A \hbar I_{z_A} (1-K_A) H_o - \gamma_X \hbar I_{z_X} (1 - K_X) H_o$$

$$+ J_{AX} h \underline{I_A} \cdot \underline{I_X} + G(t) + H_{rf}(t). \qquad (37)$$

The eigenfunctions of the time-independent part of the Hamiltonian are $|++)$, $|+-)$, $|-+)$ and $|--)$ which we number $|1)$, $|2)$, $|3)$ and $|4)$ respectively. The energy level scheme is shown in figure (4.2) where we have chosen $|E_4 - E_2| > |E_4 - E_3|$, without loss of generality. The presence of the random fields produces transitions between the eigenfunctions. We take the simplest form of G(t) which is a sum of 'single-nucleus' operators

$$G(t) = -\hbar(\gamma_A \underline{H_A}(t) \cdot \underline{I_A} + \gamma_X \underline{H_X}(t) \cdot \underline{I_X}) \qquad (38)$$

where $\underline{H_A}$ and $\underline{H_X}$ are the random fields at the A and X nuclear sites. We shall assume that the random fields at the two sites are independent. From the form of G(t) we

Figure (4.2)

Energy level diagram for the AX type grouping of nuclei showing the allowed transitions.

STATE

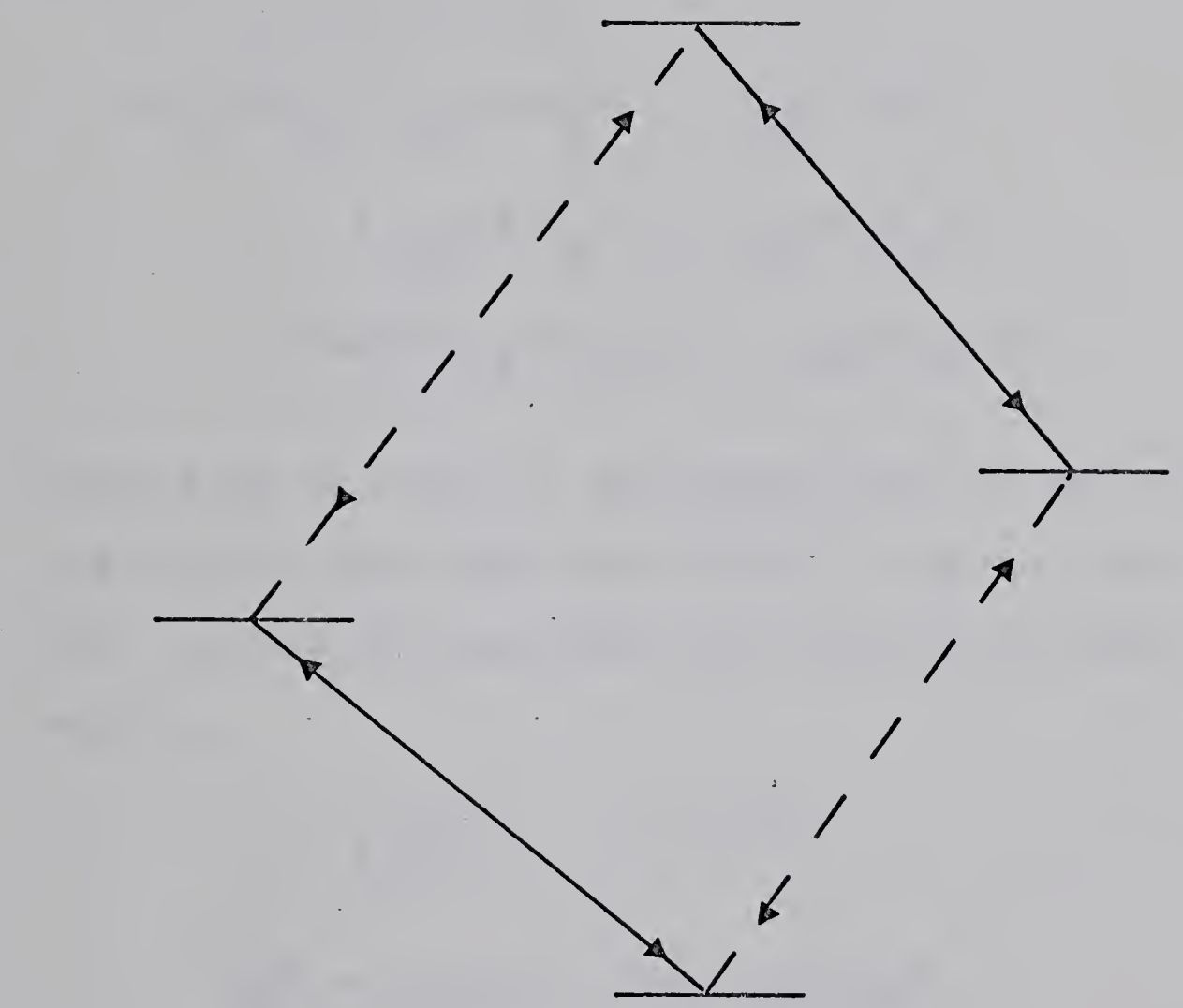

A SPECTRUM

X SPECTRUM

note that H_A will induce transitions between $|4)$ and $|2)$ and also $|3)$ and $|1)$ whilst H_X induces transitions between $|4)$ and $|3)$ and also $|2)$ and $|1)$. Imagine that we are looking at the X spectrum; then the quantity of interest is the x component of the magnetization of the X nucleus. This is

$$\begin{aligned} \langle M_x(t)\rangle_X &= \rho_{12}(2|M_x|1) + \rho_{21}(1|M_x|2) \\ &\quad + \rho_{34}(4|M_x|3) + \rho_{43}(3|M_x|4) \\ &= 2\ \mathrm{Real}\{\rho_{12}(2|M_x|1) + \rho_{34}(4|M_x|3)\} \ . \end{aligned} \tag{38}$$

Terms such as $(1|M_x|3)$ deal with lines of the A spectrum and will be zero near the X lines. Making use of equations (5), (6) and (7) we obtain, in the low rf field approximation,

$$\rho_{ii} = \rho_{ii}(T) \ , \quad i = 1 \to 4, \tag{39}$$

$$\frac{d\rho_{12}}{dt} = i\omega_{12}\rho_{12} + (\rho_{11}-\rho_{22})H_{21}/\hbar + R_{1212}\rho_{12} + R_{1234}\rho_{34} \ , \tag{40}$$

$$\frac{d\rho_{34}}{dt} = i\omega_{34}\rho_{34} + (\rho_{33}-\rho_{44})H_{43}/\hbar + R_{3434}\rho_{34} + R_{3412}\rho_{12} \tag{41}$$

where $\omega_{12} = \omega_X - J_{AX}\pi$ and $\omega_{34} = \omega_X + J_{AX}\pi$ with ω_X being

the natural frequency of the X nucleus. Evaluating the R's leads to the equations

$$\frac{d\rho_{12}}{dt} = i\omega_{12}\rho_{12} + i(\rho_{11}-\rho_{22})H_{21}/h$$

$$- \rho_{12}(2W_X + W_A) + \rho_{34}W_A \qquad (42)$$

and

$$\frac{d\rho_{34}}{dt} = i\omega_{34}\rho_{34} + i(\rho_{33}-\rho_{44})H_{43}/h$$

$$- \rho_{34}(2W_X + W_A) + \rho_{12}W_A. \qquad (43)$$

The W's are as previously defined with the suffixes denoting the nuclei with which the random fields are associated with. Ignoring terms involving W_A, the equations for ρ_{12} and ρ_{34} look just like those for the density matrix of a two-spin system with the nuclei isolated (see equation (13)). The form of the lines is Lorentzian with a linewidth determined by $2W_X$. The coupling terms, which involve W_A, produce the collapsing of the lines, a phenomenon which might well be called 'relaxation narrowing'. Trying a solution similar to that for the single nucleus we take

$$H_{rf}(t) = V \cos \omega t$$

$$\rho_{12} = r_{12} \exp(i\omega t)$$

$$\rho_{34} = r_{34} \exp(i\omega t)$$

which leads to

$$\lambda_{12}r_{12} + W\, r_{34} = -iV_{12}(\rho_{11}-\rho_{22})/2\hbar \qquad (44a)$$

and $$W\, r_{12} + \lambda_{34}r_{34} = -iV_{34}(\rho_{33}-\rho_{44})/2\hbar \qquad (44b)$$

where $$\lambda_{ij} = i(\omega_{ij}-\omega) - 3W. \qquad (44c)$$

Now

$$\rho_{ii} = \exp(-E_i/kT) \Big/ \sum_{j=1}^{4} \exp(-E_j/kT) \qquad (45a)$$

so that

$$\rho_{ii} - \rho_{i+1,i+1} \simeq \hbar\omega_o/4kT. \qquad (45b)$$

From equation (44) we obtain

$$r_{34} = 2iZ_oH_{xo}(\lambda_{12}-\omega)(\lambda_{12}\lambda_{34}-W^2)^{-1}(\gamma\hbar)^{-1} \qquad (46a)$$

and $$r_{12} = 2iZ_oH_{xo}(\lambda_{34}-\omega)(\lambda_{12}\lambda_{34}-W^2)^{-1}(\gamma\hbar)^{-1}. \qquad (46b)$$

We therefore have

$$\chi(\omega) = 2(r_{12}(2|M_x|1) + r_{34}(4|M_x|3))H_{xo}^{-1}$$

$$= 2iZ_o(\lambda_{34} + \lambda_{12} - 2W)(\lambda_{12}\lambda_{34} - W^2)^{-1}. \qquad (47)$$

If W is small compared to $2\pi J$, equation (47) describes a spectrum consisting of lines at $\omega_X \pm \pi J$ broadened by W. If $2\pi J$ is small compared to W, equation (47) describes a spectrum with a line at ω_X broadened by J and W.

Case 3: Two active nuclei in next three shells.

When both nuclei are alike and identical to the central nucleus, we again find that the nmr spectrum of the group is a single line. The spectrum is, however, split into a total of 15 lines when only two of the nuclei are the same isotope. It is possible to gain an insight on how this spectrum arises by considering the case where all the nuclei are very different. In this, so called AMX spectrum, the line from the A nucleus is split into two by the J_{AM} coupling, and each of these lines is further split by the J_{AX} coupling. A similar thing happens to the M and X lines, giving rise to a total of 12 lines. As we let the A and M nuclei become more alike, the A and M spectrum come together to give 8 lines near $(\omega_A+\omega_M)/2$. This gives the AA' part of the AA'X spectrum. The four lines near ω_X become six by the appearance of two other lines associated with the simultaneous flipping of the A and A' nuclei. The fifteenth line is a combination line (near $\omega_A+\omega_{A'},-\omega_X$) involving A, A' and X nuclei and has zero intensity unless X is similar to A.

The Hamiltonian for the three nuclei A, A' and X is

$$H = -\hbar \sum_{i=A,A',X} \gamma_i I_{z_i} (1-K_i) H_o + G(t)$$

$$+ h(J_{AA'} \underline{I_A} \cdot \underline{I_{A'}} + J_{AX} \underline{I_A} \cdot \underline{I_X} + J_{A'X} \underline{I_{A'}} \cdot \underline{I_X})$$

$$+ H_{rf}(t). \qquad (48)$$

The eigen-functions of the time-independent part of the Hamiltonian are given in table II. The determination of the eigen-functions is greatly simplified by the fact that the basis product functions with different X spins cannot be mixed . Figure (4.3) shows schematically the various allowed transitions produced by an external rf field. The transition frequencies have been given by Pople, Schneider and Bernstein (1959) and are shown in table III.

Let us first imagine that we are considering the X part of the spectrum. This means that the X atom is at the centre, surrounded by the ten sites. The lattice structure in tin is such that the probability of finding the A' and A nuclei closer together than the fourth-nearest neighbour is small. We can therefore simplify the calculation by assuming that $J_{AA'}$ is zero. This means the X spectrum now only consists of four lines. In this case we have

$$H_{xo}\chi(\omega) = 2 \sum_{ij} \rho_{ij}(j|M_x|i) \qquad (49)$$

where ij take the values 12, 36, 45 and 78. Proceeding as before, and taking

$$G(t) = - \sum_{k=A,A',X} \gamma_k \hbar \, \underline{H_k}(t) . \underline{I_k} \, , \qquad (50)$$

we find that r_{12}, r_{36}, r_{45} and r_{78} satisfy the simultaneous equation (with coefficients given in matrix form)

Table II

Wave functions for the AA'X type grouping of nuclei.

Key

$J_1 = 2\pi J_{AA'}$

$J_2 = 2\pi J_{AX}$

$J_3 = 2\pi J_{A'X}$

Wave Functions For AA'X Spectrum

$|1) = |+++)$ $\qquad$ $|7) = |--+)$

$|2) = |++-)$ $\qquad$ $|8) = |---)$

$$|3) = \cos\phi_+ |+-+) + \sin\phi_+ |-++)$$

$$|4) = -\sin\phi_+ |+-+) + \cos\phi_+ |-++)$$

$$|5) = \cos\phi_- |+--) + \sin\phi_- |-+-)$$

$$|6) = -\sin\phi_- |+--) + \cos\phi_+ |-+-)$$

where

$$D_\pm \cos 2\phi_\pm = (J_2 - J_3)/4$$

$$D_\pm \sin 2\phi_\pm = J_1/2$$

$$D_\pm = ((J_2 - J_3)^2/4 + J_1^2)^{1/2}/2$$

Figure (4.3)

Energy level diagram for the AA'X grouping of nuclei showing the allowed and forbidden transitions.

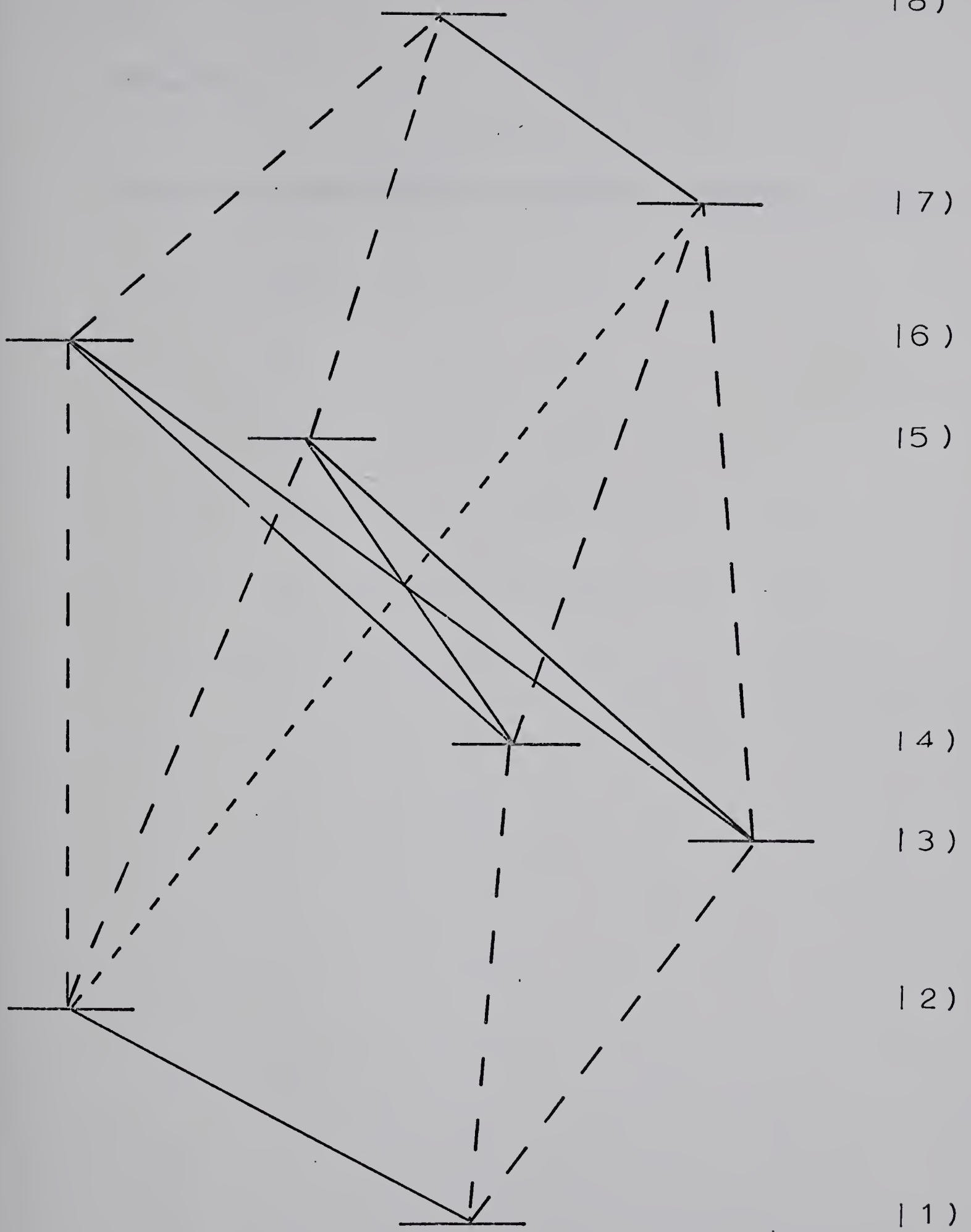
STATE
18)
17)
16)
15)
14)
13)
12)
11)
X LINES
AA' LINES
FORBIDDEN COMBINATION LINE

Table III

Transition frequencies for the AA'X grouping of nuclei.

TRANSITION FREQUENCIES FOR AA' SPECTRUM

$$\omega_{68} = \omega_A - (2J_1 + J_2 + J_3)/4 - D_-$$

$$\omega_{47} = \omega_A - (2J_1 - J_2 + J_3)/4 - D_+$$

$$\omega_{25} = \omega_A + (2J_1 - J_2 + J_3)/4 - D_-$$

$$\omega_{13} = \omega_A + (2J_1 + J_2 + J_3)/4 - D_+$$

$$\omega_{58} = \omega_A - (2J_1 + J_2 + J_3)/4 + D_-$$

$$\omega_{37} = \omega_A - (2J_1 - J_2 + J_3)/4 + D_+$$

$$\omega_{26} = \omega_A + (2J_1 - J_2 - J_3)/4 + D_-$$

$$\omega_{14} = \omega_A + (2J_1 + J_2 + J_3)/4 + D_+$$

TRANSITION FREQUENCIES FOR X SPECTRUM

$$\omega_{78} = \omega_X - (J_2 + J_3)/2$$

$$\omega_{35} = \omega_X + D_+ - D_-$$

$$\omega_{46} = \omega_X - D_+ + D_-$$

$$\omega_{12} = \omega_X + (J_2 + J_3)/2$$

$$\omega_{45} = \omega_X - D_+ - D_-$$

$$\omega_{31} = \omega_X + D_+ + D_-$$

FORBIDDEN LINE

$$\omega_{27} = 2\omega_A - \omega_X$$

$$\begin{pmatrix} \mu_{12} & W & -W & 0 \\ W & \mu_{36} & 0 & W \\ -W & 0 & \mu_{45} & -W \\ 0 & W & -W & \mu_{78} \end{pmatrix} = \frac{iZ_o}{\gamma h} \begin{pmatrix} 1 \\ 1 \\ -1 \\ 1 \end{pmatrix} \qquad (51)$$

where $\mu_{ij} = i(\omega_{ij}-\omega) - 4W$. Using equation (51) we have that

$$\chi(\omega) = -2iZ_o(i[\omega_X-\omega] - 4W)$$
$$\times [4W\{i(\omega_X-\omega) - 4W\} - \mu_{45}\mu_{36} - \mu_{12}\mu_{78}]$$
$$\times (\mu_{12}\mu_{78}\mu_{45}\mu_{36} - 4W^2\{i(\omega_X-\omega) - 4W\})^{-1} \qquad (52)$$

We now examine the AA' part of the AA'X spectrum. This is in general asymmetric about ω_A. If, however, we imagine that the A nucleus is at the centre, then A' and X are so far apart that $J_{A'X}$ is zero. This has the effect of symmetrizing the spectrum. Proceeding as before we have that

$$\chi(\omega)H_{xo} = 2\sum_{nq} \rho_{nq}(q|M_x|n) \qquad (53)$$

where nq take the values 68, 47, 25, 13, 58, 37, 26 and 14. Setting

$$\rho_{nq} = r_{nq} \exp(i\omega t) \qquad (54)$$

we find that the r_{nq}'s satisfy the simultaneous equations shown in table IV (case 1). There is nothing to be gained

TABLE IV

(a) SET OF SIMULTANEOUS EQUATIONS WHICH DETERMINE THE r's IN THE AA′ PART OF THE AA′X SPECTRUM.

(b) DEFINITION OF THE VECTOR $\underline{P}$ IN (a)

(c) DEFINITION OF THE MATRIX $\underline{\underline{A}}$ IN (a)

KEY

CASE 1 IGNORING FAR DISTANT NEIGHBOURS

$$W' = W$$

$$\mu_{ij} = i(\omega_y - \omega) - W(7+\cos^2 2\phi_+)/2$$

CASE 2 ACCOUNTING FAR DISTANT NEIGHBOURS

$$W' = W + \Delta W$$

$$\mu_{ij} = i(\omega_{ij} - \omega) - 2W - W(3+\cos^2 2\phi_+)/2 - B'$$

WHERE ΔW AND B' ARE AS DEFINED IN THE TEXT.

(a)

$$\underline{\underline{A}} \cdot \underline{r} = iH_{xo} Z_o \underline{P} / \gamma h$$

(b)

$$\underline{P} = \begin{pmatrix} C_M - S_M \\ C_P - S_P \\ C_M + S_M \\ C_P + S_P \\ C_M + S_M \\ C_P + S_P \\ C_M - S_M \\ C_P - S_P \end{pmatrix}$$

where

$$C_{\substack{P \\ M}} = \cos \phi_{\pm}$$

$$S_{\substack{P \\ M}} = \sin \phi_{\pm}$$

(C)

$$
\begin{array}{cccccccc}
\mu_{68} & C'_{PM} & C'_{MM} & 0 & 0 & S'_{PM} & -S'_{MM} & 0 \\
C'_{PM} & \mu_{47} & 0 & C'_{PP} & -S'_{PM} & 0 & 0 & -S'_{PP} \\
C'_{MM} & 0 & \mu_{25} & C'_{PM} & S'_{MM} & 0 & 0 & -S'_{PM} \\
0 & C'_{PP} & C'_{PM} & \mu_{13} & 0 & S_{PP} & S_{PM} & 0 \\
0 & -S'_{PM} & S'_{MM} & 0 & \mu_{58} & S'_{PM} & C'_{MM} & 0 \\
S'_{PM} & 0 & 0 & S'_{PP} & C'_{PM} & \mu_{37} & 0 & C'_{PP} \\
-S'_{MM} & 0 & 0 & S'_{PM} & C'_{MM} & 0 & \mu_{26} & C'_{PM} \\
0 & -S'_{PP} & -S'_{PM} & 0 & 0 & C'_{PP} & C'_{PM} & \mu_{14}
\end{array}
$$

where

$$S'_{\substack{PP \\ MM}} = W' \sin 2\phi_{\pm}$$

$$C'_{\substack{PP \\ MM}} = W' \cos 2\phi_{\pm}$$

$$C'_{PM} = W' \cos(\phi_{+} - \phi_{-})$$

$$S'_{PM} = W' \sin(\phi_{+} - \phi_{-})$$

by attempting to solve this equation algebraically and the solution is therefore obtained by computation at each point in the spectrum. The problem is not difficult as the matrix of the coefficients of the r's has a number of special properties. The method of analysis is given in appendix I.

Case 4: The effect of more distant neighbours.

In the previous analyses of tin data (McLachlan, 1968; Alloul and Deltour 1969 ; Sharma et al., 1969) the effect of far distant neighbours on the spectrum has been ignored. Approaching the analysis from the 'high resolution nmr' side shows that the distant neighbours may actually have a pronounced effect upon the line shape.

We may approximate the effect of an X nucleus in the 'continuum' on an A nucleus at the centre of a group by examining the AX spectrum in the limit of high flip rates (i.e. $W >> 2\pi J_{AX}$). We find, after considerable mathematical manipulation, that*

$$\chi_A(\omega) = i4Z_o(i\{\omega_A-\omega\} - 2W')^{-1}$$

where $2W' = 2W + 4\pi^2 J_{AX}{}^2/2W$. The 2W in the denominator of the term involving J_{AX} arises from the fact that the X nucleus is changing its spin direction at a rate 2W. Equation

---

*I would like to thank Dr. McClung of the Department of Chemistry for bringing this expression to my attention.

(57) implies that the multiplet has collapsed into a single Lorentz line whose width is slightly greater than the normal linewidth because of the presence of the residual linewidth. Each interaction with an unlike nucleus in the continuum increases the apparent linewidth. Summing over the continuum we have that

$$(2W')_{apparent} = 2W + B \tag{58}$$

where $$B = \sum_N 4\pi^2 J_{AN}^2 / 2W \tag{59}$$

with the summation being over all the X type lattice sites in the continuum. Now

$$\sum_N \pi^2 J_{AN}^2 = \int_{r_o}^{\infty} 2\pi^3 \rho r^2 J^2(r)\, dr \tag{60}$$

where ρ is the number of unlike active nuclei per unit volume of the continuum and r_o is the distance to the start of the continuum from the A lattice site (approximately 4th nearest neighbour distance). From chapter 3 we have

$$2\pi J(r) = A\, F(2k_f r) \tag{61}$$

so that

$$\sum_N J_{AN}^2 = A^2 [12\pi k_f^3 x_o^3]^{-1} \tag{62}$$

where $x_o = 2k_f r_o$. Now J_1, the nearest neighbour spin-spin coupling constant, is given by

$$2\pi J_1 = A\, F(2k_f r_1) \tag{63}$$

so that

$$\sum_N J_{AN}^2 = \rho J_1^2 \left[12\pi k_f^3 F^2(2k_f r_1) x_o^2\right]^{-1}. \qquad (64)$$

Taking typical values for the constants for tin ($k_f = 1.65 \times 10^8 cm^{-1}$, $F(2k_f r_1) = 8.4 \times 10^{-4}$, $\rho = 3.2 \times 10^{21}$ nuclei cm^{-3}, $T_1 = 150$ μsec, $J_1 = 3.1 \times 10^3$ Hz and $x_o = 15$).

leads to

$$(2W')_{apparent} = 2W + 1050 \text{ sec}^{-1}. \qquad (65)$$

As 2W is approximately 6700 sec^{-1} we see that the additional width from the far neighbours is important and should not be ignored.

We shall now try to compute the effects of the like nuclei in the continuum. Returning for a moment to the simple AA' spectrum, we find that the effect of $J_{AA'}$ is to make the A and A' nuclei exchange their spins at a rate $4\pi J_{AA'}$. If the A nucleus is in a group and the A' nucleus is in the continuum, then half of the time the exchange of spins between A and A' leaves A in a different magnetic environment in the group (i.e. the A spin flips). The rest of the time A and A' exchange equivalent spins so that the magnetic environment of A is unchanged. We may approximate the effect of the A' on the A as an increased flip rate of A . The actual effect of the A' on an AX spectrum is shown in figure (4.4). The upper spectrum shows the AA' part

Figure (4.4)

Spectra showing the effect of exchange coupling between like nuclei.

(a) The spectrum for a group of A,A' and X nuclei when there is a coupling between the A and X nuclei, and the A' nucleus is isolated from the others.

(b) The same spectrum except that there is now an exchange coupling between the A and A' nuclei.

$J_{AX} = 4$

$J_{AA'} = 0$

$J_{A'X} = 0$

(a)

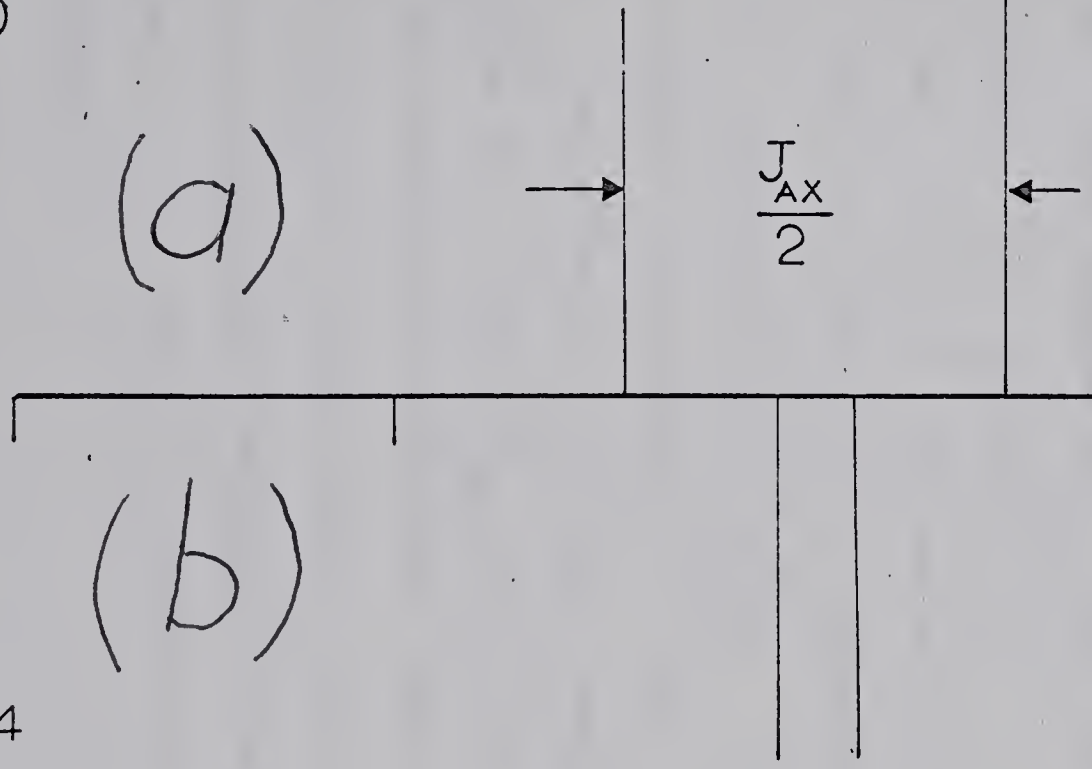

(b)

$J_{AX} = 4$

$J_{AA'} = 4$

$J_{A'X} = 0$

when the A' is not coupled to the A nucleus. The A' line is not shifted. The J_{AX} coupling splits the A line into two. Introducing the $J_{AA'}$ coupling narrows the spectrum. The narrowing could be brought about by an increased jump rate of the Aspin, but in this case the lines would not remain sharp but would become broadened. As this is only an approximation of what is actually happening, there is, unfortunately, no theoretical expression equivalent to equation (57). The apparent increased flip rate must therefore be estimated. Now a J_{AX} coupling splits the A line, of half width 2W, by an amount $2\pi J_{AX}$ but after collapse the spectrum becomes, from equation (57), a Lorentz line with half-width $2W + 4\pi^2 J_{AX}^2/W$. We can approximate this line by two Lorentz lines of linewidth 2W separated by the extra half-width, i.e. a splitting of $2\pi^2 J_{AX}^2/W$. This effectively is the same as cutting the strength of the J coupling by a fraction $\pi J/W$. The effect of the $J_{AA'}$ coupling was to exchange the spins at a rate $4\pi J_{AA'}$ but if we introduce the effect of the conduction electrons then the exchange rate drops to $4\pi^2 J_{AA'}^2/W$. We can now use this expression to determine the rate ΔW at which exchange between the A nucleus at the centre and the A' nuclear spins in the continuum occurs. It is given by

$$\Delta W = \sum_{N} 2J^2\pi^2/W. \qquad (66)$$

where the factor of $\frac{1}{2}$ arises as only half of the A' nuclei

have spins such that their exchange with A changes the A environment. It follows that

$$\Delta W = \pi^3 \rho J_1^2 [\, 6\, W k_f^{\,3} F^2(2k_f r_1) x_o^{\,3}]^{-1}. \qquad (67)$$

If, for example, we include the effects of nuclei in the continuum on the AX spectrum then we find that

$$(\lambda_{12} - \Delta W + B) r_{12} + (W + \Delta W) r_{34} = 2iZ_o/\gamma\hbar \qquad (68a)$$

$$(W + \Delta W) r_{12} + (\lambda_{34} - \Delta W + B) r_{34} = 2iZ_o/\gamma\hbar. \qquad (68b)$$

The extra broadening term B produces an increased width, whilst the increased jump rate ΔW increases the terms which collapse the multiplets in the spectrum (but are not included in the terms which broaden the spectrum).

The treatment has, however, been slightly inconsistent as the nuclei in the continuum surrounding A are affected i.e. flipped by 'their' continuum and local neighbours. We must therefore make the expressions for B and ΔW self-consistent. This implies that

$$B' = B\ 2W(2W + \Delta W')^{-1} \qquad (70a)$$

$$\Delta W' = (\Delta W) 2W(2W + \Delta W')^{-1} + \Delta W'' \qquad (70b)$$

where $\Delta W''$ is the effect, on the nuclei in the continuum, of their local neighbours. We can estimate this by taking

$$\Delta W'' = \langle \Sigma_{\text{sum over local neighbours}} \pi^2 J^2 (2W + \Delta W')^{-1} \rangle_{\text{average over sample.}} \qquad (71)$$

A plausible value for $\Delta W''$ is $0.13\, J_1^{\,2}(2W + \Delta W')^{-1}$.

Substituting this value back into equation (70b) leads to

$$\Delta W' \simeq \Delta W(1 + 0.07\pi^2 J_1^{\,2} W^{-2}) \qquad (72a)$$

and

$$B' \simeq B\, 2W(2W + \Delta W(1 + 0.07\pi^2 J_1^{\,2} W^{-2}))^{-1} \qquad (72b)$$

We can now use these expressions to correct the values of $\chi(\omega)$ for the effect of far distant neighbours (cf McConnell, 1957). Defining

$$W_e = W + \Delta W', \qquad (73)$$

then the 'isolated nucleus' spectrum becomes

$$\chi(\omega) = i4Z_o[i(\omega_o - \omega) - 2W - B']^{-1}. \qquad (74)$$

The X part of the AX spectrum becomes

$$\chi_X(\omega) = 2iZ_o(\lambda'_{34} + \lambda'_{12} - 2W_e)(\lambda'_{12}\,\lambda'_{34} - W_e^{\,2})^{-1} \qquad (75)$$

where

$$\lambda'_{ij} = i(\omega_{ij} - \omega) - 2W - W_e - B'.$$

Equation (52) describing the X part of the AA'X spectrum must be modified to read

$$\chi(\omega) = -2iZ_o Y(4W_e Y - \mu'_{45}\,\mu'_{36} - \mu'_{12}\,\mu'_{78})$$
$$\times (\mu'_{12}\,\mu'_{78}\,\mu'_{45}\,\mu'_{36} - 4W_e^{\,2}Y^2)^{-1} \qquad (76)$$

where $$Y = i(\omega_X - \omega) - 2W - 2W_e - B' \quad (77)$$

and $$\mu'_{ij} = i(\omega_{ij} - \omega) - 2W - 2W_e - B' \quad (78)$$

The new equations for the AA' part of the AA'X spectrum have been given in Table IV (case 2).

Case 5: Other configurations.

These account for the remaining 20% of the assemblies. If the nuclei in the grouping are identical, only a single line is expected. In other cases the spectra could be calculated but the proliferation of lines to be considered makes the calculation impractical. Furthermore, the probability of occurrence of each configuration is small. To ignore them entirely would be incorrect, so instead, we group them with the configurations which they most closely resemble. Any configuration with one unlike and two or more like nuclei is treated as if it consisted of one like and one unlike nucleus. All others are included in the two unlike nuclei group.

Determination of a value for W

In metals at room temperature, the spin-lattice relaxation time is mainly determined by the conduction electrons. We have, for an isolated nucleus being relaxed by the electrons (Slichter, 1963), that

$$T_1 = 1/(k_{zz} + k_{yy}) \quad (79)$$

so that 2W is equal to the reciprocal of the spin-lattice

relaxation time. The assumption, made in the first part of this chapter, that

$$k_{xx} = k_{yy} = k_{zz} \tag{80}$$

implies that T_1 is isotropic and this can be tested by measuring the orientation dependence of T_1. This has been done by McLachlan (1968) who finds that there is little variation. The absolute value of his T_1 data must be considered suspect as it appears that when compared to other work there is evidence of some systematic error (Spokas and Slichter, 1959; Dickson, 1969; App, 1970). However, a systematic error should not affect the observation of an orientation dependence of T_1.

There are a number of values of T_1 in the literature. McLachlan (1968) together with Asayama and Itoh (1962) find values of T_1 that at room temperature are equivalent to 112 μsec. This is close to the theoretical value of T_1 as determined using the known tin Knight Shift and the Korringa relationship (Korringa, 1950). However, Spokas and Slichter (1959), Dickson (1969), Alloul and Deltour (1969) and App*(1970) find values close to 150 μsec. App's work was actually performed using the same crystal

---

*I would like to thank Dr. Williams of the Department of Physics at U.B.C. for bringing my attention to this work.

used by McLachlan. Dickson (1969) tested two other samples of tin, one of high purity and the other of low purity, and obtained T_1's consistent, within experimental error, with his original result. We shall, therefore, use his value of T_1 in the determination of W.

B) Experimental Results

A typical absorption derivative nmr signal from a tin metal sample spun at 5 kHz at the 'magic' angle is shown in figure (4.5a). Figure (4.5b) shows the resonance of an unspun sample to the same scale. The complete resonance of the unspun sample, shown in figure (4.5c), clearly shows the lineshape asymmetry produced by the anisotropic Knight Shift.

The lineshape for both the tin isotopes were Lorentz-like with a peak-to-peak width of 1.70 $\pm$ 0.05 kHz for Sn^{117} and 1.90 $\pm$ 0.05 kHz for Sn^{119}. If the lineshapes had been totally determined by the spin-lattice relaxation times of the nuclei, the widths, corresponding to T_1's of 164 μsec and 150 μsec, would have been 1.14 kHz and 1.25 kHz respectively. The Sn^{117} nuclear relaxation time was calculated using the fact that $(T_1)_{Sn^{117}}/(T_1)_{Sn^{119}} = \gamma^2_{119}/\gamma^2_{117}$.

It was found that there was no change in the resonance lineshape on increasing the rotation speed from 4.2 kHz to 5.7 kHz. This was taken as evidence that the rotational-satellite lines were sufficiently weak and far from the centre line, so that the spectrum could be described by the 'liquid-like' Hamiltonian used in the first part of this chapter (see also appendix II). The variation of the resonance linewidth, as the turbine was tilted relative to the magnetic field, gave an insensitive determination of the 'magic' angle. Instead, the disappearance of the lineshape asymmetry, associated with the anisotropic Knight Shift, was used.

Figure (4.5)

Experimental Sn^{119} resonances:

(a) Resonance from a powder sample spun at 5 kHz. The resonance frequency is 6 MHz. The frequency scale is 574 Hz/div. The resonance was obtained by making 2048 runs over a period of 48 hrs.

(b) Resonance from an unspun sample to the same scale as (a).

(c) A resonance from an unspun sample on a smaller scale. The asymmetry produced by the anisotropic Knight Shift is clearly seen.

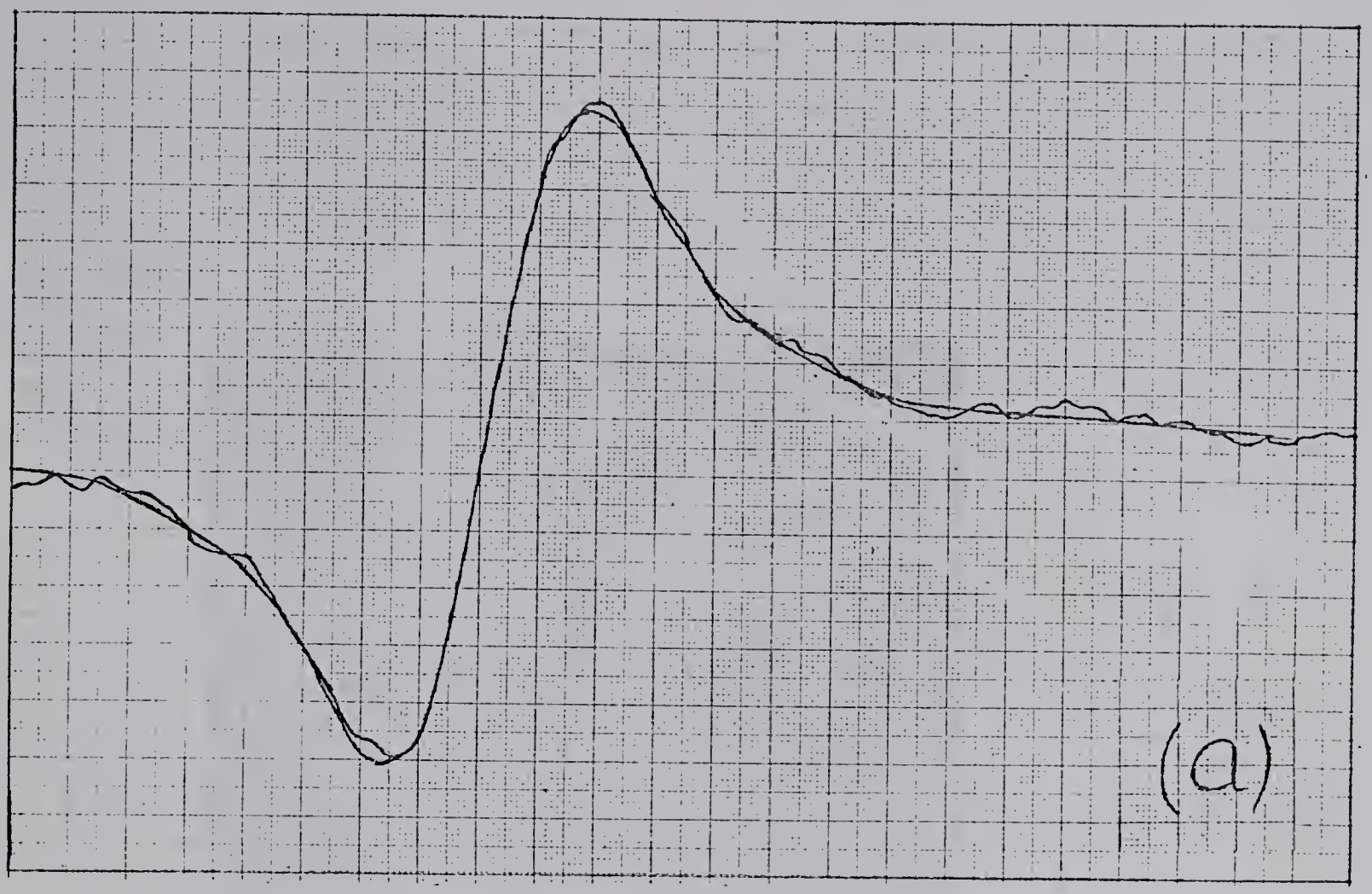
(a)

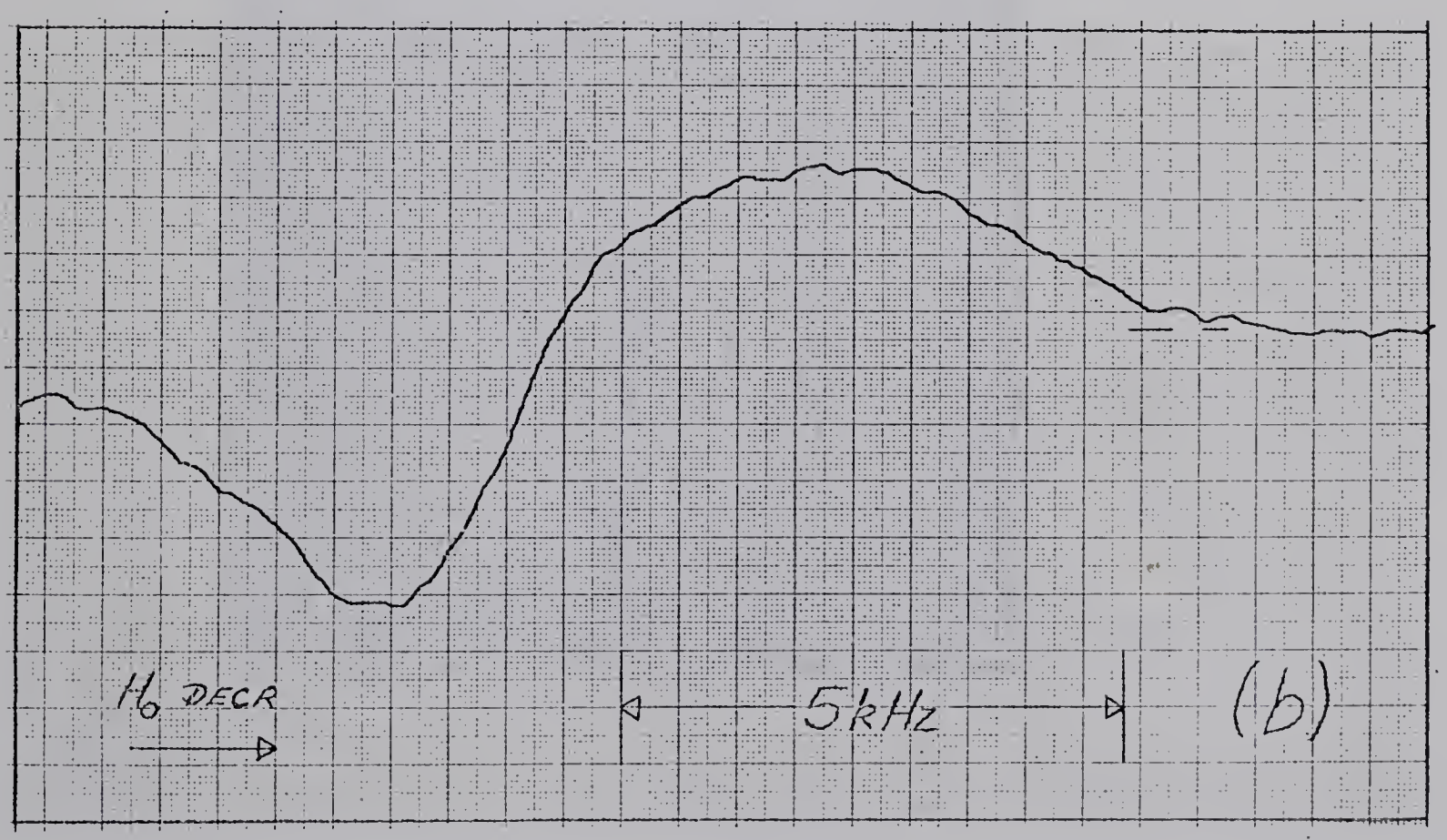
H_0 DECR
5kHz
(b)


5kHz
(C)

With the line being narrowed by the rotation, it was an excellent opportunity to accurately measure the room-temperature isotropic Knight Shift. Previous measurements have been complicated by the anisotropic Knight Shift (Borsa and Barnes, 1964) or skin-depth problems (Jones and Williams, 1964). The applied field, corresponding to a metallic tin resonance at 6 MHz, was determined by measuring the resonant frequency of an undoped saturated aqueous solution of LiCl. Knowledge of the ratios of the Li^7, Sn^{117} and Sn^{119} magnetogyric ratios lead to a value for the Sn Knight Shifts. The values for the Sn^{117} and Sn^{119} magnetic moments from the literature (Varian Associates NMR Wall Chart, 5th ed., 1965) gave values for the Knight Shifts of 0.733% and 0.747% respectively. This difference corresponds to a hyperfine structure anomaly Δ of 1.6×10^{-2} for the tin nuclei, in contrast to the expected value of the order of 10^{-4} (Eisenger and Jaccarino, 1958). Redetermination of the ratio of the Sn^{117} and Sn^{119} magnetic moments removed this discrepancy. The ratio, determined using a M/3 aqueous solution of $FeCl_3$ saturated with $SnCl_2$, was found to be

$$\gamma_{Sn^{119}}/\gamma_{Sn^{117}} = 1.046535 \pm 0.000003.$$

Using the value

$$\gamma_{Li^7}/\gamma_{Sn^{119}} = 1.0428555$$

quoted by Borsa and Barnes (1964), the isotropic Knight Shifts

for the Sn^{117} and Sn^{119} were found to be 0.745 $\pm$ 0.001% and 0.747 $\pm$ 0.001% respectively, the difference being attributed to experimental error. It was not necessary to correct the measured resonance frequencies for shifts due to χ' since the symmetry of the line indicated a negligible contribution.

To determine the value of the spin-spin coupling constant J it was necessary to compare the calculated spectra with those found experimentally. A smooth curve is drawn through each experimental curve and is fitted against the calculated spectrum. To facilitate the drawing of this curve, advantage was taken of the symmetry of the line in the following way. Each resonance was read out of the Fabri-Tek memory twice. One graph was turned relative to the other, and the smooth curve drawn through the superimposed curves. This has the effect of 'reducing' the noise by a factor of $\sqrt{2}$. The experimental curves are taken in the form of derivatives and for this reason it is necessary to calculate the theoretical spectrum in the same form. The computer programme for calculating the spectrum is given in appendix III. The final theoretical curve is 'assembled' by weighting the spectra from the various configurations of nuclei according to table I. Corrections were made to these values to take account of the 20% of the nuclei whose spectra was not directly calculated. The final probabilities are given in table V. Before this spectrum is compared to the experimental curve, it is broadened to allow for the effect of the finite field modulation and rf observing power (see

Table V

Final probabilities of the various nuclear configurations used to calculate the theoretical lineshape. These were used instead of those given in Table I.

NUCLEUS AT CENTRE OF THE 10 SITES	117	119
SURROUNDING 10 SITES CONTAIN	PROBABILITY	
0 UNLIKE NUCLEI	0.4033	0.4502
1 UNLIKE NUCLEUS	0.1740	0.1540
2 UNLIKE NUCLEI	0.2264	0.2368
1 UNLIKE NUCLEUS 1 LIKE	0.1963	0.1590

appendix IV). The spectrum is then compared to the experimental curve by a least squares fit.

The theoretical curves are determined by the parameters J_1, J_2, J_3, B', $\Delta W'$ and T_1, defined in the first part of this chapter. It is also necessary to allow for the differences in the spin-lattice relaxation times of the two isotopes. This may be appreciated by noting that the T_1 of the observed nucleus produces the lifetime-broadening effect, whilst the T_1 of the unlike nuclei produces the collapse of the satellite lines and a resultant narrowing. It is difficult to determine the appropriate values of the 'broadening factor' B' or the extra 'flip' rate $\Delta W'$ and these were therefore taken as unknowns. It was found that taking reasonable values of $\Delta W'$ ($\simeq$ 0.05 W) produced little change in the theoretical lineshape. This result could be anticipated by noting that $\Delta W'$ must add onto the effect of the nuclear relaxation processes. This parameter was therefore set as zero. The same comment cannot be made for the factor B' which has a more pronounced effect on the lineshape.

Of the two isotopes, Sn^{117} should lead to a better value of the spin-spin coupling constant. This is because the lifetime broadening is smaller ($(T_1)_{Sn^{117}} > (T_1)_{Sn^{119}}$) whilst the effect of the J coupling is larger. (A Sn^{117} nucleus has on the average more unlike neighbours than a Sn^{119} nucleus in tin metal.)

In the calculation of the theoretical curves it is necessary to know or assume the ratios between the first,

second and third nearest neighbour couplings. Whilst it would be desirable to treat all these values as unrelated parameters to be determined separately, this approach leads to computational problems and, more serious, is not justified by the present signal-to-noise ratio. Two models were used. In the first model, it is assumed that only the second-nearest neighbours interact, and there is therefore only one parameter J_2 to be determined (J_1, J_3, B' and $\Delta W'$ are taken as zero). This model was considered in view of the suggestion made by Sharma et al. (1969) that the second nearest neighbour interaction is dominant on account of the shape of the tin Fermi surface. This model gives a J_2 value of 3 kHz but the fit is poor. The theoretical curve is not as broad as the experimental one, peaking too early and fading too quickly in the wings. In the second model, it is assumed that the couplings have the form k F(x) where F(x) is the Ruderman-Kittel relationship (see chapter 3) and k is a constant. The ratio of the J values are therefore

$$J_1 : J_2 : J_3 :: 1.00 : 0.440 : -0.631,$$

and the extra broadening factor B' has the form

$$B' = BJ(2\pi^2 J_1^2)/W.$$

The undetermined constant BJ is approximately 0.02 when one takes the typical values of the tin parameters given in the first part of this chapter. Using the second model it was found that the first nearest neighbour interaction J_1 in

Sn^{117} had the values of -2.21, -2.04, -1.88, -1.76 and -1.65 ($\pm$ 0.09) kHz when BJ was 0.00, 0.01, 0.02, 0.03 and 0.04 respectively. The negative sign of the coupling is inherent in the Ruderman-Kittel model. Values from the Sn^{119} resonance are -2.40, -2.09 and -1.94 ($\pm$ 0.09) kHz when BJ was 0.00, 0.01 and 0.02. As can be seen from figure (4.6) the discrepancy between the experimental and theoretical resonances is of the order of the reading error in determining the values of the smoothed experimental curves. Figure (4.7) shows the theoretical curves superimposed on an experimental resonance.

It would be possible to calculate the theoretical curves corresponding to J values obtained from models other than those considered. However, consideration of more detailed models is not justified by the present signal-to-noise ratio.

Figure (4.6)

A graph of the normalized rms discrepancy between experiment and theory for a number of Sn^{117} resonance plots. The parameter BJ was taken as 0.02. The normalization is obtained by taking the peak-to-peak height of the experimental resonances equal to 2. The dashed-line gives an indication of the error to be expected if the smoothed experimental curve differed everywhere from the calculated spectra by an amount equal to a reading error of 0.25 mm.

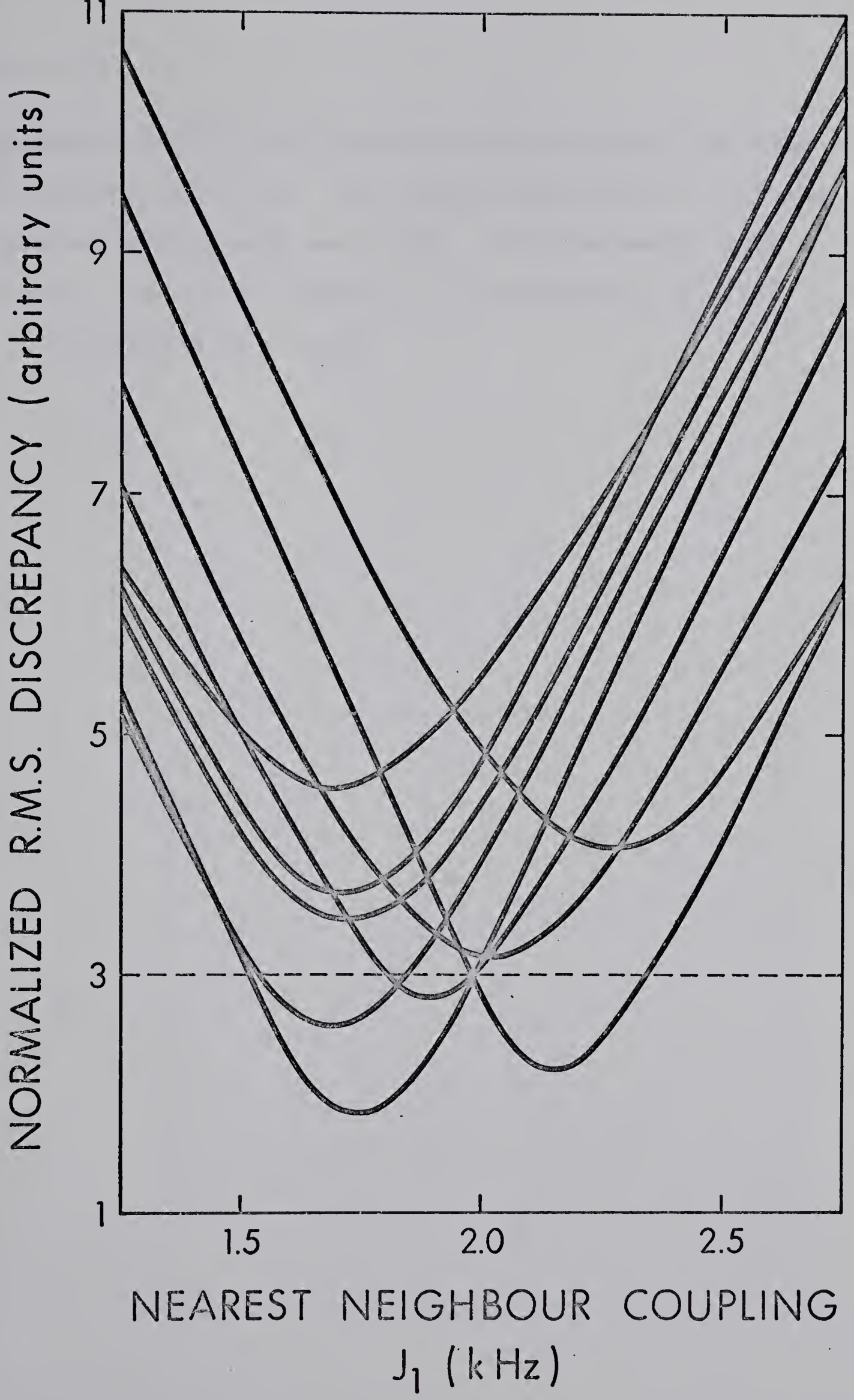
NORMALIZED R.M.S. DISCREPANCY (arbitrary units)
11
9
7
5
3
1
1.5
2.0
2.5
NEAREST NEIGHBOUR COUPLING
J_1 (kHz)

Figure (4.7)

Experimental Sn^{117} resonance obtained by making 1250 runs over a period of 29 hrs. The sample was spun at 5 kHz and the resonance frequency was 6 MHz. The frequency scale is 549 Hz/cm. The smooth curve is a theoretical fit with J_1 = 1.75 kHz and BJ = 0.02.

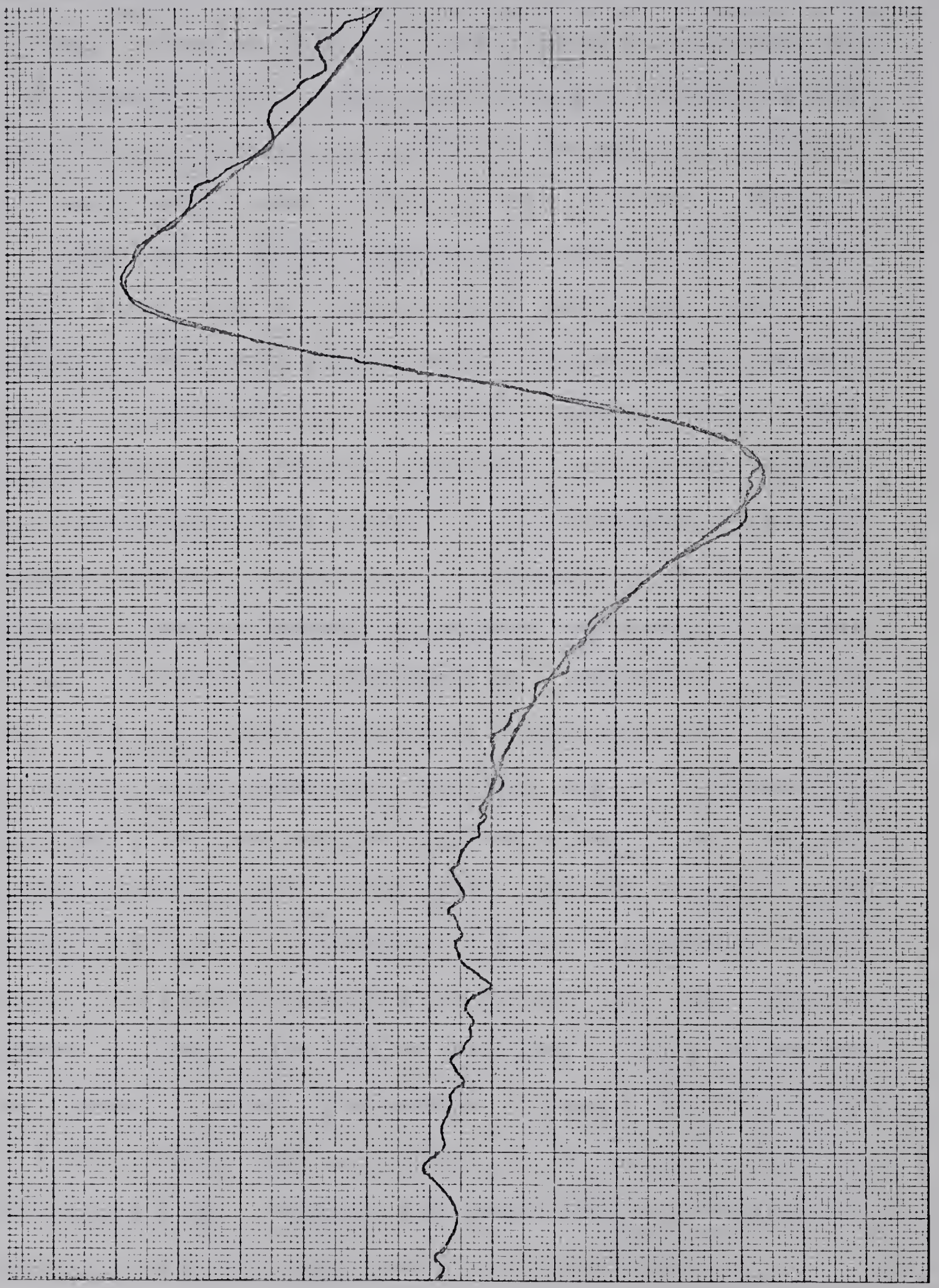

Chapter 5. Discussion and Conclusion

In this thesis we have given details of the construction of a high-speed gas turbine. This turbine was capable of rotating nmr samples at the 'magic' angle 54°44' within a Varian crossed-coil probe at speeds in excess of 5 kHz. Rotation at the magic angle at speeds greater than the equivalent frequency spread of the resonance linewidth removes the effects of the anisotropic Knight Shift, dipolar interactions and the pseudo-dipolar part of the electron-coupled nuclear-nuclear interactions. Measurements of the narrowed resonances gave accurate values of the room-temperature isotropic Knight Shifts of the Sn^{117} and Sn^{119} isotopes. In addition, the removal of the anisotropic interactions enabled the pseudo-exchange coupling in tin metal to be measured. The spectrum of the rotating sample is determined by a 'liquid-like' Hamiltonian, and enables the use of techniques usually more appropriate to high-resolution nmr to compute the lineshape of the Sn^{117} and Sn^{119} resonances. It was found that the lineshape is partly determined by the effect of the finite lifetime of the nuclear spin-states caused by the spin-lattice relaxation time in tin at room temperature. It would be interesting to repeat the measurements and remove the broadening effect of the short T_1 by spinning the sample at temperatures near liquid nitrogen or lower. This could be achieved by driving the turbine using cooled helium gas.

However, it would not be possible, because of space limitations inside the Varian probe, to convert the present system to such an operation. Two turbine systems, capable of operating at low temperatures, have been described in the literature by Beams (1971) and Potter (1971). Potter's turbine may even be propelled by liquid Helium to give operation at temperatures near 1.2°K, although with a limited speed range. Both these turbines differ in construction from the turbine described in this thesis. The propelling and supporting gas streams are separated from each other. This offers the advantage that at high flow rates of the propelling gas stream, the turbine does not shift its position, so that the flutes and gas stream remain fixed with respect to each other. This provides more effecient use of the propelling gas stream and, if the turbine remains balanced, higher rotation rates. If construction of low temperature turbines was attempted it would be advisable to prepare the sample container as large as possible to obtain the maximum signal-to-noise ratio. The problem of poor signal-to-noise ratio was one that placed the major limitation on the accurate determination of the pseudo-exchange coupling in our measurements.

The measurements of the Knight Shifts made when the metallic tin resonance was narrowed by rotation indicated, at first, that there was a significant difference in the values for the Sn^{117} and Sn^{119} isotopes. However, a re-determination of the ratio of the Sn^{117} and Sn^{119} magneto-

gyric ratios removed this difference. Our measured value of the ratio was

$$\gamma_{119}/\gamma_{117} = 1.046535 \pm 0.000003,$$

in contrast to previous values of 1.04639 (Lindgren, 1965) and 1.04648 (Varian NMR Table, fifth edition, 1965). The resonance frequencies of the rotated tin samples were measured relative to both an undoped LiCl solution and an undoped $SnCl_2$ solution. Using the LiCl reference sample and the ratio

$$\nu_{Li^7(LiCl)}/\nu_{Sn^{119}(SnCl_2)} = 1.0428555$$

quoted by Borsa and Barnes (1964) leads to values of the room-temperature isotropic Knight Shifts for Sn^{117} and Sn^{119} of $0.745 \pm 0.001\%$ and $0.747 \pm 0.001\%$ respectively. This is in good agreement with the room-temperature value of $0.750 \pm 0.002\%$ obtained by Borsa and Barnes for the Sn^{119} isotope. However, we have redetermined the ratio $\nu_{Li^7}/\nu_{Sn^{119}}$ using undoped aqueous solutions of LiCl and $SnCl_2$ and found the value

$$\nu_{Li^7}/\nu_{Sn^{119}} = 1.04264 \pm 0.00003.$$

which gives the Knight Shifts of $0.724 \pm 0.003\%$ and $0.726 \pm 0.003\%$ which are in closer agreement with the value of $0.735 \pm 0.002\%$ obtained at room temperature by Sharma et al (1969). Dr. Williams (private communication) has indicated that their measurements were made with direct reference to a

paramagnetically-doped aqueous solution of $SnCl_2$, without correcting for the effects of paramagnetic susceptibility. It appears from our measurements that the ratio of Li^7 and Sn^{119} resonance frequencies taken by Borsa and Barnes is incorrect to about 2 parts in 10^4. Using our corrected ratio the Knight Shift measurements of Borsa and Barnes come in close agreement with both our measurements and those of Sharma et al.

The synthesis of the theoretical lineshape, corresponding to a 'liquid-like' Hamiltonian, by techniques of high resolution nmr spectroscopy was made possible by the small abundance of Sn^{117} and Sn^{119}. The analysis showed that distant unlike nuclei had a significant effect on the resonance lineshape. Taking a value of 0.02, a reasonable value of the parameter BJ describing the effect of distant unlike neighbours, we have found experimentally that the nearest-neighbour pseudo-exchange coupling is -1.89 ± 0.09 kHz. This can be compared with the values of 2.5 kHz (Karimov and Schegolev, 1961) and 2.0 ± 0.5 kHz (McLachlan, 1968) obtained using second moment techniques. The latter values are rather high due possibly to the neglect of the far neighbour interactions. The broadening effect of these interactions means that a smaller value of pseudo-exchange coupling is needed to account for the width of the resonance line. Alloul and Deltour (1969) obtained a value of -4.1 kHz using a pulse method. This is of great interest as it should in principle lead to measurements of greater accuracy than the second moment

method. The technique in the pulse method is to examine the spin-echo envelopes of the tin nuclei in tin alloys. The presence of the impurity atoms leads to a spatial distribution of tin Knight Shifts related to the oscillation of the charge density of the conduction electrons (Froidevaux and Weger, 1964). The spatial distribution of Knight Shifts, provided they are large enough, makes neighbouring nuclei dissimilar, even if they are the same tin isotope. The coupling between unlike nuclei leads to a modulation of the spin-echo envelope. This was clearly shown in the envelopes obtained from Pt^{195} in platinum alloys (Froidevaux and Weger, 1964). In contrast to platinum, tin has two magnetically active isotopes, so that there should be a small modulation in the spin-echo envelope of pure tin metal. There is some evidence of such a modulation in the data shown by Alloul and Deltour (1969) though they do not draw attention to it. The modulation amplitude in tin increases on the addition of the impurity but, even so, the modulation is not as dramatic as it is in the platinum alloys. This is partly due to the difficulty in producing stable solid solutions with sufficient impurity concentrations to provide a large distribution of Knight Shifts. In platinum alloys the spin-echo envelope modulation shows fine structure (Froidevaux and Weger, 1964) but in the tin alloys the modulation dies away so fast that only the fastest modulation period will be seen. Alloul and Deltour have attributed the tin modulation to nearest-neighbour interactions.

Sharma et al. (1969) have suggested that it in fact arises from a dominant second nearest-neighbour interaction. They base this upon the presence of a flat region on the tin Fermi surface in the [001] direction which could lead to significant deviations from the Ruderman -Kittel interaction (Roth, Zeiger and Kaplan, 1966). We have shown in this thesis that the assumption of a second nearest-neighbour interaction far stronger than the other interactions does not give good agreement with the data obtained with the resonances from the spinning tin samples. It is therefore necessary to offer an explanation for the discrepancy of a factor of 2 between Alloul and Deltour and ourselves. Froidevaux and Weger (1964) have shown that the modulation of the spin-echo envelope is determined by

$$E(2\tau) = \sum_{r=0}^{N} A_r \cos^r(2\pi J\tau),$$

where A_r is the probability of having r nearest neighbour magnetic nuclei. The probability of having two magnetic nearest neighbours is close to that of having one magnetic nearest neighbour. In the case of two neighbours, the envelope will have twice the modulation period than where there is only one nearest neighbour. Because of the rapid decay of the modulation and the poor signal-to-noise ratio, it is probable that only the faster modulation period was observed, giving rise to a period determined by 2J rather than J. This interpretation of Alloul and Deltour's data would bring their value of J into closer agreement with ours.

However, it must be pointed out that the analysis of Alloul and Deltour's data is complicated by the fact that in an unspun sample it is necessary to consider the pseudo-dipolar and dipolar interactions. These have the effect of modifying the frequency of the modulation. It is also interesting to note that Froidevaux and Weger (1964) mention that their results on platinum alloys gave results which were a factor of two greater than those determined by steady-state measurements. A second possible explanation of the discrepancy may be offered if it is assumed that the modulation frequency has been correctly assigned by Alloul and Deltour. The frequency is determined by both J_1, the nearest neighbour scalar coupling constant, and B_1, the nearest neighbour 'dipolar and pseudo-dipolar' coupling constant. To determine these quantities separately it is necessary to have an additional relationship between them. Alloul and Detour calculated that M_2, the theoretical second moment of the resonance lineshape, is given by

$$M_2 = 0.40B_1^2 + 0.133J_1^2 \ .$$

As we have previously mentioned, the experimental determination of the second moment is rather difficult. Alloul and Deltour's value of 2.5 ± 0.3 $(\text{kHz})^2$ can be compared with the value 1.2 ± 0.2 $(\text{kHz})^2$ obtained by Karimov and Shchegolev (1961). Using the modulation period determined by Alloul and Deltour and our value of $J_1 = -1.9$ kHz we find that $B_1 = -1.8$ kHz.

These values lead to a second moment of 1.8 $(kHz)^2$, which is between the two experimental values. Taking this value of B_1, it follows that the pseudo-dipolar coupling between nearest neighbours is -2.3 kHz. It must be pointed out that the negative sign of J_1 is inherent in the Ruderman-Kittel model and cannot be determined from the calculated spectrum. If we take the positive sign for J_1, then this leads to a pseudo-dipolar coupling constant of 1.3 kHz.

It should be practical to repeat Alloul and Deltour's measurements in alloys for cases where the contribution from B_1 has been removed by macroscopic rotation or by a multiple pulse sequence. This would lead to a spin-echo evelope determined by J_1 only and it would therefore be hoped that a more accurate value of the pseudo-exchange coupling would be obtained.

In conclusion, we suggest that it would prove useful to attempt to obtain confirmation of the J values obtained in this thesis by applying the second moment technique to the resonances of the spinning samples. It would, however, be necessary to correct the lineshape for the broadening effect of the T_1 of the nuclei being observed. It is not necessary to remove the effect of T_1 on the neighbouring nuclei, as this interaction produces relaxation narrowing, which, in a similar fashion to the motional narrowing, leaves the second moment unchanged. However, the narrowing will tend to produce a lineshape that is somewhat Lorentzian, with the associated difficulty in making accurate determination of the second moment.

Appendix I: Calculation of the AA' part of the AA'X spectrum.

The r_{nq}'s satisfy the simultaneous equations given in table IV. The solution of the equations is not difficult as the matrix $\underline{\underline{A}}$ has a number of special properties. It is symmetric, and both the imaginary parts, and the only quantity which varies at each point of the spectrum, lie along the diagonal. The equations for r may be written

$$\underline{\underline{A}} \cdot \underline{r} = H_{xo}\ i\ Z_o \underline{P} (\gamma\hbar)^{-1} \qquad (1)$$

where $\underline{\underline{A}}$ and $\underline{P}$ are given in table IV. The nuclear susceptibility $\chi(\omega)$ has the form

$$H_{xo}\ \chi(\omega) = \underline{r} \cdot \underline{P}\ \gamma\hbar \quad . \qquad (2)$$

Let $\underline{r} = \underline{C} + i\ \underline{D}$, so that

$$H_{xo}\ \chi''(\omega) = -\ \underline{D} \cdot \underline{P}\ \gamma\hbar \quad . \qquad (3)$$

Splitting matrix $\underline{\underline{A}}$ into real and imaginary parts we have

$$\underline{\underline{A}} = \underline{\underline{F}} + i\ \underline{\underline{G}} \qquad (4)$$

so that $\underline{D}$ satisfies

$$(\underline{\underline{F}} + \underline{\underline{G}}\ \underline{\underline{F}}^{-1}\ \underline{\underline{G}})\ \underline{D} = \underline{P}. \qquad (5)$$

It is necessary to solve for $\underline{D}$ for each value of ω. This is easy since $\underline{\underline{F}}$ is not a function of ω and $\underline{\underline{G}}$ is a diagonalmatrix and can be expressed as

$$\underline{\underline{G}} = (\underline{k} - \underline{\omega})\ \underline{\underline{I}} \tag{6}$$

where $\underline{\underline{I}}$ is the unit matrix

$$\underline{k} = (\omega_{68}, \omega_{47}, \omega_{25}, \omega_{13}, \omega_{58}, \omega_{37}, \omega_{26}, \omega_{14}), \tag{7}$$

and $$\underline{\omega} = \omega \underline{I} \ . \tag{8}$$

For computational ease it is better to keep both A and A' parts of the spectrum (which gives a symmetric solution) rather than just the A line. This is justified as it will be necessary later to take account of the A' resonance. To avoid including the A' nuclei twice, the relative weight given to the AA' spectrum in determining the main spectrum must be decreased by a factor of two over the probability for finding an A nucleus at the centre position given in table I, column 3.

Experimentally, it is $\partial \chi''(\omega)/\partial \omega$ that is of interest. It is then necessary to solve for $\partial \underline{D}/\partial \omega$ which satisfies the equation

$$(\underline{\underline{F}} + \underline{\underline{G}}\ \underline{\underline{F}}^{-1}\ \underline{\underline{G}})\dot{\underline{D}} = -(\frac{\partial}{\partial \omega}(\underline{\underline{G}}\ \underline{\underline{F}}^{-1}\ \underline{\underline{G}}))\underline{D} \ . \tag{9}$$

It is necessary, first, to solve equation (5) for $\underline{D}$ and then substitute these values into equation (9).

Appendix II: Proof that the antisymmetric part $\underline{\underline{J}}^{\dagger}$ of the indirect nuclear spin-spin tensor in white tin is zero.

To have a spectrum that is determined by the 'liquid-like' Hamiltonian, it is necessary that the antisymmetric part $\underline{\underline{J}}^{\dagger}$ of the electron-coupled nuclear spin-spin interaction tensor be zero. Since the point group symmetry for white tin is $\bar{4}$ 2 m (Pearson, 1967), it is easy to show that $\underline{\underline{J}}^{\dagger}$ must be zero.

Consider a general tensor $\underline{\underline{T}}$ referred to the usual crystallographic axes of tin. Applying $\bar{4}$ symmetry requires that

$$\underline{\underline{T}} = \begin{bmatrix} T_{11} & T_{12} & 0 \\ -T_{12} & T_{22} & 0 \\ 0 & 0 & T_{33} \end{bmatrix}$$

whilst m symmetry further requires that

$$\underline{\underline{T}} = \begin{bmatrix} T_{11} & 0 & 0 \\ 0 & T_{22} & 0 \\ 0 & 0 & T_{33} \end{bmatrix}.$$

This implies that any second-rank tensor describing a physical property of white tin must be symmetric and $\underline{\underline{J}}^{\dagger}$ must be zero.

APPENDIX III : Program for calculating the theoretical lineshape.

```
T CURVE(1,50)
 1      C  CALCULATION OF THE LORENTZ-LIKE LINE-SHAPE UNDER CONDITIONS OF
 2      C  J COUPLING,RELAXATION NARROWING AND RELAXATION BROADENING
 3      C  THE PROGRAM WILL ACCOMADATE BOTH THE CALCULATION OF THE REAL AND
 4      C  IMAGINARY PARTS OF THE NUCLEAR SUSCEPTIBILITY
 5      C  THE LINESHAPES ARE GENERATED IN THE DERIVATIVE FORM
 6      C  ONLY ONE HALF OF THE LINE-SHAPE IS GENERATED AS THE RESONANCE
 7      C  IS SYMMETRIC
 8      C
 9      C  THE PROGRAM TAKES INTO ACCOUNT THE 10 NEAREST NEIGHBOUR
10      C  LATTICE SITES IN TIN     THESE SITES ARE SPLIT INTO THREE SHELLS
11      C  OF 4,2 AND 4 SITES RESPECTIVELY
12      C  THE PROGRAM GENERATES SPECTRA TAKING INTO ACCOUNT UP TO TWO
13      C  OTHER ACTIVE NUCLEI IN THE OUTER SHELLS
14      C
15            COMPLEX CB
16            DIMENSION CB(1600),CK(1600)
17            DIMENSION G(19),GG(19),X(100)
18      C
19      C  NUMBER OF THEORETICAL CURVES TO BE CALCULATED IS NRUN
20      C  NUMBER OF POINTS ON THEORETICAL CURVE IS NUM
21      C
22            READ(5,904)NRUN,NUM
23      904   FORMAT(2I3)
24            PI=3.141593
25            NUM1=NUM
26            NUM2=NUM*19
27            DO 950 NT=1,NRUN
28      C
29      C  VALUE OF FIRST NEAREST NEIGHBOUR J-COUPLING IS ASSUMED TO BE RJ HZ
30      C
31            READ(5,902)RJ
32      902   FORMAT(7F10.4)
33            SJI= 2*PI*RJ
34      C
35      C  IF CALCULATION IS TO BE PERFORMED ON THE BASIS OF SECOND NEAREST
36      C  NEIGHBOUR INTERACTIONS ONLY SET N2=2 FOR IDENTIFICATION
37      C  OTHERWISE SET N2=0
38      C
39            READ(5,904)N2
40      C
41      C  INTERVAL BETWEEN THEORETICAL POINTS IS SET AS PP HZ
42      C
43            READ(5,902)PP
44            PQ=2*PI*PP
45            DO 1 I=1,NUM
46      1     X(I)=(I-1)*PQ
47      C
48      C  SPIN-LATTICE RELAXATION TIME IS T1 SECS
49      C
50            READ(5,902)T1
L OF FILE
```

```
 CURVE(51,92)
51              W=0.5/T1
52        C
53        C   WJ MAY BE USED ON TWO COUNTS
54        C   THE FIRST IS TO ACCOUNT FOR THE DIFFERENCES IN THE SPIN-LATTICE
55        C   RELAXATION TIMES BETWEEN THE TWO ISOTOPES
56        C   AND SECOND TO TAKE ACCOUNT OF THE EFFECT OF LIKE NUCLEI IN THE
57        C   CONTINIUM
58        C
59        C   EXTRA BROADENING FACTOR B=BJ*2*PI*PI*J1*J1/W  TO TAKE ACCOUNT OF THE
60        C   UNLIKE NEIGHBOURS IN THE CONTINIUM
61        C
62              READ(5,902)WJ,BJ
63              W1=W*(1+WJ)
64              WW=W1*W1
65        C
66        C  READ IN ASSUMED RATIOS OF THE RUDERMAN -KITTEL J VALUES
67        C   THE RATIOS FOR INTERACTIONS BETWEEN UNLIKE NUCLEI ARE FED IN VIA G
68        C   RATIOS FOR UNLIKE NUCLEI VIA GG              GG(1) TO GG(4) ARE ZERO
69        C
70              READ(5,902)(G(I),I=1,19)
71              READ(5,902)(GG(I),I=1,19)
72        C
73        C   CALCULATION OF AX SPECTRUM AND A SPECTRUM
74        C
75              CALL AX(W,W1,BJ,SJI,CB,NUM,NUM1,WW,G,X)
76        C
77        C   CALCULATION OF THE X PART OF THE AA'X SPECTRUM
78        C
79              CALL XAAX(W,W1,BJ,WJ,SJI,CB,NUM,NUM1,WW,G,GG,X)
80        C
81        C   CALCULATION OF THE A A' PART OF THE AA'X SPECTRUM
82        C
83              CALL AAAX(W,W1,BJ,SJI,CB,NUM,NUM1,WW,G,GG,X,WJ)
84        962   DO 964 JJ=1,NUM2
85        964   CK(JJ)=AIMAG(CB(JJ))
86        C
87        C   THIS IS TO READ OUT THE CALCULATED SPECTRA WITH IDENTIFING PARAMETERS
88        C
89              CALL DUMP(RJ,N2,PP,T1,WJ,BJ,CK,NUM)
90        950   CONTINUE
91              STOP
92              END
OF FILE
```

```
T CURVE(93,111)
 93            SUBROUTINE AX(W,W1,BJ,SJI,CB,NUM,NUM1,WW,G,X)
 94            COMPLEX CB,U12,U34
 95            DIMENSION CB(1600),G(19),X(100)
 96            Q=2*W+W1+BJ*SJI*SJI*0.5/W
 97            DO 20 J=1,4
 98            GJ=G(J)*SJI
 99              IF(J.EQ.1)GO TO 25
100            IF(G(J).EQ.0.)GO TO 22
101        25  DO 21 JJ=1,NUM1
102            U12=-Q-X(JJ)*(0.,1.)
103            U34=(U12+GJ*(0.,1.)/2)*(U12-GJ*(0.,1.)/2)-WW
104            CB(JJ+(J-1)*NUM)=4*(1-2*(U12-W)*U12/U34)*10000/U34
105       21   CONTINUE
106            GO TO 20
107       22   DO 23 JJ=1,NUM1
108       23   CB(JJ+(J-1)*NUM)=(0.,0.)
109       20   CONTINUE
110            RETURN
111            END
 OF FILE


T CURVE(112,139)
112            SUBROUTINE  XAAX(W,W1,BJ,WJ,SJI,CB,NUM,NUM1,WW,G,GG,X)
113            COMPLEX BK,CB,U45,U36,U12,U78,DEN,E,TOP
114            DIMENSION CB(1600),G(19),GG(19),X(100)
115            DO 40 J=5,10
116            GJ=G(J)
117            GGJ=GG(J)
118            IF(GJ.EQ.0..AND.GGJ.EQ.0.)GO TO 21
119            DO 41 JJ=1,NUM1
120            X1=SJI*(GJ+GGJ)/2
121            X2=SJI*(GJ-GGJ)/2
122            Q=2*W+2*W1+BJ*SJI*SJI*0.5/W
123            BK=-Q-(0.,1.)*X(JJ)
124            U45=(0.,1.)*X1+BK
125            U36=(0.,-1.)*X1+BK
126            U12=(0.,1.)*X2+BK
127            U78=(0.,-1.)*X2+BK
128            DEN=U12*U36*U45*U78-4*WW*BK*BK
129            TOP=4*W1*BK-U45*U36-U12*U78
130            E=-(2*TOP+8*BK*(W1-BK)-2*BK*TOP*(2*BK*(U12*U78+U45*U36)-8*WW*BK)
131           C/DEN)/DEN
132            CB(JJ+(J-1)*NUM)=E*10000
133       41   CONTINUE
134            GO TO 40
135       21   DO 23 JJ=1,NUM1
136       23   CB(JJ+(J-1)*NUM)=(0.,0.)
137       40   CONTINUE
138            RETURN
139            END
 OF FILE
```

```
T CURVE(140,189)
140             SUBROUTINE AAAX(W,W1,BJ,SJI,CB,NUM,NUM1,WW,G,GG,X,WJ)
141             COMPLEX CB
142             DIMENSION CB(1600),G(19),GG(19),A(8,8),AI(8,8),TA(8,8),TC(8,8),
143            CTB(8,8),TZ(8,8),TZZ(8,8),SX(100),X(100)
144             DIMENSION FF(8),EE(8),DD(8),DDD(8)
145             DO 90 J=11,19
146             GGJ=GG(J)*SJI
147             GJ=SQRT(G(J)*G(J)*SJI*SJI)
148             IF(GJ.EQ.0..AND.GGJ.EQ.0.)GO TO 21
149             D=0.5*(SQRT(0.25*GGJ*GCJ+GJ*GJ))
150      912    SPP=0.5*GJ*W1/D
151             SMM=SPP
152             CPM=SPP
153             CPP=0.25*GGJ/D
154             CMM=-CPP
155             SPM=-CPP*W1
156             CM=SQRT(0.5+CMM/2)
157             SM=SQRT(0.5-CMM/2)
158             CP=SQRT(0.5+CPP/2)
159             SP=SQRT(0.5-CPP/2)
160             WQP=2*W +3*W1/2+W1*CPP*CPP/2+BJ*SJI*SJI*0.5/W
161             CPP=CPP*W1
162             CMM=-CPP
163             DO 71 L=1,8
164             DO 70 M=1,8
165             AI(L,M)=0.
166             A(L,M)=0.
167             IF(L.EQ.M) GO TO 69
168             GO TO 70
169       69    AI(L,M)=1.
170             A(L,M)=-WQP
171       70    CONTINUE
172       71    CONTINUE
173       83    A(1,2)=CPM
174             A(1,3)=CMM
175             A(1,6)=SPM
176             A(1,7)=-SMM
177             A(2,4)=CPP
178             A(2,5)=-SPM
179             A(2,8)=-SPP
180             A(3,4)=CPM
181             A(3,5)=SMM
182             A(3,8)=-SPM
183             A(4,6)=SPP
184             A(4,7)=SPM
185             A(5,6)=CPM
186             A(5,7)=CMM
187             A(6,8)=CPP
188             A(7,8)=CPM
189       82    CONTINUE
 OF FILE
```

```
T CURVE(190,239)
190             DO 74 L=1,8
191             DO 73 M=1,L
192             TA(L,M)=A(L,M)
193             TA(M,L)=A(L,M)
194     73       A(M,L)=A(L,M)
195     74      CONTINUE
196             FF(1)=-0.25*(2*GJ+GGJ)-D
197             FF(2)=FF(1)+0.5*GGJ
198             FF(3)=FF(1)+GJ
199             FF(4)=FF(2)+GJ
200             FF(5)=FF(1)+2*D
201             FF(6)=FF(2)+2*D
202             FF(7)=FF(3)+2*D
203             FF(8)=FF(4)+2*D
204             EE(1)=SM-CM
205             EE(2)=SP-CP
206             EE(3)=-(CM+SM)
207             EE(4)=-(CP+SP)
208             EE(5)=FF(3)
209             EE(6)=EE(4)
210             EE(7)=EE(1)
211             EE(8)=EE(2)
212     C
213     C   CALCULATION OF THE NORMAL RESONANCE CURVE
214     C
215     C
216     C   GELG IS A SUBROUTINE FROM THE FORTRAN SCIENTIFIC SUBROUTINE PACKAGE
217     C
218             CALL GELG(AI,TA,8,8,1.E-6,IER)
219             DO 76 L=1,8
220             DO 75 M=1,8
221             TB(L,M)=A(L,M)+FF(L)*FF(M)*AI(L,M)
222     75      TC(L,M)=AI(L,M)*(FF(L)+FF(M))
223     76      CONTINUE
224             DO 80 JJ=1,NUM1
225             XXJJ=X(JJ)
226             DO 79 L=1,8
227             DD(L)=EE(L)*10000
228             DO 78 M=1,8
229             TZ(L,M)=TB(L,M)-XXJJ*TC(L,M)+XXJJ*XXJJ*AI(L,M)
230     78      TZZ(L,M)=TZ(L,M)
231     79      CONTINUE
232             CALL GELG(DD,TZ,8,1,1.E-7,IER)
233             DO 196 L=1,8
234             DDD(L)=0.
235             DO 195 M=1,8
236     195     DDD(L)=DDD(L)-(2*XXJJ*AI(L,M)-TC(L,M))*DD(M)
237     196     CONTINUE
238     C
239     C   CALCULATION OF THE DERIVATIVE RESONANCE CURVE
OF FILE
```

```
 CURVE(240,251)
40      C
41            CALL GELG(DDD,TZZ,8,1,1.E-6,IER)
42            SX(    JJ)= 1*(DDD(1)*EE(1)+DDD(2)*EE(2)+DDD(3)*EE(3)+DDD(4)*EE(4
43           C)+DDD(5)*EE(5)+DDD(6)*EE(6)+DDD(7)*EE(7)+DDD(8)*EE(8))
44      30    CB(JJ+(J-1)*NUM)=(0.,1.)*SX(JJ)
45      80    CONTINUE
46            GO TO 90
47      21    DO 23 JJ=1,NUM1
48      23    CB(JJ+(J-1)*NUM)=(0.,0.)
49      90    CONTINUE
50            RETURN
51            END
OF FILE


 CURVE(252,265)
52            SUBROUTINE DUMP(RJ,N2,PP,T1,WJ,BJ,CK,NUM)
53            DIMENSION CK(1600)
54            WRITE(6,902)RJ
55            WRITE(6,904)N2
56            WRITE(6,902)PP
57            WRITE(6,910)T1
58            WRITE(6,902)WJ,BJ
59            NUM2=NUM*19
60            WRITE(6,910)(CK(JJ),JJ=1,NUM2)
61      902   FORMAT(7F10.4)
62      904   FORMAT(2I3)
63      910   FORMAT(7E10.4)
64            RETURN
65            END
OF FILE
```

Appendix IV : Correction for saturation and modulation effects.

Modulation and saturational broadening differ in their effect on the resonance line-shape. The saturation broadening, which is produced by the action of the rf field on the population distribution of the nuclear spin-states, directly affects the sample whilst the modulation broadening is totally instrumental. We therefore correct the theoretical resonances to allow for the saturation effects and then modulation broaden the resulting line-shape.

The nuclear absorption χ'', in the presence of a linear polarized rf field $2H_1$ and frequency ν, is determined by (Bloembergen, Purcell and Pound (BPP), 1948)

$$\chi''(\nu,H_1) = \chi''(\nu,0)[1 + \gamma^2 H_1^2 T_1 g(\nu)/2]^{-1} \qquad (1)$$

where $\chi''(\nu,0)$ is the unsaturated susceptibility, determined by a normalized lineshape function $g(\nu)$. The BPP theory is known to be incorrect for solids where the spin-lattice interactions are much weaker than the spin-spin interactions (Redfield, 1955). This is not the case in metallic tin, and, in this case, the saturated derivative lineshape $f_{sat}(\nu)$, proportional to $\frac{\partial \chi''(\nu,H_1)}{\partial \nu}$, is given by

$$f_{sat}(\nu) = Ag'(\nu)[1 + \rho H_1^2 \, g(\nu)/g(\nu_{max})]^{-2} \qquad (2)$$

where A is the gain of the system, ρ is $\gamma^2 T_1^2 g(\nu_{max})/2$ and ν_{max} is the frequency of one of the extrema of $g'(\nu)$ provided ω_m, the frequency of the magnetic field modulation, satisfies

$\omega_m T_1 << 1$. We may therefore use the calculated derivative lineshape $f(\nu)$ to determine the theoretical 'saturated' lineshape

$$f_{sat}(\nu) = f(\nu)[1 + \rho H_1^2 \int_o^{\nu} f(\nu')d\nu' \{\int_o^{\nu_{max}} f(\nu')d\nu'\}^{-1}]^{-2}. \quad (3)$$

The proportionality constant ρ must be determined from experiment. From equation (2) we have that

$$[f_{sat}(\nu_{max})]_{exp} = [f(\nu_{max})]_{exp}[1 + \rho H_1^2]^{-2} \quad (4)$$

so that a plot of the peak-to-peak intensity of the derivative line as a function of H_1^2 gives ρ_{exp}. Allowance must be made for the intrinsic increase in the signal intensity with H_1. In the experiment on tin, ρH_1^2 was 0.045, implying that the correction to the lineshape was small.

The technique used to calculate the modulation broadening is that given by Flynn and Seymour (1960). The modulation peak-to-peak amplitude is taken as 2a (in frequency units), so that

$$f_{sat}(\nu) = N\int_{\nu-a}^{\nu+a} (a^2 - (\nu-\nu')^2)^{1/2} f_{sat}(\nu')d\nu' \quad (5)$$

where N is a normalization constant.

REFERENCES

Abragam A, 1961, The Principles of Nuclear Magnetism, (Oxford: The University Press), p. 206.

Alloul H and Deltour R, 1969, Phys. Rev. 183, 414.

Alloul H and Froidevaux C, 1967, Phys. Rev. 163, 324.

Anderson PW, 1954, J. Phys. Soc. Japan 17, 1065.

Anderson PW and Weiss PR, 1953, Rev. Modern Physics 25, 269.

Andrew ER, 1970, Magnetic Resonance, (New York: Plenum Press), p. 163.

Andrew ER, Bradbury A and Eades RG, 1958, Nature 182, 1659.

Andrew ER, Bradbury A and Eades RG, 1959, Nature 185, 1802.

Andrew ER, Carolan JL and Randall PJ, 1971a, Phys. Letters 35A, 435.

Andrew ER, Carolan JL and Randall PJ, 1971b, Phys. Letters, in press.

Andrew ER and Farnell LF, 1968, Molecular Physics 15, 157.

Andrew ER and Jenks GJ, 1962, Proc. Phys. Soc. 80, 663.

Andrew ER and Newing RA, 1958, Proc. Phys. Soc. 72, 959.

App MJ, 1970, M.Sc. thesis, University of British Columbia.

Arnold JT, 1956, Phys. Rev. 102, 136.

Asayama K and Itoh J, 1962, J. Phys. Soc. Japan 17, 1065.

Beams JW, 1937, Jour. Applied Physics 8, 795.

Beams JW, 1964, Automotive Engineering Congress, Detroit, Michigan.

Beams JW, 1971, Rev. Sci. Instrum. 42, 637.

Bloembergen N, Purcell EM and Pound RV, 1948, Phys. Rev. 73, 679.

Bloembergen N and Rowland TJ, 1953, Acta Metallurgica 1, 731.

Bloembergen N and Rowland TJ, 1955, Phys. Rev. 97, 1679.

Borsa F and Barnes RG, 1964, J. Phys. Chem. Solids 25, 1305.

Bradbury A, Eades RG and McCarten JG, 1968, Phys. Letters 26A, 405.

Dickson EM, 1969, Phys. Rev. 184, 294.

Eisinger J and Jaccarino V, 1958, Rev. Mod. Phys. 30, 528.

Flynn CP and Seymour EFW, 1960, Proc. Phys. Soc. 75, 337.

Froidevaux C and Weger M, 1964, Phys. Rev. Letters 12, 123.

Gutowsky HS, McCall DW and Slichter CP, 1953, J. Chem. Phys. 21, 279.

Gutowsky HS and Pake GE, 1948, J. Chem. Phys. 16, 327.

Hahn EL and Maxwell DE, 1952, Phys. Rev. 88, 1070.

Henriot E and Huguenard E, 1925, Comptes Rendus 180, 1389.

Jones EP and Williams DL, 1964, Can. J. Phys. 42, 1499.

Karimov YS and Shchegolev IF, 1961, JETP (English Translation) 13, 908.

Knight WD, 1949, Phys. Rev. 76, 1259.

Korringa J, 1950, Physica 16, 601.

Lindgren I, 1965, Ark. Fys. 29, 553.

Lowe IJ, 1959, Phys. Rev. Letters 2, 285.

Mansfield P and Ware D, 1966, Phys. Letters 22, 133.

McConnell HM, 1957, J. Mol. Spectry. 1, 11.

McLachlan LA, 1968, Can. J. Phys. 46, 871.

Ostroff ED and Waugh JW, 1966, Phys. Rev. Letters 16, 1097.

Pake GE, 1948, J. Chem. Phys. 16, 327.

Pake GE, 1956, Solid State Physics 2, (New York: Academic Press), p. 1.

Pake GE and Purcell EM, 1948, Phys. Rev. 74, 1184.

Pearson WB, 1967, A handbook of Lattice Spacings and Structures of Metals and Alloys 2, (Toronto: Pergamon Press), p. 25.

Pople JA, Schneider WG and Berstein HJ, 1959, High Resolution Nuclear Magnetic Resonance, (Toronto: McGraw-Hill).

Potter WH, 1971, Rev. Sci. Instrum. 42, 618.

Redfield AG, 1955, Phys. Rev. 98, 1787.

Redfield AG, 1957, IBM Journal of Research and Development 1, 19.

Roth LM, Zeiger HJ and Kaplan TA, 1966, Phys. Rev. 149, 519.

Ruderman MA and Kittel C, 1954, Phys. Rev. 96, 99.

Schone HE, 1969, Phys. Rev. 183, 410.

Schuster NA, 1951, Rev. Sci. Instrum. 22, 254.

Schwind AE, 1967, Ann.Physik 7, 164.

Sharma SN, Williams DL and Schone HE, 1969, Phys. Rev. 188, 662.

Slichter CP, 1963, Principles of Magnetic Resonance, (New York: Harper and Row), p. 102.

Spokas JJ and Slichter CP, 1959, Phys. Rev. 113, 1462.

Van Vleck JH, 1948, Phys. Rev. 74, 1168.

Watson GN, 1922, A treatise on the theory of Bessel Functions, (Cambridge: University Press).